INSTITUTO POTOSINO DE INVESTIGACIÓN CIENTÍFICA Y TECNOLÓGICA, A.C.

POSGRADO EN CIENCIAS AMBIENTALES

Denitrification of Metallurgical Wastewater in a Novel Anaerobic Swirling Fluidized Membrane Bioreactor

Tesis que presenta

Juan Ernesto Ramírez Juárez

Para obtener el grado de

Doctor en Ciencias Ambientales

Codirectores de la Tesis:

Dr. Francisco Javier Cervantes Carrillo

Dr. Germán Buitrón Méndez

San Luis Potosí, S.L.P., julio de 2019

IPICYT

Constancia de aprobación de la tesis

La tesis "**Denitrification of Metallurgical Wastewater in a Novel Anaerobic Swirling Fluidized Membrane Bioreactor**" presentada para obtener el Grado de Doctor(a) en Ciencias Ambientales fue elaborada por **Juan Ernesto Ramirez Juárez** y aprobada el **03 de julio de 2019** por los suscritos, designados por el Colegio de Profesores de la División de Ciencias Ambientales del Instituto Potosino de Investigación Científica y Tecnológica, A.C.

Dr. Francisco Javier Cervantes Carrillo
Director de la tesis

Dr. Germán Buitrón Méndez
Codirector de la tesis

Dra. Sonia Lorena Arriaga García
Miembro del Comité Tutoral

Dra. Marisol Gallegos García
Miembro del Comité Tutoral

Dr. José René Rangel Méndez
Miembro del Comité Tutoral

Thesis committee

Promoters

Dr. Francisco Javier Cervantes Carrillo

Instituto Potosino de Investigación Científica y Tecnológica, A.C. (Universidad Nacional Autónoma de México a partir del 1 de mayo de 2019)

Dr. Germán Buitrón Méndez

Universidad Nacional Autónoma de México

Other members

Dra. Marisol Gallegos García

Universidad Autónoma de San Luis Potosí

Dra. Sonia Lorena Arriaga García

Instituto Potosino de Investigación Científica y Tecnológica, A.C.

Dr. José René Rangel Méndez

Instituto Potosino de Investigación Científica y Tecnológica, A.C.

Institutional Support

This research was conducted under the auspices of the Division of the Environmental Sciences of Instituto Potosino de Investigación Científica y Tecnológica, A. C., supervised by Dr. Francisco Javier Cervantes Carrillo and Dr. Germán Buitrón Méndez.

The hydrodynamic study presented in Chapter 3 was carried out at Laboratory of Hydraulic Models of Instituto Interamericano de Tecnología y Ciencias del Agua of Universidad Autónoma del Estado de México, supervised by Dr. Humberto Salinas Tapia.

The author of this thesis was financially supported by the Council of Science and Technology of Mexico (CONACyT), scholarship 275463, and the research project was financially supported by the Council of Science and Technology of Mexico (Grant 1289 Frontiers in Science) and by the Marcos Moshinsky Foundation.

IPICYT

Instituto Potosino de Investigación Científica y Tecnológica, A.C.

Acta de Examen de Grado

El Secretario Académico del Instituto Potosino de Investigación Científica y Tecnológica, A.C., certifica que en el Acta 017 del Libro Primero de Actas de Exámenes de Grado del Programa de Doctorado en Ciencias Ambientales está asentado lo siguiente:

En la ciudad de San Luis Potosí a los 12 días del mes de julio del año 2019, se reunió a las 16:00 horas en las instalaciones del Instituto Potosino de Investigación Científica y Tecnológica, A.C., el Jurado integrado por:

Dr. José René Rangel Méndez	**Presidente**	**IPICYT**
Dra. Sonia Lorena Arriaga García	**Secretaria**	**IPICYT**
Dra. Marisol Gallegos García	**Sinodal externo**	**UASLP**

a fin de efectuar el examen, que para obtener el Grado de:

DOCTOR EN CIENCIAS AMBIENTALES

sustentó el C.

Juan Ernesto Ramírez Juárez

sobre la Tesis intitulada:

Denitrification of Metallurgical Wastewater in a Novel Anaerobic Swirling Fluidized Membrane Bioreactor

que se desarrolló bajo la dirección de

Dr. Francisco Javier Cervantes Carrillo
Dr. Germán Buitrón Méndez (UNAM)

El Jurado, después de deliberar, determinó

APROBARLO

Dándose por terminado el acto a las 18:26 horas, procediendo a la firma del Acta los integrantes del Jurado. Dando fe el Secretario Académico del Instituto.

A petición del interesado y para los fines que al mismo convengan, se extiende el presente documento en la ciudad de San Luis Potosí, S.L.P., México, a los 12 días del mes de julio de 2019.

Dr. Marcial Bonilla Marín
Secretario Académico

Mtra. Ivonne Lizette Cuevas Vélez
Jefa del Departamento del Posgrado

INSTITUTO POTOSINO DE INVESTIGACIÓN CIENTÍFICA Y TECNOLÓGICA, A.C.
IPICYT
SECRETARIA ACADEMICA

Aknowledgements

A special mention goes to my supervisor Dr. Francisco Cervantes, thank you for trust and believe in me. I appreciate your support and guidance. It has been an absolute pleasure working with you.

I special thanks to my supervisor Dr. Germán Buitrón for believing in the project and for your support during the accomplishment of this work.

I would like to thank also to my thesis committee, Dra. Sonia Arriaga, Dra. Marisol Gallegos, Dr. René Rangel for all the useful discussions that helped me to look at situations and results from many angles. Their contribution was very helpful in carrying out this work.

A warm thanks to Dr. Humberto Salinas Tapia, Dr. Boris López and Dr. Ramiro Félix at the Instituto Interamericano de Tecnología y Ciencias del Agua for their friendship and support in the hydrodynamic study of the reactor from Chapter 3.

I special thanks to my friend Saúl Esquivel for your master thesis that help to this work as well as Carla Limberger for your support in the beginning.

I would also like to extend my thanks to the technicians of the laboratory of the Environmental Sciences Division at IPICYT, Dulce Partida, Guillermo Vidriales, Alejandra Colunga, Mario Delgado, Juan Pablo Rodas, Ma. Del Carmen Rocha, for their valuable help and technical support in this project. Thanks to Guadalupe Arriaga for helping me countless times and always showing admirable kindness. Thanks to Beatriz Adriana Rivera Escoto who attended the materials characterization and the Nanoscience and Nanotechnology Research National Laboratory (LINAN) at IPICyT, for providing access to their facilities.

Thanks to Cervantes´s team, Emilia, Eduardo, Santiago, Lupita, Paola, Iván, Mónica, Hugo, Claudia, Edgardo, Alejandra, and Mario, for their pleasant company and help with the work of the group.

Thanks to Jenny for helping me and be part of this life project as well as to all my friends from Zacatecas.

Thanks to Deny, Itzel, Joél, Migue, Janeth, Alicia, Charly, Nathalie, Max, Neto, Erick, Lupita, Cynthia, Saúl, Liz, Itzel, Francisco Guerra, Antonio Ortiz, Gerardo, Emily,

Mariana, Valeria, Andrea, Efra, Sandra, Richard, Claudia, Antonio Gamboa, Carmen, Yeraldi, Edgar, Francisco Calvillo, Dulce, Lilia, Chuy, Pao, Iván, Violeta, Marisol, JuanJo, for all the good moments, dinners, parties, trips, and discussions (Avalon) that we have shared during these years. Thanks to Karime for her friendship, and particular thanks to Alexa for all we shared and your help during the last stage. I am grateful to all of you. You were family to me!

A mi hermosa familia por hacerme sonreír a la vida y sentirme siempre acompañado. Gracias a mi mami hermosa por su ánimo, y por darme una visión de la vida que me ha hecho disfrutar de ella y buscar crecer en todo momento. Gracias a mi papá por darme ese espíritu de ayuda y amistad sincera. A mi hermana Jessica por ser un gran ejemplo de fortaleza para mi vida, te debo mucho de lo que soy. A mi hermana Nancy por su confortable compañía, y por mostrarme que no rendirse es lo mejor que puedes hacer. A mi hermanito Leo, por la agradable compañía que me da y todo lo que me ha hecho sentir en la vida. ¡Los admiro familia! ¡Gracias por ayudarme a ser feliz! ¡Los AMO!

Contributions to conferences, symposia and congress

Ramírez, J. E.; Esquivel, S.; Buitrón, G.; Cervantes, F. J. Heavy metals effects and denitrifying process in an Anaerobic Swirling Fluidized Membrane Bed Bioreactor (ASFMBR). 16th IWA World Congress on Anaerobic Digestion, 23-27 June 2019, Delft, The Netherlands.

Ramírez, J. E.; Esquivel, S.; Buitrón, G.; Cervantes, F. J. Denitrification of a synthetic metallurgic effluent through an Anaerobic Swirling Fluidized Membrane Bioreactor. XIII Taller y Simposio Latinoamericano de Digestión Anaerobia – DAAL XIII, 21-24 October 2018, Medellín, Colombia.

Ramírez-Juárez, J. E.; Buitrón, G.; Cervantes, F.J. Efecto inhibitorio del níquel en el proceso de desnitrificación: relevancia de la especiación. IX Congreso de la Red Latinoamericana de Ciencias Ambientales (RELACIAM), 2-6 October 2017, San Luis Potosí, SLP, México.

Ramírez-Juárez, J. E.; Buitrón, G.; Cervantes, F.J. Effects of heavy metals on denitrification of synthetic metallurgical wastewater. 5th IWA Mexico – Young Water Professionals Conference, 24-26 May 2017, Morelia, México.

Ramírez-Juárez, J. E.; Buitrón, G.; Cervantes, F.J. Desnitrificación de aguas residuales metalúrgicas mediante un bioreactor anaerobio de membranas con fluidización. 8° Curso-Taller “Temas Actuales en Ciencias del Agua”, Centro Interamericano de Recursos del Agua, UAEM, 23-24 November 2016, Toluca, Estado de México, Méx.

Table of contents

List of Tables

List of Figures

Abstract

Denitrification of Metallurgical Wastewater in a Novel Anaerobic Swirling Fluidized Bioreactor

Key words: denitrification; stainless-steel effluent; metal bio-recovery; fluidized bed bioreactor, swirling fluidization

The present work was focused on the application of denitrification to a stainless-steel industrial effluent, which contains a high nitrate concentration (~6.8 g $N\text{-}NO_3^-$), acidic pH (pH=3.3) and a high concentration of Fe=12.5 g/L, Cr=2.9 g/L, Ni=2.2 g/L, and other elements, such as Sn, Mn, Si, Mo, Co, Pb, Cu, V, B and Al, which are present at a concentration lower than 1 g/L. Citrate, which is a chelating agent, can also be present in this type of wastewater. Denitrification applied to this effluent has the challenge to face high nitrate and metals concentrations as well as acidic pH, which could inhibit nitrate removal rate and promote the accumulation of intermediates (NO_2^- and N_2O). The first part of the study was focused on understanding the effects of key metals present in the metallurgic effluent on denitrification performance. This was accomplished by chemical speciation analysis and by monitoring the accumulation of denitrification intermediates. The second step of the project was focused on the development of a novel technology for the treatment of a stainless-steel industrial effluent. This technology was implemented with the aim to remove high content of nitrate in the effluent, neutralize the acidic pH and to achieve metals recovery. The acidic pH can be neutralized by the by-products generated (CO_3^- and OH^-) from the denitrification process. Additionally, these compounds form insoluble species with the metals, promoting their bio-recovery.

The project innovation considers the design and test of the process previously described through an Anaerobic Swirling Fluidized Membrane Bioreactor (ASFMBR). Fluidization of granular carbon (GC) through the hydrodynamic conditions established inside the ASFMBR has the objective of promote the collision

of GC particles with the microfiltration hollow fiber membranes surface as a mechanical cleaning strategy to prevent membrane fouling. Likewise, a denitrifying biofilm was supported on GC particles to carry out the denitrification process. Swirling fluidization is produced both by the novel reactor geometry (hydrocyclone type) and by a tangential inlet. Membrane module design allows the free GC particles circulation around the membranes. The outlet of the reactor is just composed by the line of permeate flow. This allows the saturation of the chemical species, their precipitation, and rejection by the membranes. The treatment concept was also integrated by a preliminary precipitation column in which high recirculation of the alkalinity produced from the denitrifying process was introduced to drive the precipitation and recovery of metals present in the industrial wastewater. Two external electron donors (ethanol and citrate) were added to balance the C/N ratio to achieve denitrification.

The effects of the chemical speciation metal-citrate complexes on denitrification performance was conducted in batch assays. Fe(II) improved nitrate removal and Ni(II) affected the reduction of NO_3^-, NO_2^- and N_2O. Cr(III) inhibited only the nitrate reduction step. A continuous metal addition in ASFMBR decreased the negative effects of Ni(II) on denitrification performance. Fe(II) stimulated the process by promoting autotrophic denitrification, and Cr(III)-citrate complexes were difficult to break. The novel reactor configuration achieved high nitrate removal (>94 %) with marginal accumulation of intermediates (nitrite and N_2O) with both electron donors tested. Furthermore, the acidic pH was efficiently neutralized in the reactor, by recycling the alkalinity produced from the denitrifying process. The operational strategies also allowed to recover over 40% of the metals present in the precipitation column and higher to 90% inside the ASFMBR. Membrane fouling was avoided by the hydrodynamic regime established in the ASFMBR and GC fluidization. The treatment concept is promising to achieve efficient removal of nitrate and recovery of metals, while preserving the membrane fouling by the hydrodynamic conditions prevailing inside the ASFMBR. This treatment concept could also be applicable for other anaerobic processes, such methanogenesis and sulfate reduction demanded for the treatment of industrial effluents.

Resumen

Desnitrificación de aguas residuales metalúrgicas en un novel Bioreactor Anaerobio con Fluidización en Remolino

Palabras clave: desnitrificación; efluente de acero inoxidable; bio-recuperación de metales; bioreactor de lecho fluidizado; fluidización en remolino.

El presente trabajo estudia la aplicación del tratamiento de desnitrificación al efluente de la industria del acero inoxidable, el cual contiene una alta concentración de nitratos (~6.8 g $N\text{-}NO_3^-$), un pH ácido (pH=3.3) y una alta concentración de Fe=12.5 g/L, Cr=2.9 g/L, Ni=2.2 g/L, y otros elementos, tales como Sn, Mn, Si, Mo, Co, Pb, Cu, V, B y Al, los cuales están presentes en una concentración menor a 1 g/L. Citrato también puede estar presente en este tipo de efluentes, el cual es un agente quelante. La aplicación de la desnitrificación a este efluente tiene el reto de enfrentar altas concentraciones de nitratos y metales, así como un pH ácido, que podrían inhibir la tasa de eliminación de nitratos y promover la acumulación de intermediarios (NO_2^- y N_2O). La primera parte del estudio está enfocada en entender el efecto de los metales predominantes en el efluente de la industria metalúrgica sobre el rendimiento del proceso desnitrificante. Esto se logró mediante el análisis de especiación química y monitoreo de la acumulación de intermediarios del proceso de desnitrificación. El propósito de la segunda etapa del proyecto de investigación fue el desarrollo de una tecnología novedosa para el tratamiento del efluente de la industria del acero inoxidable. Los principales objetivos de esta tecnología son remover el alto contenido de nitrato en el efluente, neutralizar el pH y lograr la recuperación de los metales. El pH ácido puede ser neutralizado por los subproductos generados del proceso de desnitrificación (CO_3^- y OH^-). Adicionalmente, estos compuestos forman especies insolubles con los metales, promoviendo si bio-recuperación.

La innovación del proyecto considera el diseño y la prueba del proceso descrito anteriormente mediante un Bioreactor Anaerobio de Membranas con Fluidización en Remolino (ASFMBR, por sus siglas en inglés). La fluidización del carbón granular (CG) a través de las condiciones hidrodinámicas establecidas dentro del ASFMBR tiene el objetivo de promover la colisión de partículas de CG con la superficie de las membranas de fibra hueca de microfiltración como una estrategia de limpieza mecánica para evitar el taponamiento de la membrana. Asimismo, una biopelícula desnitrificante se soportó sobre partículas de CG para llevar a cabo el proceso de desnitrificación. La fluidización en forma de remolino es producida tanto por la novedosa geometría del reactor (tipo hidrociclón) como por una entrada tangencial que alimenta al reactor. El diseño del módulo de membranas permite la libre circulación de CG alrededor de las membranas. La salida del reactor está compuesta solamente por la línea de flujo de permeado. Esto permite la saturación

de especies químicas, su precipitación, y su rechazo mediante la filtración por membranas. El tren de tratamiento también está integrado por una columna de precipitación previa al ASFMBR, la cual es alimentada por una recirculación con alta concentración de alcalinidad que es producida por el proceso desnitrificante para inducir la precipitación y recuperación de metales presentes en el agua residual industrial. Se adicionaron dos fuentes donadoras de electrones (etanol y citrato) para balancear la relación C/N para llevar a cabo la desnitrificación.

Los efectos de la especiación química de los complejos metal-citrato sobre el desempeño de la desnitrificación fue llevado a cabo en ensayos batch. Fe(II) mejoró la remoción de nitrato, mientras que el Ni(II) afectó la reducción de NO_3^-, NO_2^- y N_2O. Cr(III) inhibió la etapa de reducción de nitrato. La adición continua de metales en el ASFMBR disminuyó el efecto negativo de Ni(II) en el proceso desnitrificante. Fe(II) estimuló el proceso mediante desnitrificación autotrófica mientras que la ruptura del complejo de Cr(III)-citrato fue difícil. La novedosa configuración del reactor logró una alta remoción de nitrato (>94 %) con escasa acumulación de intermediarios (nitrito y N_2O) para ambas fuentes de electrones experimentadas. Además, el pH ácido alimentado al reactor fue neutralizado por la recirculación de la alcalinidad producida por el proceso desnitrificante. Las estrategias operacionales permitieron una recuperación arriba del 40% de los metales en la columna de precipitación y una recuperación mayor al 90% dentro del ASFMBR. El taponamiento de las membranas se evitó por el régimen hidrodinámico impuesto en el reactor y la fluidización del CG. El concepto de tratamiento promete lograr una eliminación eficiente del nitrato, así como una alta recuperación de metales, al tiempo que se preserva el taponamiento de la membrana debido a las condiciones hidrodinámicas que prevalecen dentro del ASFMBR. Este concepto de tratamiento también podría aplicarse a otros procesos anaeróbicos, como la metanogénesis y la reducción de sulfato requeridos para el tratamiento de efluentes industriales.

1. General introduction

1.1 Pickling and passivation effluent

Pickling of stainless-steel is a chemical operation that is performed by immersion of the metal in acidic baths to remove the layer of metallic oxides formed on the stainless-steel surface, which promotes a chromium enrichment of the passive surface [1]. Two principal baths are used with this purpose: (a) nitric acid + hydrofluoric acid [2] and (b) sulfuric acid + oxygen water [3]. During metallic passivity, the active state in concentrated nitric acid solution suddenly turns into a passive state where almost no corrosion is observed, forming an oxide film of several nanometers thick on the surface of passivated metals [4,5]. Because inherent characteristics of oxidizing and reducing acids, mixture of nitric and hydrofluoric acid is the most frequently used solution for pickling stainless steel parts. Nitric acid is oxidizing in character, whereas hydrofluoric acid is reducing. Nitric acid tends to promote and preserve the corrosion-resistant qualities (passivity) of stainless steel, while hydrofluoric acid reduces the oxides over the metal. At the same time, it reduces the protective oxide film on stainless steel [6].

Metallic iron in the passive state dissolves in the form of hydrated ferric ions, indicating that the passive film is ferric oxide, Fe_2O_3 [4].

$$2Fe + 3H_2O \rightarrow Fe_2O_3 + 6H^+_{(aq)} \text{ passive film formation (1.1)}$$

$$Fe_2O_3 + 6H^+_{(aq)} \rightarrow 2Fe^{3+}_{(aq)} + 3H_2O \text{ passive film dissolution (1.2)}$$

Nickel dissolution produces divalent nickel ions, implying that the passive film is divalent nickel oxide.

$$Ni + H_2O \rightarrow NiO + 2H^+_{(aq)} \text{ passive film formation (1.3)}$$

$$NiO + 2H^+_{(aq)} \rightarrow Ni^{2+}_{(aq)} + H_2O \text{ passive film dissolution (1.4)}$$

For chromium, the anodic dissolution produces divalent chromium ions in the active state and the passivation occurs forming an extremely thin, trivalent chromium oxide film on the metal surface.

$$2Cr + 3H_2O \rightarrow Cr_2O_3 + 6H^+_{(aq)} \text{ passive film formation (1.5)}$$

$$Cr_2O_3 + 6H^+_{(aq)} \rightarrow 2Cr^{3+}_{(aq)} + 3H_2O \text{ passive film dissolution (1.6)}$$

Then, the main species of Fe, Cr and Ni found in solution are present as ferric iron Fe(III), Ni(II) and Cr(III) [2]. During the pickling operation, the acidic baths are consumed while the metals are dissolved. Prevailing iron followed by chromium and nickel. In consequence, the spent acidic baths are periodically changed by fresh acids [3].

Organic acid chelates can be used to clean light oxides or scales and free iron particles from stainless steel surface. The complex formed remove a variety of metallic ions that would otherwise adversely affect the corrosion resistance of the alloy. The organic compounds combine acid solution activity with sequestrant and buffering properties. This type of treatment is used as a final cleaning step for fabrications for the food and chemical industries [6]. Citric acid is a commonly used acid, which is cheap and safe as compared with other compounds. The concentration used in the pickling process is between 2–10 % (wt) [7].

1.2 Environmental risk and legislation of the discharge

The discharge of stainless-steel effluents without previous treatment can generate a huge environmental damage by the high nitrate content, presence of fluoride, acidic pH and a high concentration of metals. Furthermore, citric acid, which is commonly present in this wastewater, increases metals mobility. Nitrate concentration of metallurgic effluents could be between 500 to 1000 mg $N\text{-}NO_3^-$/L [8,9]. For the present work, two samples of wastewater generated from stainless-steel industry were analyzed. For a factory which produces stainless-steel containers for the food industry, the wastewater contained ~500 mg $N\text{-}NO_3^-$/L and ~1656 mg citrate/L with

a pH of 3.17. Moreover, for stainless-steel pipe factory, it was found an extreme nitrate concentration with a range of 6.9-19.6 g N-NO_3^-/L without organic matter content, and a pH between 1.67 and 3.34. The concentrations of the main metals present in the first effluent were 133.2, 47.9 and 30.3 mg/L, for Fe, Cr and Ni, respectively. For the effluent from the stainless-steel pipe factory, the concentrations were in a range of 12.5-33.5 g Fe/L, 2.9-9.5 g Cr/L and 2.2-10.8 g Ni/L. The permissible discharge according to Mexican regulation stablishes a maximum concentration ≤35 mg Total-N/L with a range of pH between 6.5 and 8.5 [10]. European legislation establishes a limit between 10 and 15 mg Total-N/L in the most sensitive areas of discharge [11]. For metals, they must be discharged according to the following concentrations: Cu ≤ 6 mg/L, Cr ≤ 1.5 mg/L, Ni ≤ 4 mg/L, Pb ≤ 0.4 mg/L, Zn ≤ 20mg/L [10]. In addition, a problem with the presence of the citrate as chelating agent of metals is that the wastewater treatment hardly degrades this compound, increasing metals mobility, which implies that metals can be transported through the wastewater treatment system to the discharge. Therefore, the characteristics of the effluents are extremely distant from the limits indicated by legislation.

1.2.1 Nitrate

The discharge of nitrogenous compounds may cause an important accumulation in groundwater and surface water sources, which excess results into eutrophication of these reservoirs [12]. Large concentrations of nitrate cause cyanobacterial and algal blooms, as well as problems of reduced water clarity, taste, odor, and cyanotoxins in drinking water, which diminish water quality and ecosystem services [13]. Human health can be affected by nitrate and nitrite in food causing methemoglobinemia in babies. Other health risks include oral and gastrointestinal cancer [14].

1.2.2 Metals

Metals are of nutritional significance to humans. These can be essential elements, elements which are probably essential, and potentially toxic elements, some of which may nevertheless have some essential functions at low levels. Some essential nutrients are cobalt, copper, chromium, iron, magnesium, manganese, molybdenum, nickel, selenium and zinc. These are required for various biochemical and physiological functions. Inadequate supply of these micro-nutrients results in a variety of deficiency diseases or syndromes to human health [15]. However, an excess amount of such metals produces cellular and tissue damage leading to a variety of adverse effects and human diseases [16].

The essential heavy metals exert biochemical and physiological functions. They are important constituents of several key enzymes and play important roles in various oxidation-reduction reactions. On the other hand, their bioavailability can be influenced by both physical, chemical and biological factors. Physical factors include temperature, phase association, adsorption and sequestration. Moreover, chemical factors influence speciation at thermodynamic equilibrium, complexation kinetics, lipid solubility and octanol/water partition coefficients. Biological factors, such as species characteristics, trophic interactions, and biochemical/physiological adaptation, also play an important role [16]. For biological systems, some heavy metals serve as cofactors in several enzymes [17]. However, heavy metals have also been reported to affect cellular organelles and components, such as cell membrane, mitochondrial, lysosome, endoplasmic reticulum, nuclei, and some enzymes involved in metabolism, detoxification, and damage repair, as well as interacting with cell components, such as DNA and nuclear proteins, causing DNA damage and conformational changes that may lead to cell cycle modulation, carcinogenesis or apoptosis [16].

Unlike organic contaminants, heavy metals are not biodegradable and tend to accumulate in living organisms. Toxic heavy metals of concern in the treatment of industrial wastewaters include zinc, copper, nickel, mercury, cadmium, lead and

chromium. Nickel might bring about serious lung and kidney problems aside from gastrointestinal distress, pulmonary fibrosis and skin dermatitis, and may cause cancer in humans. For chromium, Cr(VI) is more toxic than Cr(III). Cr(VI) affects human physiology, accumulates in the food chain and causes severe health problems ranging from simple skin irritation to lung carcinoma [16]. Cr(III) is relatively insoluble and considerably less toxic, environmental friendly and safe, and may be economical as well [18]. Beyond complying with environmental regulations, heavy metals are environmental priority pollutants and are becoming one of the most serious environmental problems. Thus, these toxic heavy metals should be removed from the wastewater to protect people and the environment [19].

1.2.3 Citric acid and heavy metals

Citric acid is a multidentate chelating agent, which forms stable complexes with metal ions. A chelating agent forms multiple bonds with metal ions. These bonds essentially form a ring in which the metal ion is held, so that it is not free to form an insoluble salt [20]. The chemistry of citrate is complex with a variety of different binding modes reported due to the four ionizable groups (Fig. 1.1). Binding of metal ions can occur at four sites: namely through the three carboxylate groups (pKa_1=3.13, pKa_2=4.76, pKa_3=6.40) and the hydroxyl group (pK_4~11), although the stability constants are sensitive to the medium [21,22]. The structural chemistry of the metal citrate is quite complex with bidentate complexes binding through dicarboxy, bidentate complexes involving the hydroxy group, and tridentate complexes [22]. Numerous studies have been performed to reveal the chemistry between citrate and metals with different purposes, such as Fe(II)-Fe(III) [23–27], Cr(III) [25,28], Ni(II) [29–33], Sn(II) [34], Sn(IV) [35], Ca(II) [36,37], Cu(II) [24,30,31], Co(II) [31,32,36], Mn(II) [31,32], Mo(VI) [38], Ce(III) [31], Al(III) [39], Pb(II) [22], Zn(II) [32], Mg(II) [36,37], Sr(II) [36], Ba(II) [36], Cd(II) [36], Na [37], K [37], V [40]. Also, the study of the existence of mixed complexes formed between Cu(II)-citrate and other divalent cations has been reported [41]. The use of software has been implemented

as a technique to predict the chemical speciation, such as MINEQL+, visual MINTEQ and Make Equilibrium Diagrams Using Sophisticated Algorithms (MEDUSA), giving information about the chemical equilibrium reactions of the species formed.

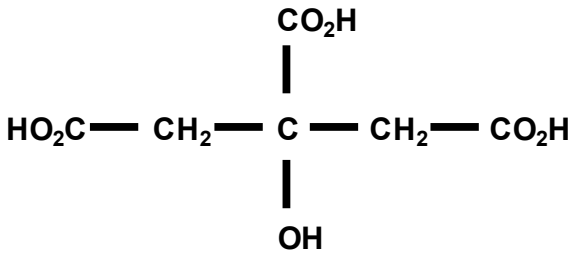

Figure 1.1Citric acid

1.3 Treatment of stainless-steel effluent

The usual treatment of the stainless-steel effluent is carried out by neutralization and slurry disposal, but it produces large volume of sludge with residual nitrogenous species in the liquid phase. Additional treatments include retention of acids by resins, dialysis, electrodialysis, and evaporation. These treatments have difficulties by the residues generated and the operational conditions, as well as high costs [3]. Other range of treatment technologies can be applied to remove the metals, such as chemical precipitation, coagulation-flocculation, flotation, ion exchange and membrane filtration, being the most frequently studied ion-exchange, adsorption and membrane filtration. The last can remove heavy metals ions with high efficiency [19]. Physical and chemical methods are suitable for removing low levels of nitrate. On the other hand, denitrification converts nitrate into dinitrogen gas in a cost-effective process [42], and can be adapted to remove high concentrations of nitrate from wastewater [9,43]. Some studies have applied denitrification combined with metals precipitation. Generally, $Ca(OH)_2$ is used to remove fluoride and metals in the form of sludge, thus obtaining treated wastewater which still contains high nitrate concentrations as well as dissolved calcium. Denitrification performed in a sequential batch reactor (SBR) showed a negative effect of Ca on the process and the

requirement to add an external electron source to support denitrification, while fluoride ions did not cause inhibition [8].

1.3.1 Denitrification applied to the stainless-steel effluent treatment

1.3.1.1 Denitrification process

Denitrification is an important process of the global nitrogen cycle sustained by bacteria. Nitrate reduction consists of four consecutive reduction steps by specific enzymes concomitant to the oxidation of an electron donor. These enzymatic steps include nitrate (NO_3^-) reduction to nitrite (NO_2^-) by *nitrate reductase* (Nar), nitrite to nitric oxide (NO) by *nitrite reductase* (Nir) and NO to nitrous oxide (N_2O) by *nitric oxide reductase* , and finally, N_2O to nitrogen gas (N_2) by *nitrous oxide reductase* [44]. Denitrification is part of the bioenergetic apparatus of the bacteria cell, where the N oxyanions, nitrate and nitrite, and the gaseous N oxides, NO and N_2O, serve as terminal acceptors for electron transport phosphorylation [44]. An important issue in wastewater denitrification is the accumulation of N-oxide intermediates (NO_2^-, NO and N_2O). Among these, NO_2^- and N_2O are the main intermediates, since NO is not a major product in denitrification [45,46]. N_2O is a powerful greenhouse gas, with a global warming potential of around 300 times that of CO_2 and with a life-cycle of 114 years, so that its emission has a long-term influence on climate [47]. Ammonium can also be accumulated by means of dissimilatory nitrate reduction to ammonium [44].

The oxidation of an electron donor can be either organic (organotrophic denitrification) or inorganic (lithotrophic denitrification) source. Organotrophic denitrification is a biological process where organic matter oxidation is coupled to N oxide reduction. For this case, the electron donor can also act as a carbon source and it is called organo-heterotrophic denitrification. Numerous organic compounds have been tested as electron donors, such as methanol, acetate, ethanol, lactate, glucose, glycerol, succinic acid, formic acid, among others [48,49]. Regarding lithotrophic denitrification, the oxidation of an inorganic source is coupled to N oxide

reduction [44]. Some electron donors used in lithotrophic denitrification are sulfide (S^{2-}), sulfur (S^0) and thiosulfate ($S_2O_3^{2-}$) [48]. For industrial wastewaters, the organic content is commonly low, thus it is necessary to add an external electron donor. Organic electron donors are commonly used since they are easily available. Taking in consideration the possible presence of citrate in stainless-steel effluents, its use as electron donor is an option for the treatment of this type of effluents. However, scarce information about the use of citrate as electron donor in denitrification is available. Additionally, the interaction between metals and citrate should be considered since the stability of the complexes formed can affect denitrification.

The pH is another factor affecting the respiratory process of denitrification. Enzymes are dependent of the pH, which can either inhibit or improve the process. The pH has influence on the mechanisms of transport affecting the consumption efficiency and rate due to changes in the physical-chemical properties of lipids and proteins of the cell membrane. A good performance is achieved in the range of 7-8.5 where the metabolic changes are tolerable [48].

1.3.1.2 Metals and metal-citrate effects on denitrification

The presence of heavy metals can stimulate or inhibit the microbial activity of denitrifying bacteria. Supply of trace concentrations of metals can enhance metabolic degradation, while at certain concentration, they can suppress the microbial activity [50]. However, microorganisms have developed mechanisms to tolerate the presence of heavy metals, such as efflux of metal ions outside the cell, complexation of metal ions inside the cell, reduction of metal ions to a less toxic state or their use as terminal electron acceptors in anaerobic respiration [51,52]. However, at higher concentrations, metals can change the microbial enzyme conformation and block essential functional groups [53]. In denitrification, inhibition by metals of the enzymes responsible for the nitrogen species reduction can cause the accumulation of denitrification intermediates. Addition of Ni has caused accumulation of both nitrate and nitrite in denitrifying FBR [54]. In batch assays, Cu has been reported to

decrease nitrate removal rate and NO_2^- accumulation, whereas a deficient concentration could increase N_2O production [55,56]. Likewise, long term-acclimation to Cu in continuous-flow tests can decrease its inhibition in comparison with short-term tests [57]. Co also causes nitrite accumulation in batch assays [58]. High Ca concentration decreases microbial growth and denitrification rates in a Sequential Batch Reactor (SBR) [8]. However, the presence of Fe(II) could contribute to nitrate reduction by autotrophic denitrification. Electrons derived from the oxidation of Fe(II) to Fe(III) are transferred to nitrate for denitrification. This process is relevant for the treatment of industrial wastewaters since they lack enough organic electron donors to stimulate heterotrophic denitrification. This process can be enhanced by the supply of organic electron donors since many Fe(II)-oxidizing denitrifying microorganisms can grow under mixotrophic conditions. Better denitrification performance occurred at neutral pH in comparison with that observed at low pH values. The presence of other metals could also affect Fe(II) oxidation [59–61].

Considering the biological importance of the metal-citrate system, the chemistry of the complex has influence on the denitrification process. The experimental conditions, such as stoichiometry, pH, as well as other ligands or bases, lead to different species, which modify the form of citrate in solutions [21], and thus the effect of metal on denitrifying microorganisms. Likewise, citric acid oxidation changes the concentration of the species formed. On the other hand, citric acid might result in the transformation of higher toxic forms of metals into lower toxic forms, reducing the toxicity of some metals [62]. Some works report the degradation of ferrous and ferric iron-citrate complexes [23], Fe(III)- and Ni-citrate complexes [63] and mix-metal-citrate-complexes of Fe-U-citric acid [64] by *Pseudomonas fluorescens* under aerobic conditions, in which the characteristics of the complex formed between the metal and citric acid play an important role in determining its biodegradability. Under similar conditions, other study reports the improvement of metal removal from the medium by the incorporation of inorganic phosphate as a precipitant, with formation of nickel and cobalt phosphates confirmed by X-ray powder diffraction analysis [65].

However, studies reporting the degradation of citrate coupled to metals under denitrifying conditions are scarce.

1.3.1.3 Denitrification coupled to metals bio-recovery

Precipitation is a physical-chemical process, in which the addition of a precipitation agent converts soluble metals into relatively insoluble species and inorganic salts. Some aspects are needed to obtain a successful precipitation, such as the maintenance of a proper pH range during the reaction time and subsequent settling time, as well as the addition of a suitable precipitating agent. Hydroxide precipitation effectively removes cadmium, Cr(III), copper, iron, manganese, nickel, lead, and zinc. Sulfide precipitation effectively removes cadmium, Cr(VI), cobalt, copper, iron, mercury, manganese, nickel, silver, tin, and zinc. Carbonate precipitation effectively removes nickel, cadmium, lead and zinc [20]. The solubility-product constant (K_{sp}) represents the product of the maximum ions concentration that can have under equilibrium conditions for a given temperature. When the product of the molar concentration of the ions is lower than the solubility-product constant, the species will be dissolved, and it is called unsaturated solution. In a supersaturated solution, the product of the molar concentration of the ions is greater than the solubility-product constant. In this case, if internal forces allow the formation of crystal nuclei, the precipitation will occur [20]. Therefore, supersaturated conditions are needed so that precipitation take place. The presence of complexing agents can prevent the removal of heavy metals by conventional treatment processes. Complex formation is determined by factors, such as pH, complex stability constants, and concentration of participating species. Citrate affects the extent of metal precipitation due to the competition between the formation of the metal insoluble species and the metal complexes. Precipitation could be improved by coprecipitation, occurring when metal is adsorbed onto the precipitate of target metals. Another strategy is the oxidation (e.g. Fe(II) to Fe(III)) or reduction (e.g. Cr(VI) to Cr(III)) to change the oxidation state to more precipitable species [20].

The kinetics and the free energy change of the process depends on the chemical structure of citrate or other organic compounds used as electron donor [48]. Nevertheless, the use of organic electron donors produce alkalinity that increase the pH. Production of alkalinity by microorganisms promote precipitation of minerals by changing the chemical conditions, which modify the saturation index (SI) with respect to the produced minerals, as well as provide mineral nucleation sites. Bacterial surfaces also provide nucleation sites for precipitation and crystalline growth by lowering the activation energy (i.e., supersaturation) required for biomineralization. This interaction occurs by the positively charged ions (e.g. Ca(II), Mg(II)) Fe(III) linked to negatively charged surface groups. Extracellular polymeric substances (EPS), which is secreted by microorganisms, also promote metals precipitation [66]. Denitrifying metabolism carried out by *Pseudomonas stutzeri* was found to promote biomineralization under pH and alkalinity conditions, which was not observed with nonmetabolizing bacteria [66]. Autotrophic denitrification also promotes Fe(III) precipitation, in which the bio-oxidation of Fe(II) to Fe(III) is followed by the bio-precipitation/bio-recovery of Fe(III) (hydr)oxides with possible co-precipitation or adsorption with other metals [59,61,67].

1.4 Bioreactor configurations

1.4.1 Fluidized bed bioreactor (FBR)

Fluidized bed bioreactors are characterized by two-phase mixture of fluid and solid, in which the bed of solid particles is fluidized by means of downward or upward recirculation stream (Fig. 1.2). FBRs are widely used for multiple environmental engineering solutions, such as wastewater treatment, as well as some industrial applications. FBR offers many benefits, such as compact bioreactor size due to short hydraulic retention time, long biomass retention on the carrier, high conversion rates due to fully mixed conditions and consequently high mass transfer rates, no channeling of flow, dilution of influent concentrations due to recycle flow, suitability for enrichment of microbes and reduced toxic effects via solution recycling [68]. Due

to the negative effects on denitrification caused by acidic pH and high metals concentration, the characteristics of the FBR allow to neutralize the pH by the alkalinity produced by microbial metabolism and the recycled flow, which dilutes influent concentrations and acidity. Application of FBR in denitrification, including wastewater with heavy metals, has been reported through a denitrifying biofilm supported on granular activated carbon (GAC). Inhibitory effects of heavy metals have been decreased by high dilution rates established inside of the reactors and by pH neutralization of the acidic feed with denitrification by-products; in addition to the precipitation of a fraction of heavy metals with the medium composition [58,69]. Despite the high nitrate removal and pH neutralization obtained, heavy metals precipitation is low, offering an effluent with high content of metals [54]. Other disadvantages of FBRs include bioreactor size limitations due to the height-to-diameter ratio, high energy requirements due to high recycle ratios, and long start-up periods for biofilm formation. However, this technology has many potential new uses, as well as hydrodynamic characteristics, which enable environmental and industrial applications [68].

1.4.2 Anaerobic membrane bioreactor (MBR)

Membrane bioreactor combines the biological removal of organic substances and nutrients, followed by solids-water separation with a membrane module. The use of membranes has different tasks, such as separation, selective extraction of compounds, retention of a biocatalyst, distribution/dosing of a reactant and as biocatalysts support, as well as a combination of them [70]. MBR has been widely studied and applied for the treatment of domestic wastewater and the application on industrial wastewater treatment is of growing interest [71]. Lately, the confidence in the use of MBR for industrial applications is increasing, even when several challenges remain [72]. The nature of MBR process allows efficient biological treatment of contaminants for the high solids retention time (SRT) and low hydraulic retention time (HRT) [73]. Additionally, high removal of organic and inorganic

compounds, as well as microorganisms, are accomplished through physical filtration [72,74], which allows the compliance of environmental regulations and the possibility of water reuse [71,75]. Microfiltration in membrane bioreactors has emerged offering high retention of cells and solids, thus high quality of treated water to be reused. Despite the benefits mentioned, membrane fouling is an inevitable phenomenon occurring by diverse mechanisms at internal or external membrane locations [75]. Fouling reduces permeate productivity and frequent implementation of antifouling techniques or cleaning and replacement of membranes demand time, energy and operational costs [76]. Consequently, great interest on fouling characterizations and control has been taken during the last years [77]. Application of MBR in domestic wastewater has revealed that heavy metals can be joined to sludge components and be rejected by membranes [78]. However, negative effects, such as affectation to the biological process, change in the sludge characteristics, and inorganic fouling by the precipitation or incrustation on the membrane surface have also been observed [79,80]. In industrial wastewater, using Osmotic Membrane Bioreactor (OMBR) for nutrients removal resulted in poor sludge characteristics, treatment performance and intense membrane fouling with the addition of more than 5 mg/L of chromium and more than 2 mg/L of lead [81].

1.4.3 Anaerobic Fluidized Membrane bioreactor (AFMBR)

Membrane fouling in MBRs is often simultaneously caused by more than one mechanism, categorized in simplistic form as internal fouling and external fouling. The internal fouling is caused of dissolved matter adsorption into the membrane pores and pore blocking, whereas the external fouling occurs by biosolids deposition onto it, forming the cake layer on membrane surface. Internal and external fouling produce irreversible and reversible fouling, respectively. In most cases, external fouling could be removed with an appropriate physical washing and internal fouling through chemical cleaning. Both phenomena are considered to occur by physicochemical interactions between the bulk phase compounds and the

membrane material [76,82]. The cake layer formation is considered as one of the main mechanisms of fouling in anaerobic membrane bioreactors [83–85]. Total suspended solids (TSS) and soluble microbial products (SMP), are usually assumed to be the major factors responsible for fouling in MBRs [86–88]. The development and implementation of strategies anti-fouling must include both the less energy consumption and environment friendly. Usually, membrane cleaning consists of backwashing and chemical cleaning [76]. However, several fouling control strategies have emerged to take care of fouling, such as aeration scouring, biological control, electrically-assisted, and nanomaterials-based membranes [77]. Gas scouring has been widely adopted as a strategy antifouling; however, this comprises the fraction of operational costs [89,90]. Recently, fluidization of scouring agents in MBR has resulted in a technique with lower energy requirements in comparison with cross flow systems and gas sparging techniques used in typical operating conditions [91–94]. Particle fluidization is an unsteady-state shear means energetically efficient in which particle solids are dispersed and suspended according to the liquid phase movement. The presence of particles enhances the shear stress at the membrane surface and prevents deposition of solutes and foulants, preventing membrane fouling [92]. Through media fluidization, scouring agents cross the boundary layer and hit the membrane surface removing and/or avoiding the cake layer formation on the membrane [75,91,95,96]; hydrodynamic turbulences or air bubbles hardly reach the membrane surface [94]. On the other hand, particle fluidization near the membrane improve back-transport of solutes in the polarization layer [97,98] and across the boundary layer.

Kim et al., 2011 developed the concept of particle fluidization using GAC as scouring agent in an anaerobic fluidized bed membrane bioreactor (Fig. 1.2). GAC was additionally used as supporting material anaerobic biofilm. Bulk recirculation suspends the media to produce a mechanical cleaning of membrane surfaces through physical contact and movement of GAC. In addition, the use of GAC prevents cake layer formation by its capacity of organic matter adsorption [95,100,101]. Several investigations have evaluated the effect of different aspects on membrane fouling control with the aim to understand and optimize an effective

control antifouling with low energy requirement, evaluating factors, such as size of media, carrier dosage, adsorbing media capacity and process configuration [96,101–103]. AFMBR has even been tested at pilot scale [104]. However, the scouring agent for mechanical cleaning of membrane can affect membrane integrity [105]. Thus, it is critical to achieve membrane cleaning effectively without potential decrease in membrane life time.

An important factor, which affects the mechanical cleaning of membranes is the hydrodynamic regime of multiphase flow systems, such as AFMBR, which depends on several parameters, such as the geometry of the reactor, diffuser/distributor, membrane module configuration, media characteristics (size, shape, density, dosage), as well as bulk medium characteristics. All these aspects will affect the mechanical cleaning response. The appropriate use of fluid instabilities, which could be produced by the geometry of the reactor and membrane configurations could be factors that improve the performance of membrane filtration [106]. Reactor design is highly relevant because particles distribution along the membranes depends on flow circulation. Cylindrical configuration allows better mixing than parallelepiped rectangle reactor design, which are commonly used geometries. Bad reactor design could be reflected in dead zones of flow and the media could be trapped both in the reactor and through the membranes [94]. Another relevant element to design and optimize is the diffuser/distributor, which determines the distribution of flow and scouring agents in the reactor. The flow field in FBR is predominantly in one direction, induced by an upward flow and tends to be non-uniform vertically and laterally, which could be reflected in a non-uniform control of fouling [107]. In experiments with GAC as scouring media in AFMBR, the distributor consists of nozzles directed downwards in an inverted-V configuration and spread evenly along a central pipe traversing the reactor bottom [101,104,108,109]. In gas sparging systems, the modification of the sparger could increase liquid velocity [110], and a homogeneous shear stress could be obtained with the rotation of the nozzle aperture [111]. Therefore, in solid media fluidization, the diffuser in reactor design needs to be considered to achieve optimal performance of mechanical cleaning [94]. In addition, the movement of scouring agents inside the reactor depends on the

membrane module design. Most experimentation has been conducted in membrane modules with hollow fiber and flat-sheet membranes. The last allows a better movement of the scouring media to membrane surface, whereas systems with a bundle hollow fiber membrane can significantly restrict the accessibility inside of fiber bundles by the narrow space among the membranes. Few studies have been performed with spacing between hollow fiber membranes, surface shear forces were observed to be higher for the wide module spacing than narrow module spacing in sparging gas systems [112] and in solid fluidization [96]. Proper spacing allows good contact of liquid and scouring media with the membrane surface, facilitating homogeneous shear forces distribution along the membrane [94].

Recently, some reports have been focused on hydrodynamic aspects in AFMBR with the aim to understand the associated characteristics of fluidized GAC particles throughout the membranes. Wang et al., 2016b determined, through accelerometer signal response, that solid phase dynamics correlated well with the extent of fouling mitigation in a filtration test. In another work, the use of image analysis via high-speed video camera technique, to characterize GAC particle velocity and concentrations, revealed that momentum transfer between the GAC particles and membrane represents a key mechanism effecting the scouring to diminish membrane fouling [108]. Cahyadi et al., 2017 implemented computational fluid dynamics (CFD) to report negative correlations (improved fouling control) between fouling rate versus particle momentum and water shear stress. Notably, reactor design and membrane configuration dictated dynamics of the scouring media particles, which is closely related to the effectiveness of fouling mitigation. Membrane modules and reactor geometry must allow the movement of particles without blockages throughout the system [92,112], with the objective of achieving an efficient use of the energy between the expenditure for the particle fluidization and an effective scouring [77,92]. However, manipulation of hydrodynamic conditions around membrane surface to avoid the membrane fouling has not been explored, becoming an important area of research [74].

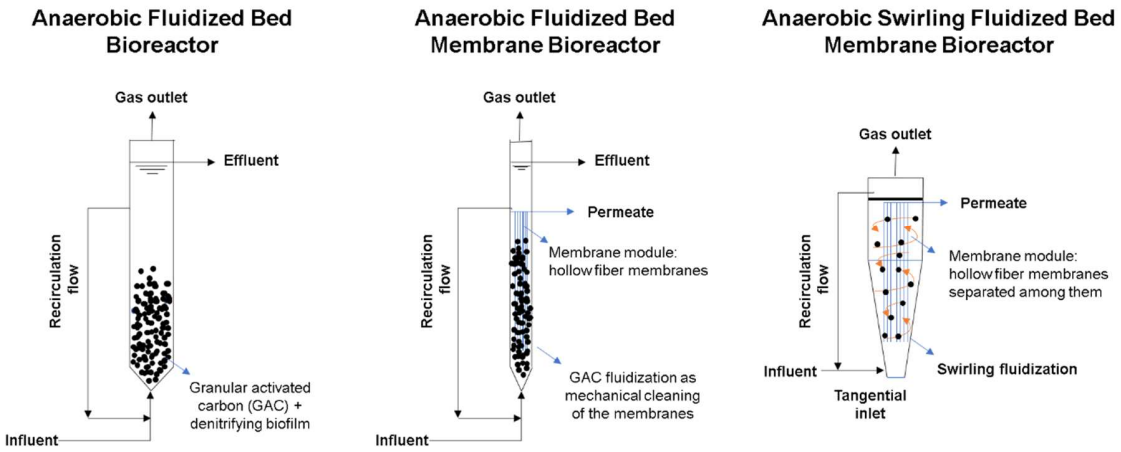

Figure 1.2. Schematic diagrams of FBR, AFMBR and ASFMBR.

1.5 Research needs and outline of this thesis

1.5.1 Significance of the study

The treatment of stainless-steel effluents is necessary to fulfil environmental regulations. Treatment of this industrial effluent has the challenge to remove high nitrate concentration, neutralize the acidic pH, in addition to metals precipitation. The presence of citrate in this type of effluents challenges the treatment due to the metals-complexes formed. Denitrification is a cost-effective technique in which an electron donor is demanded to carry out nitrate reduction. Citrate could be a suitable electron donor for denitrification. However, scarce information is available on the use of citrate as electron donor for denitrification, and on the effects of metals-citrate complexes on denitrification. In addition, the use of a suitable reactor for the treatment of metallurgical effluents is required to remove its high content of nitrate, neutralize the acidic pH and achieve metals recovery. The study of the treatment of the stainless-steel industry effluent are involved in three main aspects:

1) The use of citrate as electron donor to carry out denitrification process. For metal-citrate complexes, citrate limitation and decrease of denitrification inhibition by metals presence can occur.

2) The use of a novel Anaerobic Fluidized Membrane Bed Bioreactor with Swirling Fluidization can serve to remove the nitrate and neutralize the acidic pH from the metallurgical wastewater, while the swirling fluidization of granular carbon preserves the membrane filtration.
3) The characteristics of the novel Anaerobic Fluidized Membrane Bed Bioreactor with Swirling Fluidization can serve to reduce the negative metal effect on denitrifying microorganisms and achieve metal bio-recovery, while the granular carbon fluidization preserves the membrane filtration for the treatment of synthetic and real metallurgical wastewater. The treatment concept also is integrated by a preliminary precipitation column that can serve as a unit of precipitation and recovery of metals.

1.5.2 Scope and outline of thesis

The objective of this dissertation is to evaluate the denitrification of metallurgical wastewater through a Novel Anaerobic Swirling Fluidized Bioreactor. The study is divided in three phases: (i) evaluate the effects of the most abundant metals in the stainless-steel effluent (Fe, Cr and Ni) at different concentrations and pHs, (ii) evaluate de denitrification, pH neutralization and membrane fouling mitigation through the design, construction, and test of a novel Anaerobic Swirling Fluidized Bed Membrane Bioreactor (ASFMBR) and (iii) evaluate de denitrification and metal bio-recovery for the treatment of synthetic and real metallurgic wastewaters through an ASFMBR, including a previous precipitation column.

In Chapter 2, three different heavy metals concentrations of Fe, Cr, and Ni at two initial pH values (6 and 7) were evaluated through denitrifying batch assays on the N_2 production rate and intermediates accumulation (nitrite and N_2O). This for single and multi-metal assays, using citrate and ethanol as electron donors. The results were linked to speciation analysis and minerals precipitated during the denitrifying process. For Chapter 3, the denitrification and filtration performance of a novel ASFMBR was evaluated for the treatment of synthetic metallurgic wastewater absent

of metals. Neutralization, nitrate removal and intermediates production (nitrite and N_2O), as well as granular carbon fluidization on fouling mitigation capacity, is discussed. Hydrodynamic characterization through experimental and numerical results of the ASFMBR and its relation to membrane fouling mitigation also is presented. The treatment of synthetic and real metallurgical wastewater was achieved through the ASFMBR and its described in Chapter 4. Two external electron donors (ethanol and citrate) was tested to simulate real treatment. The denitrification and filtration performance, as well as the fate and characterization of the metals during the treatment is presented. The last Chapter includes discussion about relevant results obtained during the batch assays and ASFMBR performance, likewise, a recommendation for the future studies to obtain an optimized treatment system. Furthermore, the comparison of the accomplished of the treatment with Mexican normative is commented.

2. Denitrification of metallurgic wastewater: mechanism of inhibition by Fe, Cr and Ni

2.1 Abstract

Metallurgic wastewaters are acidic effluents containing large amounts of nitrate and heavy metals. Citric acid is one of the acids used by this industry and forms stable complexes with metal ions. The aim of this study was to elucidate the chemical aspects driving inhibitory or stimulatory effects of heavy metals on denitrifying processes, based on speciation analysis and monitoring key denitrification intermediates (nitrite and N_2O). Denitrifying sludge incubations were conducted with iron, chromium and nickel, in single and multi-metal assays, using citrate and ethanol as electron donors. Ferric-citrate complex, $[Fe\text{-}cit]_{(aq)}$, was readily consumed, while complexes of divalent metals, $[Fe\text{-}cit]^-$ and $[Ni\text{-}cit_2]^{4-}$, remained very stable affecting denitrification. Nitrate reduction was affected by Ni(II), while nitrite and N_2O accumulation was observed with $NiCO_3$ and $Ni(OH)_2$ oversaturation. $[Cr\text{-}cit_2]^{4-}$ resulted in overall denitrification inhibition, while species of $[Cr\text{-}cit]^{2-}$ caused denitrification stimulation. Fe and Cr inhibited the overall denitrification process, while Ni caused accumulation of intermediates. Synergistic inhibition imposed by multi-metal systems revealed lower inhibitory effects as compared to those observed by the sum of individual effects of metals. This study elucidates chemical aspects determining the effects of heavy metals on denitrification, which is relevant to develop efficient biological processes for metallurgic effluents.

This Chapter has been published as:

J.E. Ramírez, J.R. Rangel-Mendez, L. Lopes, S.D. Gomes, G. Buitrón, F.J. Cervantes, Denitrification of metallurgic wastewater: mechanisms of inhibition by Fe, Cr and Ni, J. Chem. Technol. Biotechnol. 93 (2017) 440–449. doi:10.1002/jctb.5374.

2.2 Introduction

Effluents from the stainless-steel pickling and passivation processes are highly acidic and contain large amounts of nitrate and heavy metals. Predominant metals in these industrial wastewaters are iron, chromium and nickel [3,8,9]. Contamination of both surface and ground water with nitrate is a current menace causing serious environmental and public health problems. Nitrogen-containing compounds released into environment can promote eutrophication of rivers due to excess nutrients [113–115]. In the case of heavy metals, their toxicity to plants and animals is well known. One important feature is the non-biodegradability of heavy metals, and having entered the environment, their potential toxicity is controlled to a great extent by biological and geochemical factors [116]. Therefore, metallurgic effluents containing these pollutants must be properly treated prior their discharge to the environment.

Processes used for treating nitrate-rich wastewaters include reverse osmosis, ion exchange, catalysis and denitrification. Wastewater generated in the stainless-steel pickling process are commonly pretreated through a precipitation process (generally with $Ca(OH)_2$) to remove fluorides and metals in the form of sludge, thus obtaining treated wastewater still containing high nitrate concentrations (between 500 and 1000 mg $N\text{-}NO_3^-/L$) as well as dissolved calcium as a consequence of the aforementioned treatment [8,9].

Biological treatment systems have emerged as suitable technologies to remove nitrogen from wastewaters, which have been shown to be efficient and economical compared to physical-chemical treatment processes [117]. Denitrification reduces nitrate to nitrogen gas by four sequential stages in accordance with the following sequence: $NO_3^- \rightarrow NO_2^- \rightarrow NO \rightarrow N_2O \rightarrow N_2$. Each of these steps is regulated by different enzymes, which are controlled by several parameters. The presence of inhibitors, such as heavy metals, may cause accumulation of undesirable intermediates: NO_2^-, NO and N_2O. Among these, the main intermediates are NO_2^- and N_2O, since NO is not a major product in denitrification [45,46,56,118]. Ammonium can also be accumulated by means of dissimilatory nitrate reduction to

ammonium. In addition to the environmental problems generated by these nitrogenous compounds, they have the potential to increase risks of methaemoglobinaemia and cancer [114,115]. N_2O is a powerful greenhouse gas, with a global warming potential of around 300 times that of CO_2 and with a life-cycle of 114 years, so that its emission has a long-term influence on climate [47].

In general, effluents derived from the metallurgic industry do not contain a carbon source; however, stainless steels intended for the food and chemical industries require an extra treatment involving citric acid [6,119], which is a multidentate chelating agent that forms complexes with metal ions [23]. The biodegradability of these complexes depends on many factors, such as the nature of the complex, the metal/chelating agent ratio, the type of metal, and the solution pH [120]. Despite the relevance of medium chemical speciation on metal-citrate complex biodegradability, just a few studies have examined the chemical aspects determining inhibition of nitrogen removing processes [121]. However, studies elucidating the fate of both citric acid and metals in denitrifying processes are missing in the literature and are crucial to optimize and apply these nitrogen-removing processes for metallurgic wastewaters. Based on a preliminary characterization of a stainless-steel industry effluent, we performed batch incubations with denitrifying sludge to assess the inhibitory effects of iron, chromium and nickel (main metals found in this industrial wastewater). Next, using speciation analysis and following key denitrification intermediates (NO_2^- and N_2O), the chemical aspects determining their accumulation were revealed under two relevant initial pH values (6 and 7) with citric acid and ethanol as electrons donors. Ethanol was considered as a reference as it has been extensively used in denitrifying processes [45,122–125].

2.3 Materials and methods

2.3.1 Stainless-steel wastewater

Synthetic metallurgical wastewater was used on denitrification tests with the aim to simulate parameters as real wastewater contains (presence of citric acid, nitrate at high concentration and predominant heavy metals: Fe, Cr and Ni). The stainless-steel pickling effluent has an acid pH of 3.17 and oxidation-reduction potential (ORP) of 543 mV. The nitrogen species and principal metal concentrations are present in Table 2.1, which agrees with those reported in the literature [1,126]. Total dissolved solids (TDS) were lower than values reported causing inhibition to denitrification [127,128]. Citric acid concentration was measured in terms of chemical oxygen demand (COD). Dissolved iron, chromium and nickel were present as Fe(III), Cr(III) and Ni(II), respectively [2,4]. For this reason, these metals were added as ferric iron nitrate nonahydrate (98%), chromic nitrate nonahydrate, and nickel nitrate nonahydrate (98.5%) in batch incubations.

Table 2.1. Metallurgic effluent characterization

Parameter	Concentration (mg/L)
$N\text{-}NO_3^-$	457.5
$N\text{-}NO_2^-$	1.7
$N\text{-}NH_4^+$	9.5
COD	123.2
TDS	2448.5
Iron, Fe	133.2
Chromium, Cr	47.9
Nickel, Ni	30.3
Silicon, Si	32.8
Tin, Sn	26.3

Table 2.2 pH and metal concentrations in assays at the preliminary (Prel.), initial and final conditions for the two electron donors: ethanol (EtOH) and citrate (Cit).

Concentration (mg L^{-1})		Prel.	Initial pH 6		Final pH	Initial pH 7		Final pH
			Initial	final		initial	final	
Ni	EtOH	2.2	2.0±0.2	0.0±0.0	9.8	2.0±0.1	0.0±0.0	9.8
		5.1	5.3±0.2	0.0±0.0	8.9	5.0±0.3	0.0±0.0	9.7
		10	10.2±0.5	2.2±0.2	9	9.7±0.6	0.1±0.1	9.5
	Cit	10	10.3±2.5	2.2±1.2	8.9	7.1±1.0	5.6±0.4	9.2
		35.3	35.2±0.3	25.9±4.6	8.6	33.4±0.6	28.0±0.8	9.2
		60.5	57.9±0.4	51±0.4	8.4	57.0±0.8	50.7±0.4	9.1
Cr	EtOH	5.3	0.16±0.0	0.0±0.0	9.7	0.04±0.0	0.00±0.0	9.6
		100.2	0.04±0.0	0.0±0.0	9.6	0.24±0.0	0.00±0.0	9.7
		150.3	0.62±0.0	0.0±0.0	9.9	0.40±0.0	0.05±0.0	10
	Cit	5.3	4.1±0.2	3.4±0.6	8.4	3.9±0.2	3.3±0.1	9.4
		100.2	95.9±1.5	77.4±3.4	8.6	93.0±0.5	78.4±1.8	9.5
		150.3	148.8±1.4	142.3±1.4	8.7	144.0±1.9	137.6±1.7	9.3
Fe-Cit	total Fe	25.1	24.7±0.6	22.1±0.9	9.4	26.1±1.9	26.4±0.7	9.6
		70.5	71.1±2.8	63.6±0.7	8.8	71.8±3.6	43.8±2.4	9.2
		149.8	145.6±2.1	143.1±3.2	8.8	151.2±2.0	105.6±3.6	9.4
	Fe(III)		17.1±0.6	13.8±0.8		17.1±2.1	12.1±4.7	
			67.0±3.4	52.5±0.7		64.3±2.8	41.8±1.5	
			116.1±1.0	136.3±2.3		122.5±1.1	95.6±1.2	
	Fe(II)		7.6±0.4	8.3±0.6		9.0±0.2	14.3±2.6	
			4.7±0.2	5.5±0.7		7.6±1.2	1.8±0.7	
			29.5±3.4	6.9±3.2		28.6±1.0	10.3±0.9	
Fe-Cr-Ni-Cit	Ni	10.2	7.9±0.3	6.6±0.2	8.5	8.0±0.3	5.9±0.1	9.1
		35.3	23.5±1.3	19.7±0.8	8.7	23.7±0.9	21.0±0.4	9.3
		60.4	39.7±1.1	34.5±0.9	8.7	39.0±1.2	34.4±1.1	9.3
	Cr	4.9	4.5±0.2	4.3±0.2		4.8±0.2	4.2±0.1	
		99.8	78.5±2.8	73.0±2.0		79.5±2.5	74.4±1.7	
		150.2	112.2±3.5	103.5±2.3		111.2±2.8	104.8±3.2	
	total Fe	25.1	19.0±1.1	27.4±2.2		19.7±1.4	22.8±1.1	
		69.8	53.6±1.9	59.6±2.6		54.0±1.6	54.1±1.1	
		148.9	102.9±3.2	107.2±2.4		100.0±2.6	96.3±1.2	
	Fe(III)		13.5±1.2	17.0±2.8		9.2±0.6	13.8±1.7	
			46.9±3.7	38.3±5.3		36.0±1.0	30.3±1.8	
			78±2.5	75.6±2.3		56.9±3.1	72.4±2.9	
	Fe(II)		5.5±0.3	10.3±1.2		10.5±1.0	9.0±0.6	
			6.8±0.3	21.3±3.1		17.9±0.6	23.8±2.8	
			24.9±0.2	31.5±0.4		43.1±1.0	23.8±3.6	

2.3.2 Biomass

Anaerobic granular sludge originated from a wastewater treatment plant treating effluents from a brewery factory (Cd. Obregón, México) was used. The biomass was acclimated under denitrifying conditions in two up-flow anaerobic sludge blanket (UASB) reactors with a working volume of 1.1L. The hydraulic retention time was set at one day. Both reactors were fed with 500 mg N-NO_3^-/L and were supplied with stoichiometric amounts of either ethanol or citrate as electron donor. Medium used for bioreactors operation contained (mg/L): KH_2PO_4, 300; $MgSO_4 \cdot 7H_2O$, 61.3; $FeSO_4 \cdot 7H_2O$, 17.2; $CaCl_2 \cdot H_2O$, 75 and 1 mL/L trace elements with the following composition (g/L): $MnCl_2.4H_2O$, 0.5; H_3BO_3, 0.05; $ZnCl_2$, 0.05; $CuCl_2$, 0.03; $Na_2MoO_4 \cdot 2H_2O$, 0.01; $CoCl_2 \cdot 6H_2O$, 0.5; $NiCl_2.6H_2O$, 0.01 and Na_2SeO_3, 0.01. The pH of the feed was adjusted to 7 with NaOH as required.

2.3.3 Batch assays

Experimental conditions applied in batch tests were designed to reflect the actual conditions prevailing in the studied metallurgic effluent and they are summarized in Table 2.2. Incubations were performed in serological bottles (124 mL) with 2 g of volatile suspended solids (VSS)/L of biomass and 100 mL of mineral medium, which was supplied with 500 mg of N-NO_3^-/L and with carbon source at double stoichiometric C/N ratio: 1.43 (g/g) and 2.86 (g/g) for ethanol and citrate, respectively. Mineral medium and trace elements were prepared with the same composition as for reactors feeding through biomass acclimation. Medium was bubbled with argon to remove any traces of dissolved oxygen. The pH of the medium was adjusted to the corresponding values with NaOH as needed. The medium was stored overnight before being added to incubation bottles to allow reaches the equilibrium. All bottles were sealed with rubber stoppers and aluminum caps. Headspace of bottles was exchanged with argon at atmospheric pressure. Experiments were performed using sacrificial bottles and triplicates from all

experimental treatments were taken for measuring at each sampling point. The concentration of $N\text{-}NO_3^-$, $N\text{-}NO_2^-$, $N\text{-}NH_4^+$, and $N\text{-}N_2O$ was quantified over time, while mass balances of all nitrogenous species, except for NO that was dismissed, derived production of $N\text{-}N_2$. In addition, COD, pH, ORP and dissolved metals concentrations were also measured. Sludge samples were also collected at the end of the incubation period and were analyzed by X-ray diffraction (XRD) to identify precipitated species of studied metals. For experiments performed with iron, the concentration of ferric iron was calculated from the difference between quantified concentrations of total iron and ferrous iron.

2.4 Results and discussions

Overall denitrification reactions with the two carbon sources considered in this study, ethanol and citrate, proceed as follows:

$$C_2H_5OH + 2.4\ NO_3^- \rightarrow 2HCO_3^- + 1.2N_2 + 0.4OH^- + 1.8H_2O \quad (2.1)$$

$$\Delta G° = -1230.7\ kJ/mol$$

$$C_6H_5O_7^{3-} + 3.6NO_3^- + 0.6H^+ + 0.2H_2O \rightarrow 6HCO_3^- + 1.8N_2 \quad (2.2)$$

$$\Delta G° = -1881.0\ kJ/mol$$

According to Gibbs free energy values, citrate is a better carbon source than ethanol to perform denitrification from the thermodynamic point of view. This premise was experimentally corroborated in the control experiments, which did not contain heavy metals; μ_m of 17.96 ± 0.81 and 26.02 ± 0.4 mg $N\text{-}N_2\ L^{-1}h^{-1}$ at pH 6 and 7, respectively, were obtained with ethanol; while the values obtained with citrate were 43.06 ± 0.95 and 47.29 ± 0.75 mg $N\text{-}N_2\ L^{-1}h^{-1}$ at pH 6 and 7, respectively. The pH increased during incubations, according to equations (2.1) and (2.2), corresponding to the metabolism of the electron donor sources. In addition, no buffer was added to control the pH, thus explaining this increase. Table 2.2 shows the preliminary (acidic pH), initial (pH adjusted to 6 or 7) and final pH (end of incubations) of the tests with their respective metals concentrations. In all experiments, the decrease of COD concentration

agreed with N_2 production. No accumulation of intermediates was observed in incubations supplied with citrate. However, nitrite transitorily accumulated reaching a maximum concentration of 10 mg N-NO_2^-/L at initial pH of 6, but was further reduced to N_2 at the end of the incubation period. Ammonium concentration was quantified in a very low concentration in all experiments. Our results contrast with findings reported by Arbel et al.[132], who found nitrate removal rates higher (and absence of nitrite accumulation) with ethanol as compared to experiments performed with citrate. This discrepancy might have been due to different microbial populations and thus with distinct metabolic capabilities.

2.4.1 Iron effects

In experiments conducted with ethanol, added concentrations of 24.9, 71.2 and 150.3 mg Fe/L resulted in complete precipitation of iron just after the medium was adjusted to the initial pH values (6 and 7). The presence of hematite (Fe_2O_3) in the precipitate was confirmed by XRD analysis; this is shown in Figure 2.1(a). Nitrite was the only intermediate evolved during the course of incubations with concentrations lower than 10 mg N-NO_2^-/L, which yielded mild inhibition of the denitrifying process. ORP progressively decreased (150.6 to -48.7 mV) during the incubation period, which agreed with the reduction of nitrate [133], while pH increased due to alkalinity generated from ethanol metabolism. Papirio et al.[69], whose results revealed almost complete precipitation of iron at pH 7 during the course of denitrification with ethanol as electron donor, reported similar denitrifying activities.

In incubations with citrate, the total iron concentration was conserved by adjusting the pH to the initial established values for the kinetics. In some experiments, iron concentration even increased during the course of kinetics, which could be due to re-solubilization of iron that was present in the granular sludge; this agrees with similar observations by Papirio et al.[69]. Iron was added as ferric iron; however, a certain concentration of this species was reduced to ferrous iron, see Table 2.2. In all incubations, complete denitrification was obtained without the presence of

intermediates. With respect to μ_m, a clear inhibition was observed at pH 6 with the increase of iron concentration, whereas at pH 7 an opposite pattern was observed. Similar to ethanol experiments, the ORP progressively decreased (137.7 to -123.9 mV) during the incubation period. Figure 2.2 shows the level of inhibition or stimulation promoted by iron additions.

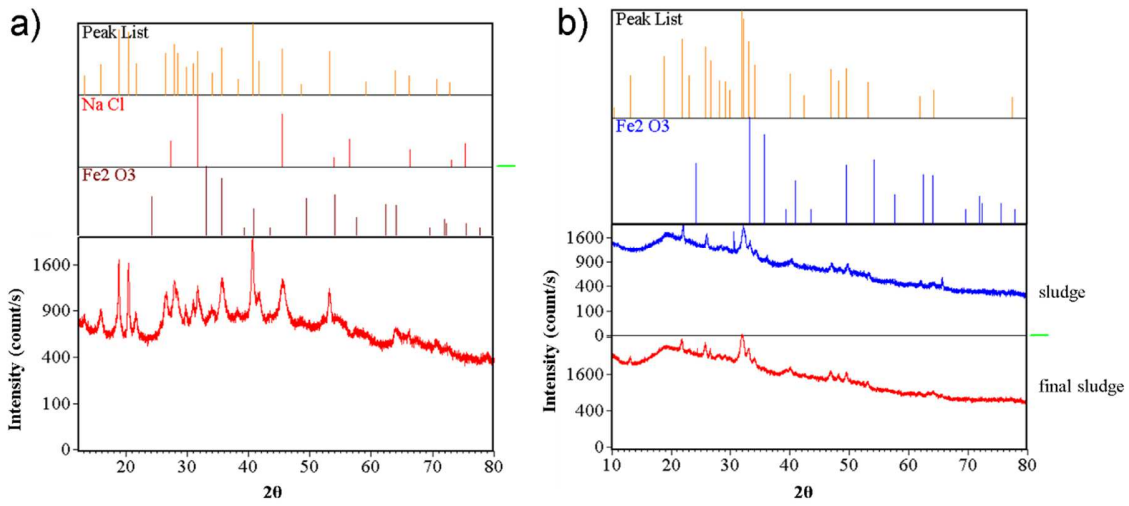

Figure 2.1 a) XRD patterns of medium mineral precipitated at pH 6 and 7 in ethanol incubations for the control experiments and b) XRD patterns of granular sludge at the end of incubations with iron and citrate as electron donor.

According to speciation analysis, increase on iron concentration caused a lower concentration of free citrate (cit^{3-}, $C_6H_5O_7^{3-}$) by the formation of the citrate-iron complex. The concentration of this species decreased during the kinetics; interestingly, its consumption rate is related to the level of inhibition or stimulation on the denitrifying process. In experiments performed at pH 7, a higher initial concentration of this species was detected as compared to that observed in experiments started at pH 6. Evolution of the Fe-citrate species during the experiments is different for the two pH values evaluated. At pH 6, the predominant species is ferric-citrate, $[Fe\text{-}cit]_{(aq)}$, during the lag phase, which was maintained at the same concentration or in some cases even increased. At the beginning of the exponential phase, this species decreased by consumption of citrate and by the increase on pH. Released iron forms soluble hydroxides, due to its amphoteric

property. At pH 7, the $[Fe\text{-}cit]_{(aq)}$ species began to decrease from the beginning of the kinetics, then the released iron produced soluble hydroxides, just like in the case observed at pH 6. The conversion of $[Fe\text{-}cit]_{(aq)}$ to soluble Fe-hydroxides occurred at the same rate as can be seen in Fig. 2.3(b).

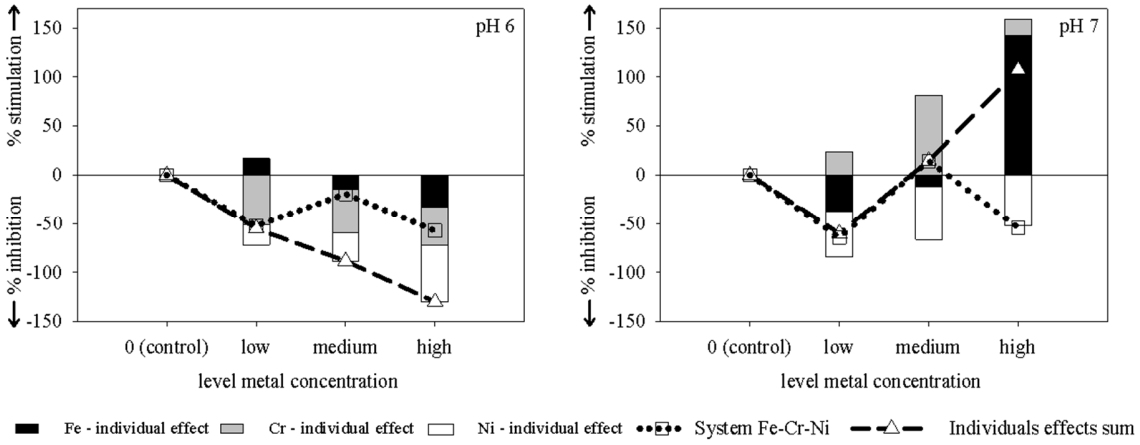

Figure 2.2 Percentage of inhibition or stimulation of μm with respect to the control incubated in the absence of metals, versus three levels of Fe, Cr and Ni concentrations, as well as the Fe-Cr-Ni mixture; and the sum of the individual metal inhibition. Details of concentrations tested are described in Table 2.2.

In the case of species formed with ferrous iron, species $[Fe\text{-}cit]^-$ is predominant and is maintained throughout the whole incubation period. Its consumption is related to the level of inhibition or stimulation on the μ_m value. Similar effects were observed under aerobic conditions by Francis and Dodge [23]. At pH 6, this species remained constant or increased its concentration. At the highest concentration of iron (145.6 mg/L), an increase of this species was observed during the exponential phase, and this was the experimental treatment showing the highest extent of inhibition (Fig. 2.3(a)). The presence of $[FeH\text{-}cit]_{(aq)}$ was also proportional to the degree of μ_m inhibition. At pH 7, citrate in $[Fe\text{-}cit]^-$ species was consumed during the course of the kinetics. For the experiments conducted with the highest concentration of iron (151.2 mg/L), the concentration of this species was drastically decreased within a few hours at the beginning of the experiment, which agrees with high denitrifying activity stimulated. In contrast, this species remained constant for a longer period in

incubations performed with the other two iron concentrations (26.1 and 71.8 mg/L). Ferrous iron released from this complex, subsequently formed species with bicarbonate and soluble hydroxides, while another fraction remained in ionic form (Fig. 2.3(a)). Furthermore, a fraction of both ferrous and ferric iron precipitated during the experiments, and according to the saturation index obtained from speciation analysis, precipitates could be oxy(hydroxides) and iron carbonate. Results derived from XRD analysis also showed the presence of hematite (Fig. 2.1(b)).

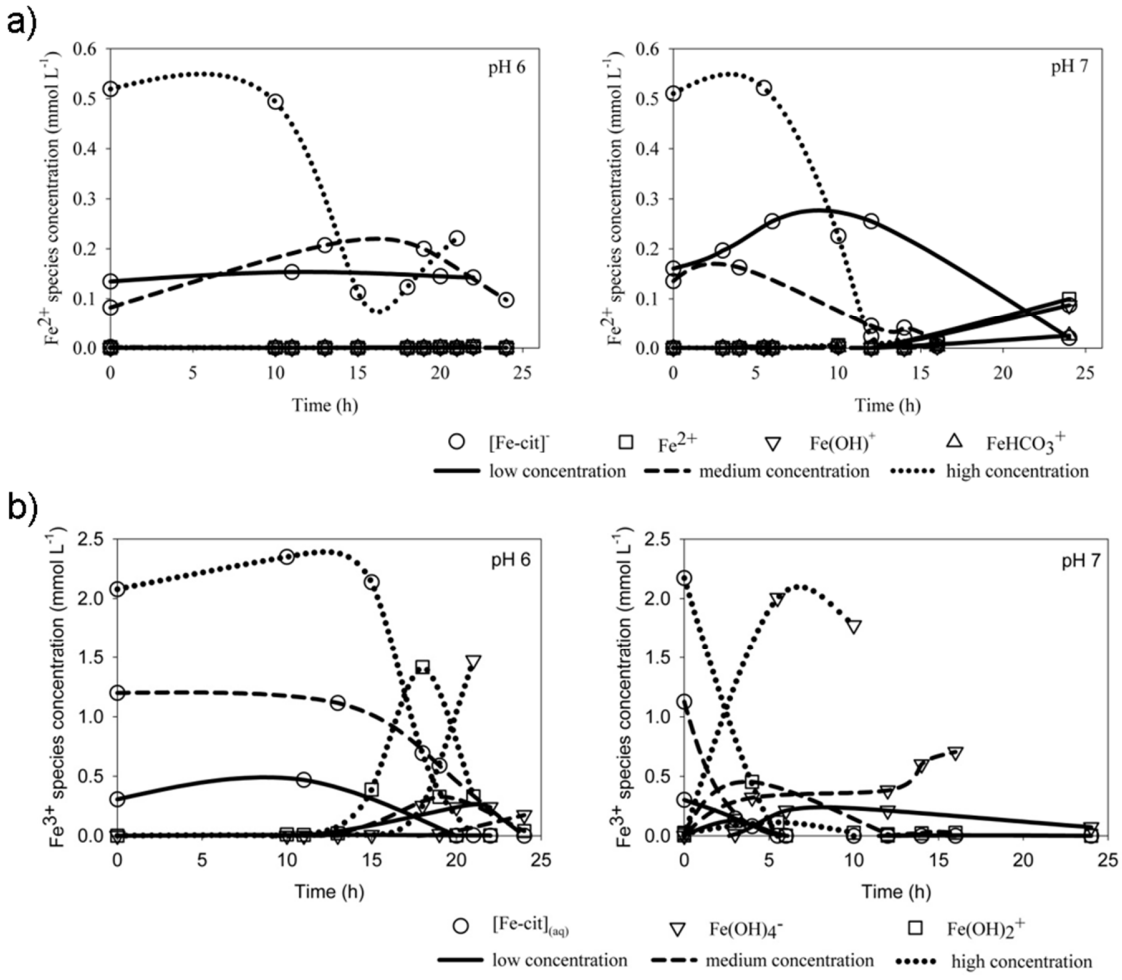

Figure 2.3 Distribution of (a) ferrous iron and (b) ferric iron species during kinetics performed with citrate as electron donor.

The pH showed relevance on the iron-citrate complex stability. High pH values on incubations caused important release of iron from the complex, thus contributing with

an important amount of free citrate available to support denitrification. This was observed in the experiment with the highest μ_m stimulation, which elevated pH in the first hours of incubation caused a high release of the two iron species and their precipitation. This considerable increase of pH could also be due to other processes.

Traces of H_2 were detected in some incubations but could not be quantified precisely because of the method used. The detection of H_2 could be explained by the presence of Fe(II). Certainly, Karadag and Puhakka reported that high concentrations of Fe(II) promoted hydrogen production by anaerobic sludge [134].

2.4.2 Nickel effects

In ethanol assays, initial nickel concentrations remained constant after the initial pH adjustments (Table 2.2). Nonetheless, nickel concentrations decreased during denitrification kinetics, particularly for experiments started at pH 7. μ_m inhibition and intermediates accumulation was more prominent at this pH as compared to incubations started at pH 6. In fact, there was a correlation between the amount of intermediates accumulated and the concentration of nickel observed in both series of experiments. At pH 6, the most affected denitrification step was nitrate reduction (Fig. 2.4). Speciation analysis further revealed that decrease on nickel concentration in solution promoted accumulation of nitrite and N_2O, while the permanence of free nickel ions affected the nitrate reduction step. At initial pH of 6, the concentration of free nickel ions was higher and decreased at a lower rate compared to experiments with initial pH of 7. Additional species, such as nickel carbonates, were produced in lower proportion as denitrification took place; at the beginning, $NiHCO_3^+$ species is formed, but when pH increased, its concentration drop, while the concentration of $Ni(CO_3)_{(aq)}$ increased (Fig. 2.5). In kinetics with initial pH of 7, these species are present at low concentrations since nickel in solution considerably decreased at initial kinetic points. Zou et al.[58] obtained an inhibition of 18 and 65% in a denitrifying process at concentrations of 26.4 and 75.2 mg L^{-1} of Ni, respectively, with nitrite as the only intermediate monitored, which did not exceed 10 mg NO_2^--N

L^{-1} during the experiments and was completely reduced at the end of the experiments. These results indicate lower inhibitory effects by nickel as compared to those observed in the present work. This could be explained by the use of phosphate buffer in their work, which could have significantly changed the solubility of nickel species. Considering the speciation of phosphate and nickel (50%-$NiHPO_4$ and 50%-$Ni_3(PO_4)_2$, at pH 7) previously reported [135,136], an exercise of speciation analysis by Visual MINTEQ at pH 7 for a equimolar mixture of Ni(II) and PO_4^{3-} revealed an oversaturation of 0.716 for $Ni(OH)_{(c)}$ and 7.454 for the species $Ni_3(PO_4)_{2(s)}$. With respect to ORP values, experiments with low inhibition showed ORP values from 95.5 to -124.1 mV and complete nitrate reduction was accomplished; while for experiments with incomplete nitrate reduction and intermediates accumulation, the ORP remained at positive values (185.0 to 176.1 mV). This ORP pattern agrees with works demonstrating the effect of ORP on denitrification process [137].

According to speciation analysis, nickel was totally complexed with citrate, with $[Ni\text{-}cit_2]^{4-}$ and $[Ni\text{-}cit]^{-}$ prevailing as predominant species (Fig. 2.5), which agrees with those reported in potentiometric and spectroscopic studies of species formed by Ni^{2+} and citric acid at similar pH values [29,30,138]. μ_m inhibition was more prominent with the increase on initial nickel concentration at both initial values of pH as compared to experiments performed with iron and chromium. Furthermore, a higher concentration of $[Ni\text{-}cit_2]^{4-}$ and a greater inhibition of N_2 production occurred at pH 7 as compared to experiments performed at pH 6. Decrease of nickel concentration during the course of the kinetics was greater at initial pH of 6, indicating a higher complex stability formed at pH 7. The decrease of species $[Ni\text{-}cit_2]^{4-}$ along the kinetics occurred slowly, showing stability with increasing pH and throughout the denitrification process. This stability hinders biodegradation of citrate while linked to nickel. This complex is formed by two molecules of citrate bound to one molecule of Ni, which decreases the amount of free citrate available for denitrification. During the course of the kinetics, $[Ni\text{-}cit]^{-}$ formation is observed as $[Ni\text{-}cit_2]^{4-}$ decreases, which could indicate that degradation of $[Ni\text{-}cit_2]^{4-}$ yields $[Ni\text{-}cit]^{-}$, releasing in turn a citrate molecule. Regarding denitrification intermediates, accumulation of NO_2^{-} and N_2O

was present in experiments with medium and high nickel concentrations. No obvious effects on nitrate reduction were observed. ORP showed a similar pattern with ethanol incubations, it was reduced (from 168.6 to -276.0 mV) in incubations with complete denitrification, while it remained constant or increased to positive values (from 97.8 to 126.1 mV) in kinetics with final intermediates accumulation.

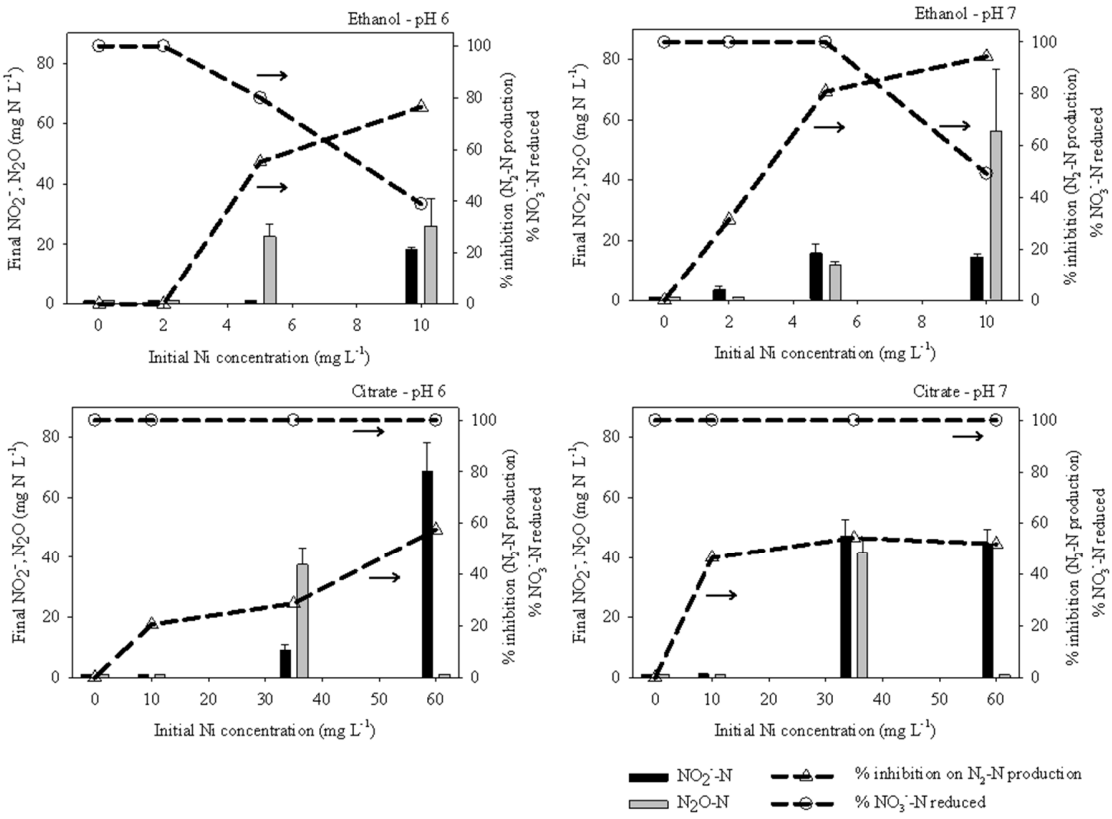

Figure 2.4 Accumulation of denitrifying intermediates and extent of inhibition in incubations performed with different nickel concentrations with ethanol and citrate as electron donors.

Inhibition of μ_m was lower in experiments conducted with citrate even though the concentrations of nickel prevailing in these assays were much higher than in incubations with ethanol. This could be due to the complex formed that maintained nickel less bioavailable. At the common tested concentration with the two carbon sources (initial concentration of 10 mg Ni L^{-1}), citrate experiments also showed lower inhibition and not accumulation of intermediates as compared to ethanol assays. One of the most important observations is the lack of affectation of the nitrate

reduction step in experiments with citrate. A possible explanation for the affectation of the nitrate reduction step in ethanol amended cultures is the presence of free nickel ions, which did not prevail in citrate incubations due to the previously described complex formed.

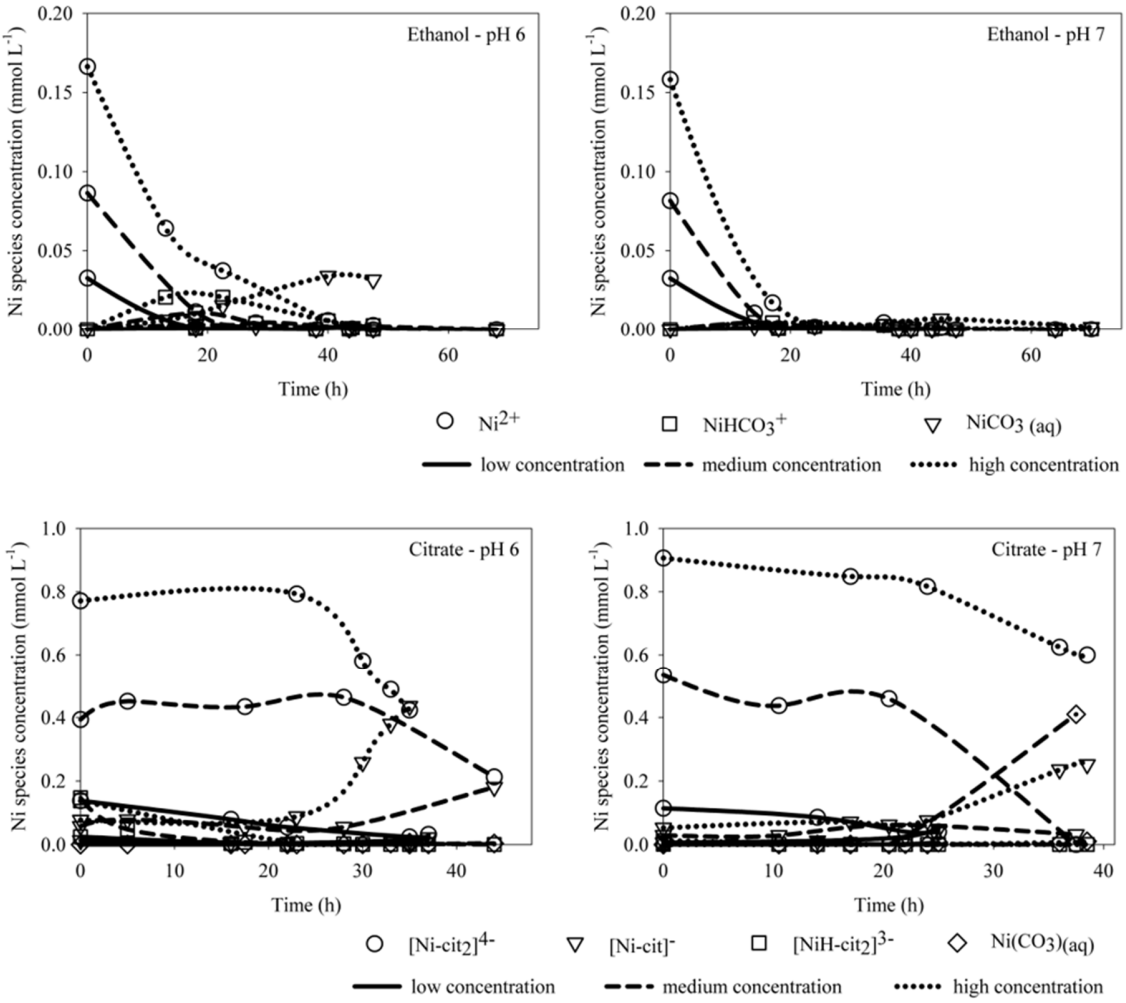

Figure 2.5 Distribution of the nickel species during kinetics performed with ethanol and citrate as electron donors.

Regarding saturation index species with possibility to precipitate in all experiments for the two carbon sources tested are: $Ni(OH)_{2(am)}$, $Ni(OH)_{2(c)}$ and $NiCO_{3(s)}$. In all experiments, $NiCO_{3(s)}$ had higher oversaturation followed by $Ni(OH)_{2(c)}$ and finally $Ni(OH)_{2(am)}$. However, species of nickel were not observed in XRD analysis. A correlation between intermediates concentration and saturation index during the

course of kinetics was obtained; this is shown in supporting information (Figures 2.6 and 2.7). These figures illustrate a pattern of NO_2^- accumulation with $NiCO_{3(s)}$ oversaturation, and N_2O presence with $Ni(OH)_{2(c)}$ or $Ni(OH)_{(am)}$ oversaturation. During the experiments performed with citrate as electron donor, chromium and iron precipitations were observed on the liquid surface, while this was not observed for nickel experiments. However, under both pH values tested and at an initial concentration of 35 mg Ni L^{-1}, accumulation of NO_2^- and N_2O occurred along with a change of color in the surface of the granular biomass, probably due to the described above. An additional observation was the production of traces of H_2 in some experiments. This agrees with findings of Karadag and Puhakka, described in previous section, which showed that an increase of Ni concentration stimulated hydrogen production[134].

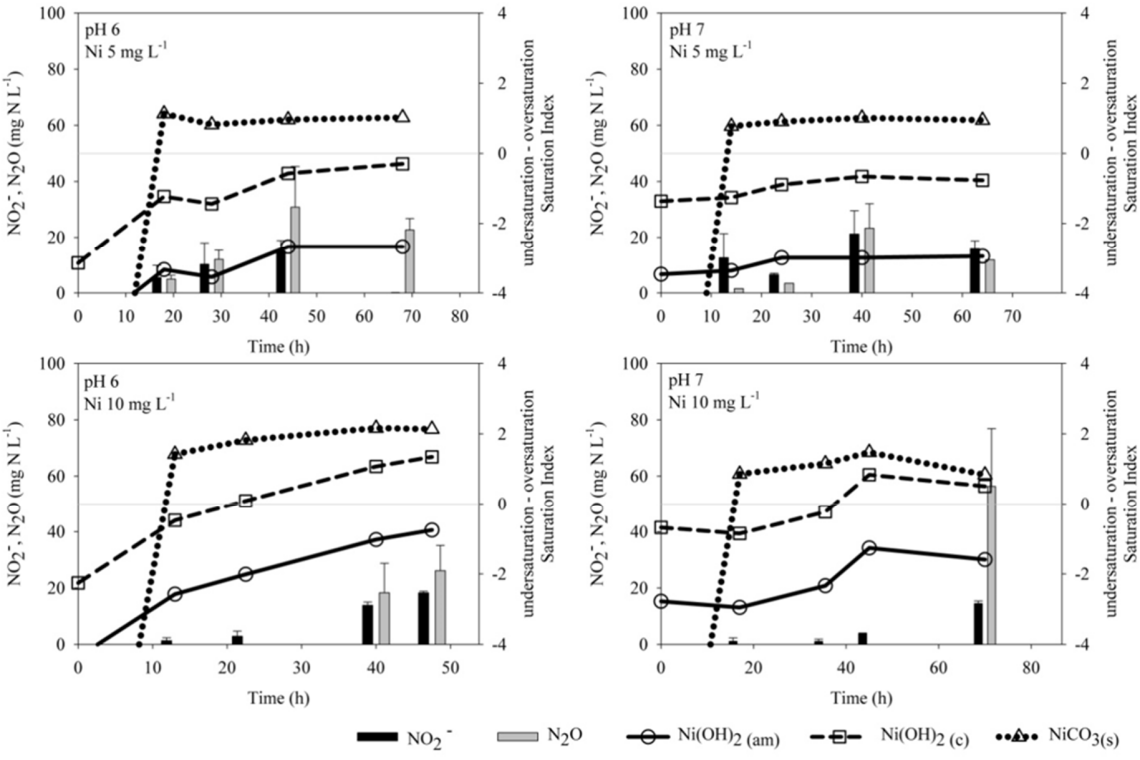

Figure 2.6 Intermediates (NO_2^- and N_2O) production and nickel species saturation index during the course of the incubations with ethanol as electron donor.

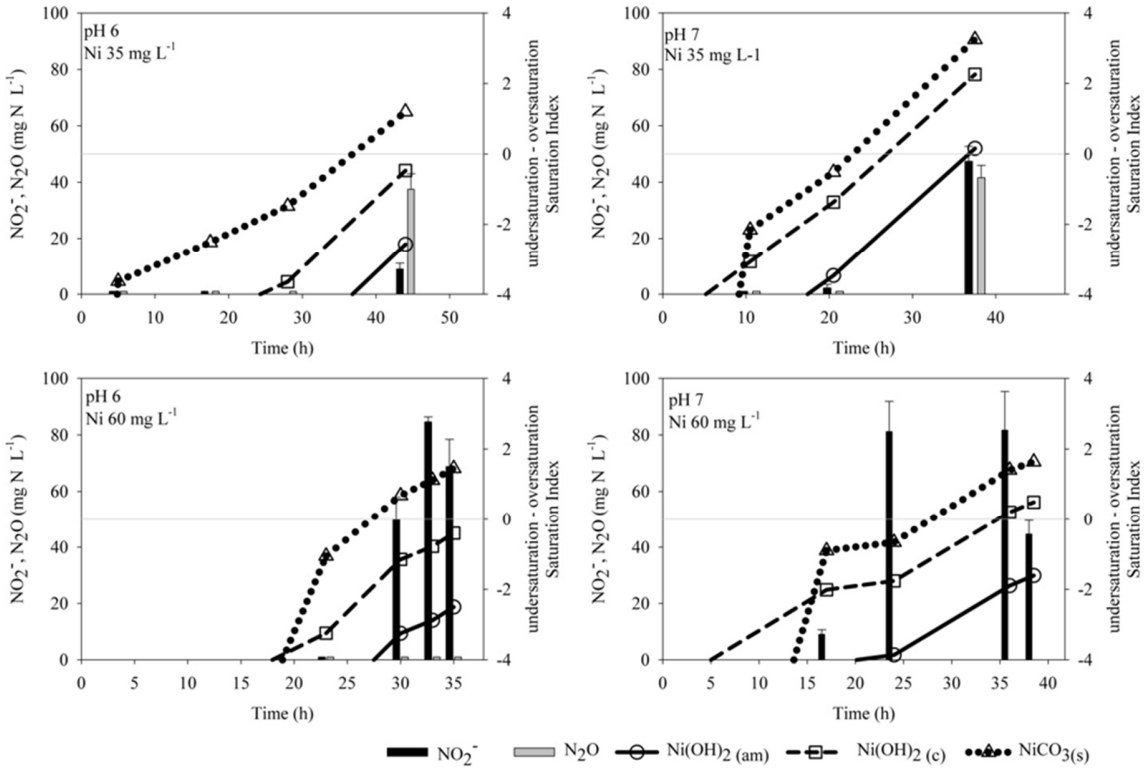

Figure 2.7 Intermediates (NO_2^- and N_2O) production and nickel species saturation index during the course of the incubations with citrate as electron donor.

2.4.3 Chromium effects

In ethanol assays, added chromium precipitated almost entirely by adjusting the pH to the initial values (Table 2.2). According to XRD analysis, this precipitate contained Cr_2O_3 and Fe_2O_3; these solids were also observed at the final sludge (Figures 2.8 and 2.9(a), respectively). Traces of chromium were measured during the course of the kinetics, which resulted in μ_m stimulation in most cases: mainly at initial pH of 6 with values of 71.7, 63.0 and 24.5 % at the low, medium and high preliminary chromium concentration, respectively. Cr(III) is thought to be rather harmless due to both its low solubility and requirement in some metabolic processes [18,139–142]. In the case of initial pH 7, μ_m inhibition of 12.1% was obtained at the lower preliminary chromium concentration, and a stimulation of 12.56 and 11.3% at the medium and

high concentrations, respectively. Similarly, high precipitation and low nitrate reduction inhibition at traces of Cr(III) in denitrifying batch experiments at pH of 8-8.5 have been reported [143]. No evident effects on the reduction of NO_2^- and N_2O were observed. NO_2^- transitorily accumulated up to 50 mg $N\text{-}NO_2^-/L$, but was further reduced to N_2. ORP values showed highly reductive conditions (92.1 mV to -290.2 mV) during the incubations; this is in agreement with the stimulation of N_2 production observed.

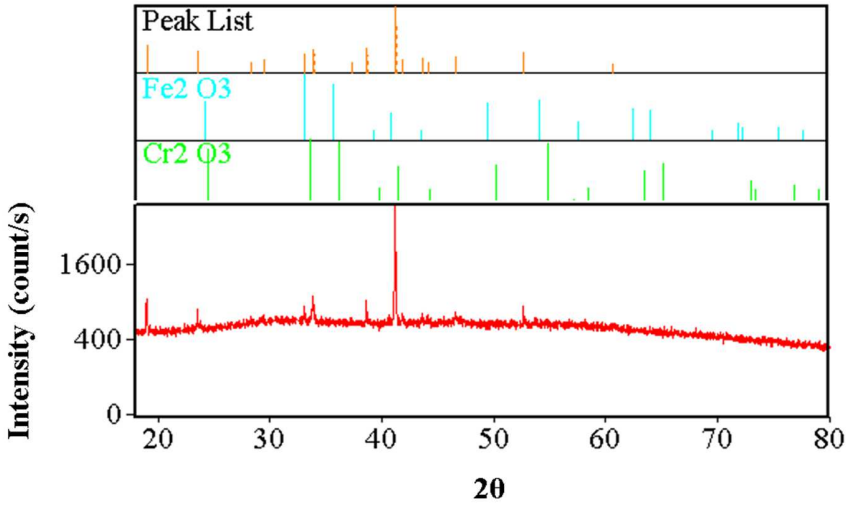

Figure 2.8 XRD patterns of medium precipitated at pH 6 and 7 in ethanol incubations for experiments with chromium.

Unlike ethanol experiments, citrate amended assays kept chromium in solution, indicating the formation of complex between citrate and Cr(III). Chromium concentration was maintained during the kinetics, decreasing less than 20% (Table 2.2). Speciation analysis indicated that chromium could have precipitated as $Cr(OH)_{3(am)}$ and $Cr_2O_{3(c)}$ for all cases, and XRD analysis confirmed the presence of Cr and $Cr_2O_{3(c)}$ (Fig. 2.9(b)). Nitrate was completely reduced, while nitrite was the only transient intermediate accumulated (<20 mg $N\text{-}NO_2^-/L$). ORP values were higher than those observed in incubations exposed to the other metals and decreased, but at a slow rate without reaching negative values (from 352.9 to 181.8 mV).

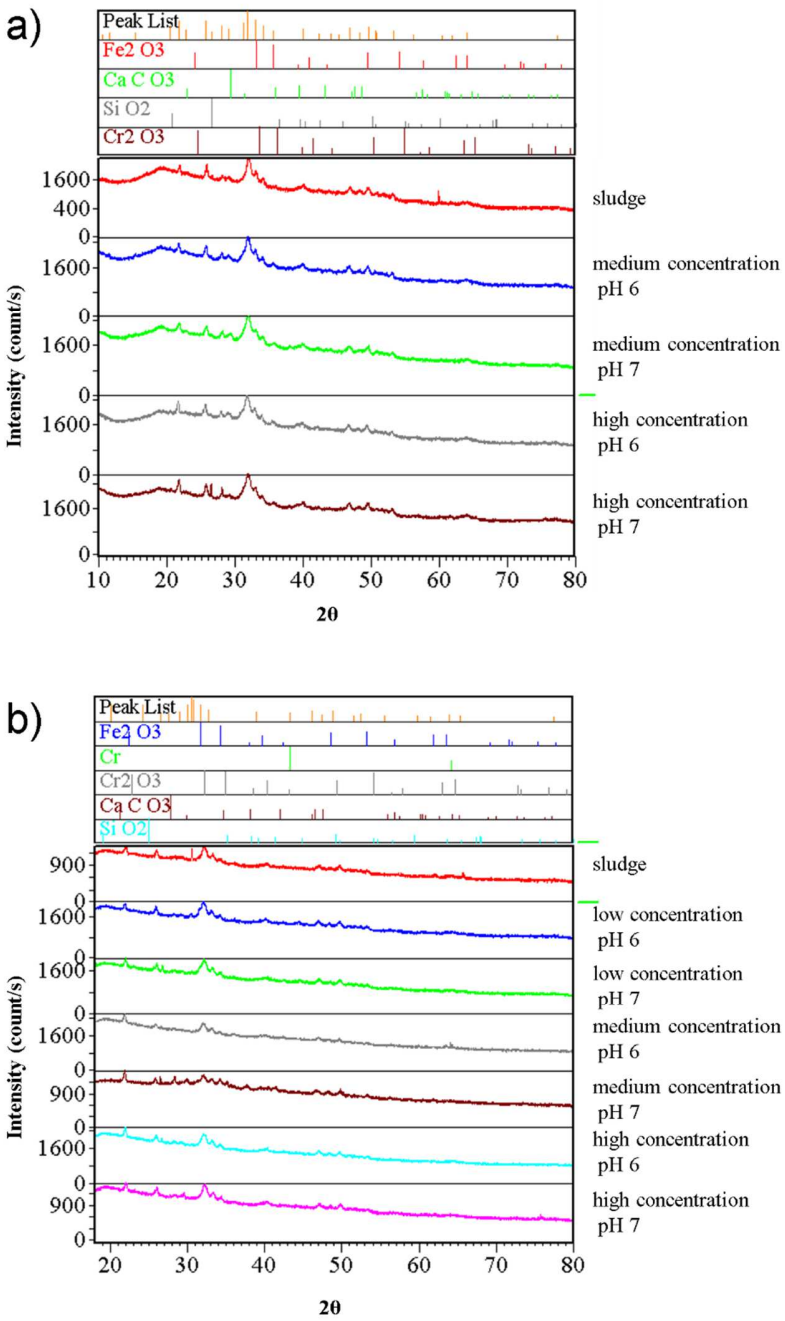

Figure 2.9 XRD patterns of granular sludge at the end of incubations with chromium and (a) ethanol or (b) citrate as electron donors.

An μ_m inhibition was quantified in experiments with initial pH 6, while an opposite pattern was observed at initial pH 7 (Fig. 2.2). This performance could not be explained by means of speciation analysis. It is important to mention that Visual

MINTEQ database does not contain Cr(III)-citrate complex species. However, this species along with its respective formation constant was determined by Gabriel et al.[28], which were incorporated into our software. Nevertheless, Cr^{3+} ionic form cannot be added to the software, only as $Cr(OH)_2^+$[144], which could affect species reported. Regarding species obtained in the speciation analysis, soluble hydroxides of Cr(III) are predominant, while Cr(III)-citrate complex is in low concentration. The concentrations of soluble hydroxides were close for both initial pH values and were maintained throughout the whole incubation period (Fig. 2.10). This indicates that these species do not have a relevant effect on the denitrifying process. However, the presence of chromium-citrate complex in high concentration was evident, due to the low decrease of chromium in solution at high pH in contrast with ethanol experiments where chromium precipitated almost completely. The μ_m inhibition at pH 6 could be explained with the Cr(III)-citrate species reported by Gabriel *et al.* [28] at different pH values. For instance, at initial pH of 6, the following proportions of Cr(III) species are present: $[Cr\text{-}cit_2]^{4-}$ in approximately 50%, followed by $[Cr\text{-}cit]^-$ with 22%, and finally $[Cr\text{-}cit]^{2-}$ with 19%. Meanwhile, species $[Cr\text{-}cit_2]^{4-}$ is reduced to 20 and 10% at pH 7 and 8, respectively; and species $[Cr\text{-}cit]^{2-}$ increased to 60 and 80% at pH 7 and 8, respectively. At pH 7 and 8, the amount of chromium bounded to a single citrate molecule is higher than the amount quantified at pH 6. As a result, a higher amount of free citrate is released to be utilized in the process, while at pH 6, less amount of free citrate is available due to predominant complexes with two molecules of citrate bounded to one molecule of chromium.

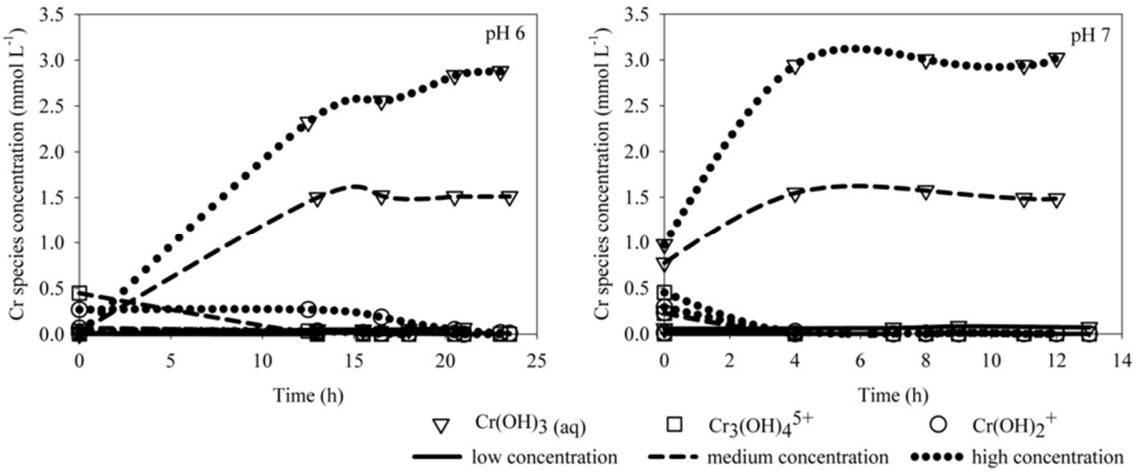

Figure 2.10 Distribution of the chromium species as a function of the time assays for ethanol and citrate as electron donors.

2.4.4 Multi-metal effects

In order to get further insight on the effects of metals on denitrification under similar conditions prevailing in the metallurgic effluent studied, additional experiments were performed with the three metals altogether and citrate as electron donor. Similar μ_m inhibition (<60%) was obtained in all experimental treatments at both initial pH values. This inhibition was compared with the sum of the individual effects (inhibition or stimulation) of each metal (Fig. 2.2). Cumulative effects were obtained at the lowest metals concentrations for both pH values, whereas for the medium and high metals concentrations, antagonist and synergistic effects were observed at pH 6 and 7, respectively. Respect to accumulation of intermediates, combined effects of metals during the course of denitrification kinetics resulted in synergism. Nitrite reduction was the most affected step, which maximum quantified concentration was nearly 160 mg NO_2^--N L^{-1}. N_2O production was observed at medium and high metal concentrations in experiments with initial pH of 6, which concentration was lower than 50 mg NO_2^--N L^{-1}. These intermediates were subsequently converted to N_2.

ORP measurements showed reductive conditions in all experiments, starting at 132.4 mV and decreasing to -121.3 mV.

Through speciation analysis, a similar species evolution was observed in the multi-metal system as compared to individual metals experiments (Fig, 2.11). The concentration of species that showed *μm* inhibition in individual experiments, [Fe-cit]$^{-}$ and [Ni-cit]$_2^{4-}$, remained approximately constant. In incubations showing less inhibition in the denitrifying process, [Ni-cit]$_2^{4-}$ concentration decreased and [Ni-cit]$^{-}$ concentration increased, which was also observed in individual experiments with Ni. Chromium species had similar pattern as individual experiments. An additional species showing oversaturation was $FeCr_2O_{4(s)}$, which contains Cr(III) and Fe(II). Further analysis by XRD revealed the presence of hematite, Cr and $Cr_2O_{3(s)}$ in precipitates (Figure 2.12).

The Fe-Cr-Ni system showed similar inhibition (expressed as μ_m) for the two pH values evaluated, perhaps due to the approximately same metals concentrations prevailing at initial time of incubations and to the nearly same evolution of species during the course of the kinetics. The milder effects obtained in multi-metal system as compared to the sum of individual metals effects could be a result of metals interactions, such as co-precipitation. Cr(III)-Fe(III) (oxy)hydroxide can be formed via co-precipitation at neutral to alkaline pH values [145]. On the other hand, decrease on nickel toxicity and increase on Ni-citrate biodegradation could be obtained by trapping the nickel [65] or by co-precipitation with iron [63], respectively. These factors can modulate Ni bioavailability and its toxicity during the bioremediation of metallurgic waste streams. The interactions between metals are simplified in lower metals concentrations in solution, which are mainly observed due to the lower initial metals concentrations in solution, at the beginning of the incubation, and to a less pronounced decrease on Ni concentrations during the incubations (Table 2.2). On the other hand, the stimulatory effect of iron and chromium on μ_m could help to decrease the negative effects observed by nickel.

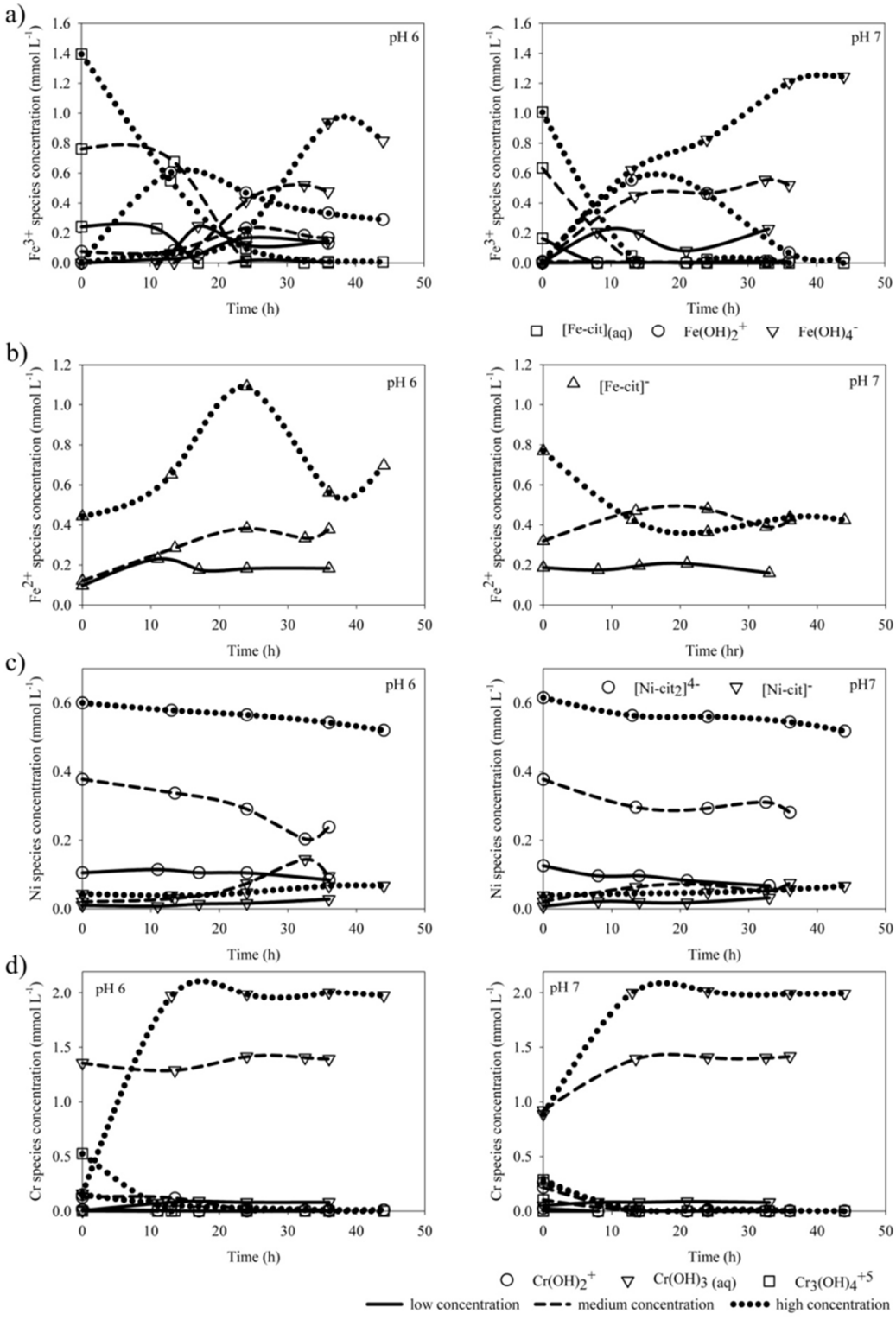

Figure 2.11 Distribution of the a) Fe(III); b) Fe(II); c) Ni(II) and d) Cr(III) species in the system Fe-Cr-Ni as a function of the time assays with citrate as electron donor.

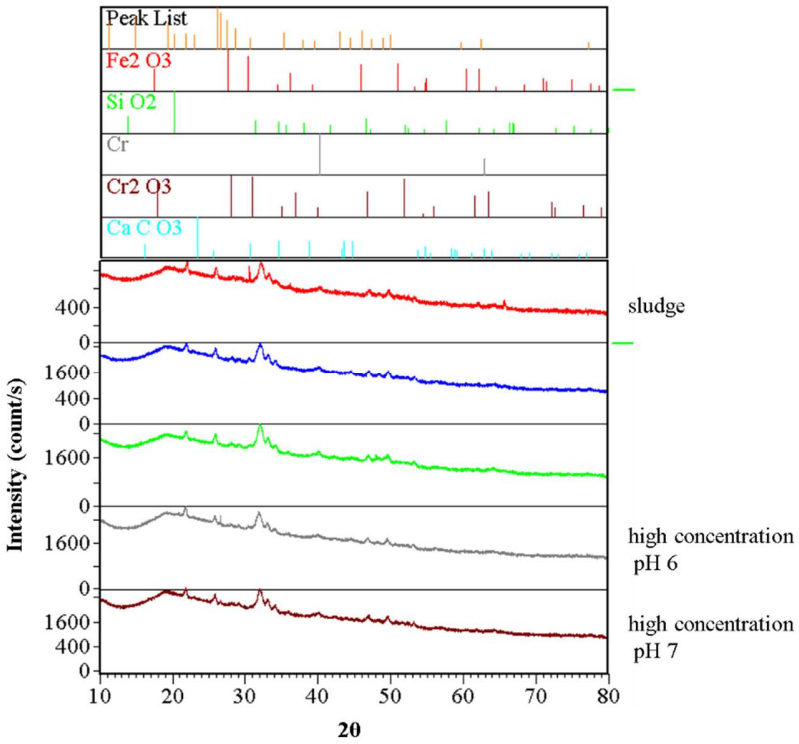

Figure 2.12 XRD patterns of granular sludge at the end of incubations for the system Fe-Cr-Ni and citrate as electron donor.

2.5 Conclusions

This study elucidates chemical aspects determining the inhibitory effects of Fe, Cr and Ni on denitrification of synthetic metallurgic wastewater. These aspects include the influence of metals-citrate complexes conformation and their subsequent bioavailability affecting the denitrification process. $[Fe\text{-}cit]_{(aq)}$ was readily biodegraded, while ferrous citrate complex, $[Fe\text{-}cit]^-$, was resistant to biodegradation. Nickel formed strong complexes, such as $[Ni\text{-}cit_2]^{4-}$ that in turn formed [Ni-cit], which were slowly biodegraded leading to μ_m inhibition. Predominant chromium species like $[Cr\text{-}cit_2]^{4-}$ resulted in μ_m inhibition and a simpler form of this species, $[Cr\text{-}cit]^{2-}$, resulted in μ_m stimulation. Iron and chromium affected the overall process (N_2

production rate), while nickel inhibited all denitrification steps. Multi-metal system showed milder inhibitory effects than individual metals systems. This information is pertinent to develop efficient biological processes to remove nitrate and citrate from metallurgic effluents.

3. Swirling fluidization in an Anaerobic Membrane Bioreactor as antifouling technique

3.1 Abstract

Scarce attention has been placed on the geometry of anaerobic fluidized bed membrane bioreactors (AFMBR) affecting the hydrodynamic pattern inside the reactor and, consequently, on the mechanical cleaning driven by granular carbon (GC) around the membrane. The present work determined the feasibility of applying a swirling fluidization, produced by a reactor with hydrocyclone geometry and by a tangential inlet, with the aim to avoid membrane fouling and to perform the denitrification process. The study includes 3D-hydrodynamic description of the flow and particles fluidization through computation fluid dynamics (CFD), experimentally validated with the particle image velocimetry (PIV) technique. Water shear stress and GC momentum acting over the membranes were also determined, in addition to monitoring the filtration and denitrification performance. The conical section resulted in higher shear stress and particle momentum compared with the cylindrical zone. Soluble microbial products (SMP) accumulated on the membrane walls with lower shear stress and particle momentum. The operation of the AFMBR was maintained with a continuous permeate flow without any change in suction pressure and the nitrate removal efficiency was above 90% with negligible accumulation of NO_2^- and N_2O. This novel reactor configuration could be suitable to design AFMBR for the treatment of industrial effluents.

This chapter will be submitted for publication as:

J. Ernesto Ramírez, S. Esquivel-Gonzalez, Boris López-Rebollar, H. Salinas, J.R. Rangel-Mendez, Germán Buitrón, Francisco J. Cervantes, Swirling fluidization in an Anaerobic Membrane Bioreactor as antifouling technique, Journal of Membrane Science.

3.2 Introduction

Membrane fouling is one of the major challenges in membrane reactors, as poor reactor design can lead to high energy and chemicals demand to recover membrane permeability. Cake layer formation is considered as one of the main mechanisms of fouling in anaerobic membrane bioreactors [83–85] and usually membrane cleaning consists of backwashing and chemical cleaning [76]. Currently, several fouling control strategies are emerging to take care of fouling, such as aeration scouring, biological control, electrically-assisted cleaning, and application of nanomaterials-based membranes [77]. Another recent strategy is the fluidization of scouring agents in membrane bioreactors (MBR), in which the bulk recirculation suspends the media to produce a mechanical cleaning of surfaces through physical contact and shearing on the membranes [99] increasing the critical flux [91,95]. Circulation of particles around the membrane surface enhances the shear stress and prevents the deposition of solutes and foulants [146]. This has led to lower energy requirements in comparison with cross flow systems and gas sparging techniques [91,93,94,146]. However, upward fluidization commonly used to fluidize media in rectangular and cylindrical reactors has disadvantages, such as incomplete scouring along the membranes caused by an inconsistent fluidization [107]; thus, the new challenge is to create a more efficient fluidization.

During fluidization, the scouring agent crosses the boundary layer and hit the membrane surface removing and/or avoiding cake layer formation on the membrane; hydrodynamic turbulences or air bubbles hardly reach the membrane surface[94]. In addition, particle fluidization improves the back-transport of solutes in the polarization layer [97]. Kim et al. [99] developed the concept of particle fluidization using granular activated carbon (GAC) as scouring agent in an AFMBR; GAC was additionally used as supporting material for anaerobic microorganisms to improve the treatment process. The use of GAC prevented cake layer formation by its capacity of organic matter adsorption [100,101]; however, GAC could be saturated after long-term operation and thus must be replaced. This could increase the operational costs due to frequent replacement. Some investigations have been

performed to evaluate the effect of different factors, such as size and dosage of the media, adsorbing media capacity and process configuration [96,101,102]; which has been tested even at pilot scale [147]. Additionally, mathematical modelling has been developed with the aim to understand the scouring mechanisms on membrane fouling mitigation [87,88,148].

The appropriate use of fluid instabilities driven by the geometry of the reactor and membrane module configuration are factors that could improve the performance of membrane filtration [106]. Hydrodynamic conditions of the multiphase flow system prevailing in AFMBR depend on the geometry of the reactor, type of distributor of the media, membrane module configuration, media characteristics (size, shape, density, dosage), as well as the bulk medium conformation. Typically, the geometry of the reactors is cylindrical, which appears to allow better mixing than parallelepiped rectangle reactors [94], and have a distributor to improve the dispersal of the flow and scouring agents inside the reactor. The distributor consists of nozzles directed downwards in an inverted-V configuration and spread evenly along a central pipe traversing the reactor bottom [101,102,108]. Flow field in the reactors is predominantly in the upward direction and tend to be non-uniform vertically and laterally, which is reflected in a non-uniform control of fouling [107]. The manipulation in the distribution system could increase the flow velocity [110] or obtain a homogeneous shear stress [111]. Moreover, the movement of scouring agents inside the reactor also depends on the membrane module design. Spacing between hollow fiber membranes has been observed to enhance the surface shear stress, facilitating a homogeneous shear forces distribution along the membrane [96,112]. Additionally, flow shear stress increases the back transport of the particles away from the membrane surface, preventing membrane fouling [149]. Recently, hydrodynamic study in AFMBR has been implemented as a tool to understand the local behavior of both flow and GAC fluidization through the membranes and its relation to membrane fouling mitigation. Wang et al.[102] determined through the accelerometer signal response that, solid phase dynamics correlated well with the extent of fouling mitigation. In another work, the use of image analysis via the high-speed video camera technique to characterize the concentrations and particle

velocity of the GAC, determined that momentum transfer between the GAC particles and membrane was the key mechanism affecting the scouring to diminish the membrane fouling [108]. Some optical techniques are difficult to apply by the GAC concentration, but this can be solved with the CFD capacity. For instance, Cahyadi et al. [107] found an improved fouling control between the fouling rate versus particle momentum and water shear stress using CFD in a 2-D study. Notably, the reactor design and membrane configuration dictate the dynamics of the scouring media particles, which is closely related to the effectiveness of fouling mitigation. However, the manipulation of the hydrodynamic conditions around the membrane surfaces has been poorly evaluated, becoming an important area of research.

The aim of the present work was to develop an innovative Anaerobic Swirling Fluidization Membrane Bioreactor (ASFMBR) design to avoid membrane fouling while performing a denitrifying process. The biological process proved in this work was denitrification of an acidic synthetic metallurgical wastewater. The denitrification and filtration processes were studied in the same reactor following the next points: (i) hydrodynamic study of the ASFMBR system through the CFD modeling in three-dimensional (3D) system, previously experimental validated by PIV to describe the flow patterns and GC trajectories, as well as to determine the shear stress and GC momentum along the membranes; (ii) filtration and denitrification tests with the monitoring of the membrane fouling through the suction pressure and the concentrations of the total suspended solids (TSS) and soluble microbial products (SMP), usually assumed to be the major factors responsible for fouling in MBRs [86–88]; furthermore, denitrification was studied using citric acid (commonly present in metallurgical effluents) as electron donor with the evaluation of the nitrate removal efficiency and undesirable denitrification intermediates (nitrite and nitrous oxide) generation, as well as, the neutralization of the acidic feed in the reactor.

3.3 Experimental section

3.3.1 Bioreactor description

Fig. 3.1(a) presents the schematic diagram for the ASFMBR. The geometry is composed of conical (upper) and cylindrical (lower) sections, with a volume of 1.57 L. The inlet flow to the reactor was pumped by a centrifugal pump through a tangential inlet located in the lower part of the conical section (see Fig 3.1(b)), which together with the geometry, creates a swirling fluidization inside the reactor; the tangential inlet serves as diffuser of the scoring media. The recirculation flow rate was adjusted to 3.8 L/min to expand the GC in the entire reactor covering the membranes. Wash-out of GC particles was prevented by the hydrodynamic conditions and with traps located before the outlet of the recirculation line. These traps were designed according to Rios-Del Toro et al. [150]. The gas phase was recovered at the upper part of the reactor for N_2O measurements. The membrane module was submerged inside the reactor and the design consists of 18 polyvinylidene difluoride (PVDF) hollow fiber membranes (HINADA). The porous size and outer diameter of the membrane are 0.1 μm and 1.2 mm, respectively. A structure holds the membranes in vertical position, which were spaced among them in a star configuration as shown in Fig. 3.1(c). This arrangement was set with the aim to allow free scouring particles circulation around the membranes. The lower extreme of the membranes was sealed, and the other extreme was joined and connected to a peristaltic pump (MasterFlex) to produce a continuous permeate flux of 3.4 $L/m^2 \cdot h$. The permeate line was monitored with sensors of pressure (Pure palmer, Model C206) and flow (Alicat Scientific Model #: L-200CCM-D) and were connected to a computer with Lab-View application with a data acquisition card (National Instruments, Austin, USA). Biochar of coconut shell based granular carbon (from Carbotecnia) was used as scoring media and as denitrifying biofilm supporting material with three different mesh sizes: 8x14, 8x30 and 12x40 with a density of 0.909, 1.250 and 1.666 g/mL, respectively. This GC did not receive activation with

the aim to use a material with high mechanical strength and to reduce costs. The use of GC of different sizes and densities allowed its fluidization in the entire reactor.

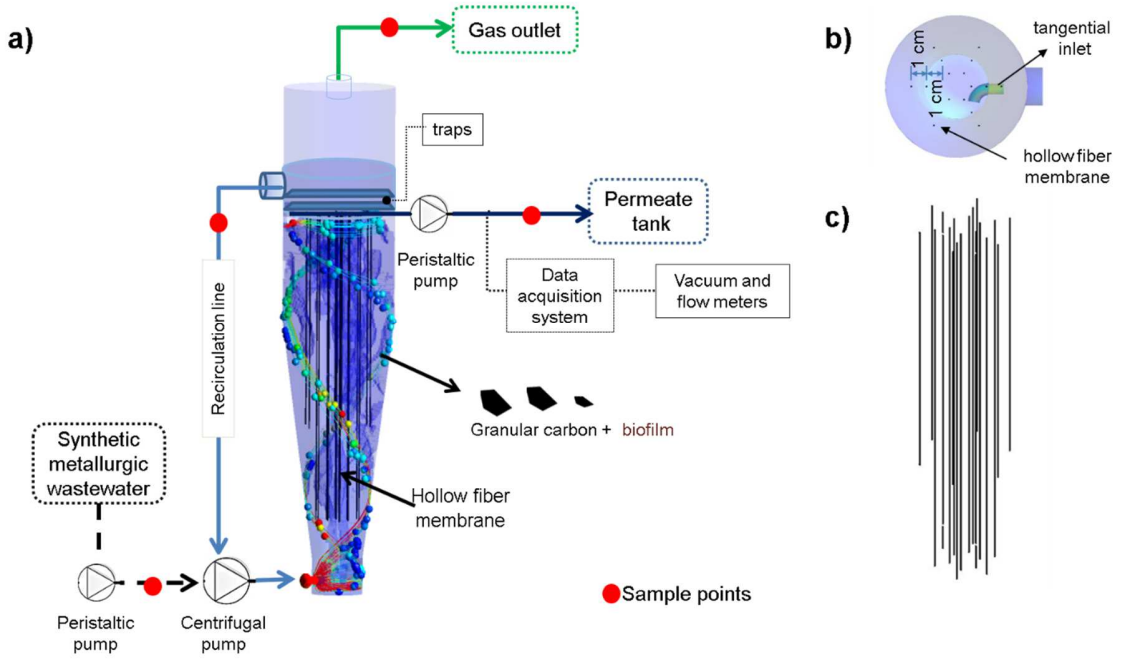

Figure 3.1 Schematic diagram of the ASFMBR: a) schematic set-up diagram of the ASFMBR; b) superior view of the ASFMBR and c) membrane module configuration.

3.3.2 Hydrodynamic study

3.3.2.1 Experimental study: Particle Image Velocimetry

Flow patterns within the reactor were experimentally obtained using the PIV technique [151] (Fig. 3.2(a)), for the cases with flow circulation in the presence and in the absence of the membrane module. Clean water was used with a recirculation flow of 3.42 and 3.54 L/min, and with an inlet pressure of 12.6 and 13.2 kPa, for experiments conducted without and with membranes, respectively. Polyamide particles with 25 μm of diameter and density of 1.03 g/mL were used as tracer particles. The region of analysis was lighting with a 15 mJ double pulsed Nd:YAG laser (New Wave, Fremont, USA); the exposure time of each light pulse was 0.4 μs. The light was driven through optical accessories (mirrors and lenses). Image capture

was carried out with a high-speed CCD camera (Pulnix Jai, Japan) model CV-M2CL equipped with a 50 mm AF Micro-nikkor lens (NIKON), which has a temporal and spatial resolutions of 60-250 fps and 1600×1195 pixels, respectively; the CCD pixel size was 7.4 μm. A synchronizer NI (trigger) was used to control the image acquisition sequence and light. An average of 50 pairs per run with separation times of 2 ms among images were recorded to obtain averaged values of velocity. Images processing and results visualization were carried out with PROVision XS and Tecplot 360 software. The axial and radial velocities were obtained through vertical captures at 5 heights and three depths, starting from the center of the reactor and separately 1 cm among them with the aim to cover the planes where the membranes were located (see Fig. 3.2(b)).

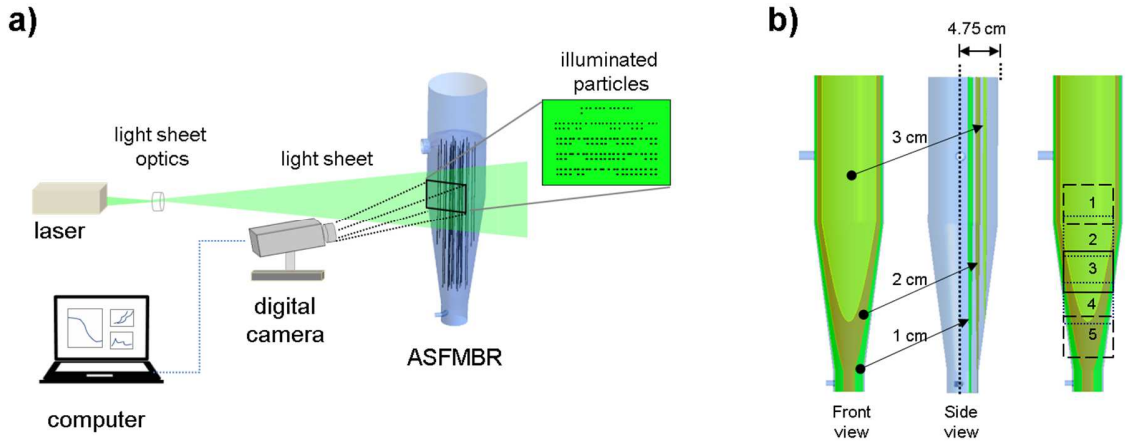

Figure 3.2 Particle image velocimetry: a) set-up of image acquisition system and b) vertical planes captured for 5 heights and three depths.

3.3.2.2 Numerical study: Computational fluid Dynamics

Numerical simulations were performed to validate experimental data with PIV results obtained with flow circulation in the presence and in the absence of the membrane module. After validations, simulation of particles fluidization was performed to determine the distribution, velocities, and momentum of the GC along the reactor. Figure 3.3 (panels a and b) shows the dimensions of the reactor model and the mesh

used to accomplish the numerical simulation. The mesh of the model and simulation were conducted with Ansys-Fluent R17.0 and the geometry of the reactor with Solid Works 2013. The minimum and maximum sizes of the unstructured tetrahedral mesh were $1x10^{-3}$ m and $8x10^{-3}$ m, respectively. The number of elements was 579,109, which corresponds to 645,424 nodes, with fine meshing near the walls of the membranes to capture the shear stress (Fig. 3.3(c)). The outlets of the recirculation line and biogas were established as pressure outlets, which allow the flow in both directions. The direction of flow was specified in normal direction to the boundary outlets and the intensity of turbulence was set at 5%. The operational pressure was established as the pressure at which the experimentation was conducted. Water properties of 0.998 g/mL of density and viscosity of 0.001 Pa s were used. Firstly, simulations of flow were performed under steady state conditions with the reactor filled with water at the start of the simulation. Reynolds Stress Model (RSM) was used as turbulence model and Volume of Fluid Model (VOF) was employed to obtain the interface between liquid and gas phases [152]. An explicit scheme of solution was used. The simulations were performed until reaching steady state conditions and when a swirling flow was developed in the entire reactor. Secondly, for simulations with GC fluidization, with the results obtained for flow circulation in the reactor with the membrane module, Discrete Phase Module (DPM) was enabled with the injection of particles and it was simulated under steady state conditions. For this case, the solid phase (GC) is sufficiently diluted (less than 10%). Thus, particle-particle interactions are negligible and the discrete phase formulation of Fluent can be utilized to obtain the GC modelling. Three injections were established with the characteristics of every GC mesh sizes, previously described.

3.3.3 Denitrification performance

The denitrifying biofilm formation over the GC particles was developed with the mixture of 50 mL of every GC mesh size portion and 150 mL of disintegrated anaerobic granular sludge (8% Volatile suspended solids (VSS)) collected from a

brewery factory in Sonora, Mexico, which was previously acclimated under denitrifying conditions in a column (1.1 L). Nitrate was added as KNO_3 while citric acid was added as electron donor, and a hydraulic retention time (HRT) of 1 day was established. The basal medium contained (mg/L): KH_2PO_4, 300; $MgSO_4 \cdot 7H_2O$, 61.3; $FeSO_4 \cdot 7H_2O$, 17.2; $CaCl_2 \cdot H_2O$, 75 and 1 mL/L of trace elements with the following composition (g/L): $MnCl_2.4H_2O$, 0.5; H_3BO_3, 0.05; $ZnCl_2$, 0.05; $CuCl_2$, 0.03; $Na_2MoO_4 \cdot 2H_2O$, 0.01; $CoCl_2 \cdot 6H_2O$, 0.5; $NiCl_2.6H_2O$, 0.01 and Na_2SeO_3, 0.01; and the pH of the feed was adjusted to 7 with NaOH as required. Biofilm formation was achieved after nearly 3 months at different hydraulic regimes: at the beginning, the operation was in batch mode, followed by a continuous operation with a HRT of 1 day, and finally in batch mode with high recirculation rate.

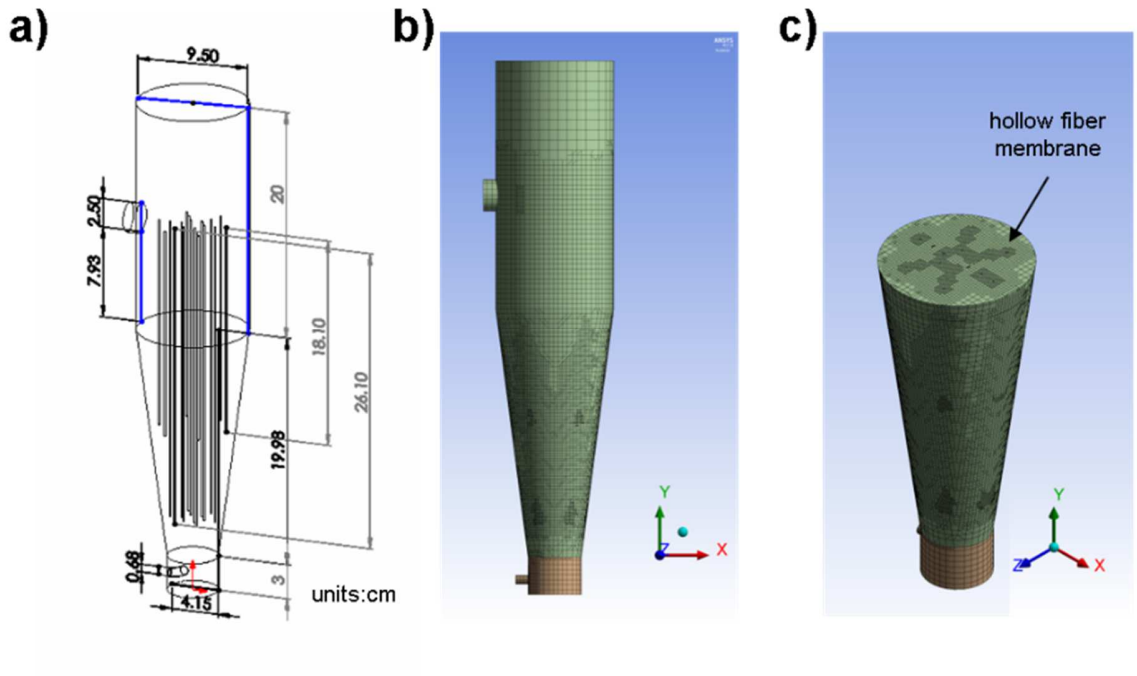

Figure 3.3 3-D model of the ASFMBR: a) geometry and dimensions of the model; b) meshing of the geometry and c) cut-away view showing the refinement mesh around the membranes.

For the reactor start-up, a volume of 150 mL of GC (0.56 g VSS/L) from the column of biofilm formation was added to the ASFMBR, which represents 9.55% of the volume of the reactor. All the solids were maintained in the reactor during the test and the HRT was set at 26 h. The synthetic metallurgic wastewater composition was fed with an acidic pH of 2.5, 500 mg N-NO_3^-/L and citrate in a ratio of 2.86 g C/g N. The mineral medium and trace elements added were the same used in the biofilm formation, previously described. Flows of the synthetic wastewater and permeate were established at the same value (1 mL/min) to maintain a balance in the AFMBR. These were adjusted to obtain a high nitrate removal efficiency and a pH neutralization of the acidic feed. Nitrate (NO_3^-), nitrite (NO_2^-), ammonium (NH_4^+), pH, TSS, turbidity, and SMP of the liquid phase in terms of proteins (SMPp) and carbohydrates (SMPc) were monitored in the reactor and at the permeate line. NO_3^-, NO_2^-, NH_4^+, TSS and VSS were measured according to the Standard Methods [130]. Turbidity was measured by a turbidimeter (2100N HACH) in nephelometric turbidity units (NTU). Measurement of pH was done using a pH meter (Thermo Scientific, Orion 4-star). N_2O was determined in the gas phase by gas chromatography (Agilent 6850 Series GC System) using a thermal conductivity detector at 250 °C. With a column 10’ × 1/8" SS packed with HayeSep D 100/120 mesh. The injector temperature was at 250 °C. Nitrogen was the carrier gas to 6 ml/min. 100 µl of sample was directly injected into the chromatograph. The VSS determination of the biofilm supported in the GC was achieved by the detachment of the biofilm of 1 g of GC in 10 mL of distilled water by ultra-sound treatment for 30 min, at the beginning and at the end of the test. For the control experiment without GC fluidization and at the end of the experiment with GC fluidization, the material on the membrane surface (cake layer) was carefully removed from a known membrane surface area at different heights and its composition of SMP was analyzed. The soluble concentration of proteins and carbohydrates were determined by the colorimetric method of Bradford [153] and Dubois [154], respectively.

3.4 Results and discussion

3.4.1 Numerical validation and general flow pattern

The flow field within the reactor is complex due to 3D whirlpool motion, but it is important because it largely determines the movement of the GC particles around the membranes. This was experimentally obtained with the PIV results and compared with numerical results to validate the CFD modelling for water circulation in the presence and in the absence of the membrane module. The experimental determination of flow patterns with GC fluidization was not conducted due to technical difficulties arising from the presence of GC on the PIV technique application. The flow patterns inside the reactor were driven by the conical-cylindrical body of the reactor and by the flow that enters tangentially on the lower part of the conical section. All these hydraulic conditions, in conjunction, produce streams curling upward. For this reason, the higher flow velocities occurred in the lower part of the reactor and subsequently decreased as the flow circulation went upward until reaching an equilibrium with the reactor outlet and the gas phase in the upper part of the reactor. Through the PIV images processing, the axial (y-direction) and radial (x-direction) mean velocities were determined (see Fig. 3.4 and 3.5). For the axial velocity, the positive values represent an upward flow, while the negative ones correspond to downward flow. Nearby the reactor walls, the planes located to 2 and 3 cm from the center of the reactor show a predominant upward flow, being predominant in the conical section and reduced in the cylindrical part. The plane nearest to the center has an upward flow only in the zones close to the walls and lower or negative values in the center, this means that the fluid flows upward along the reactor walls and downward in the central section. On the contrary, the radial velocity has the lowest values in the zones adjacent to the walls and the highest values at the center of the reactor; this velocity is related to the centrifugal force. At the beginning of the conical section, lower experimental values of velocity in comparison with the CFD results were obtained. This could be due to the high turbulence produced in this zone, which was hardly determined experimentally, while

in the cylindrical section and transition between cylindrical-conical section a good approximation was obtained.

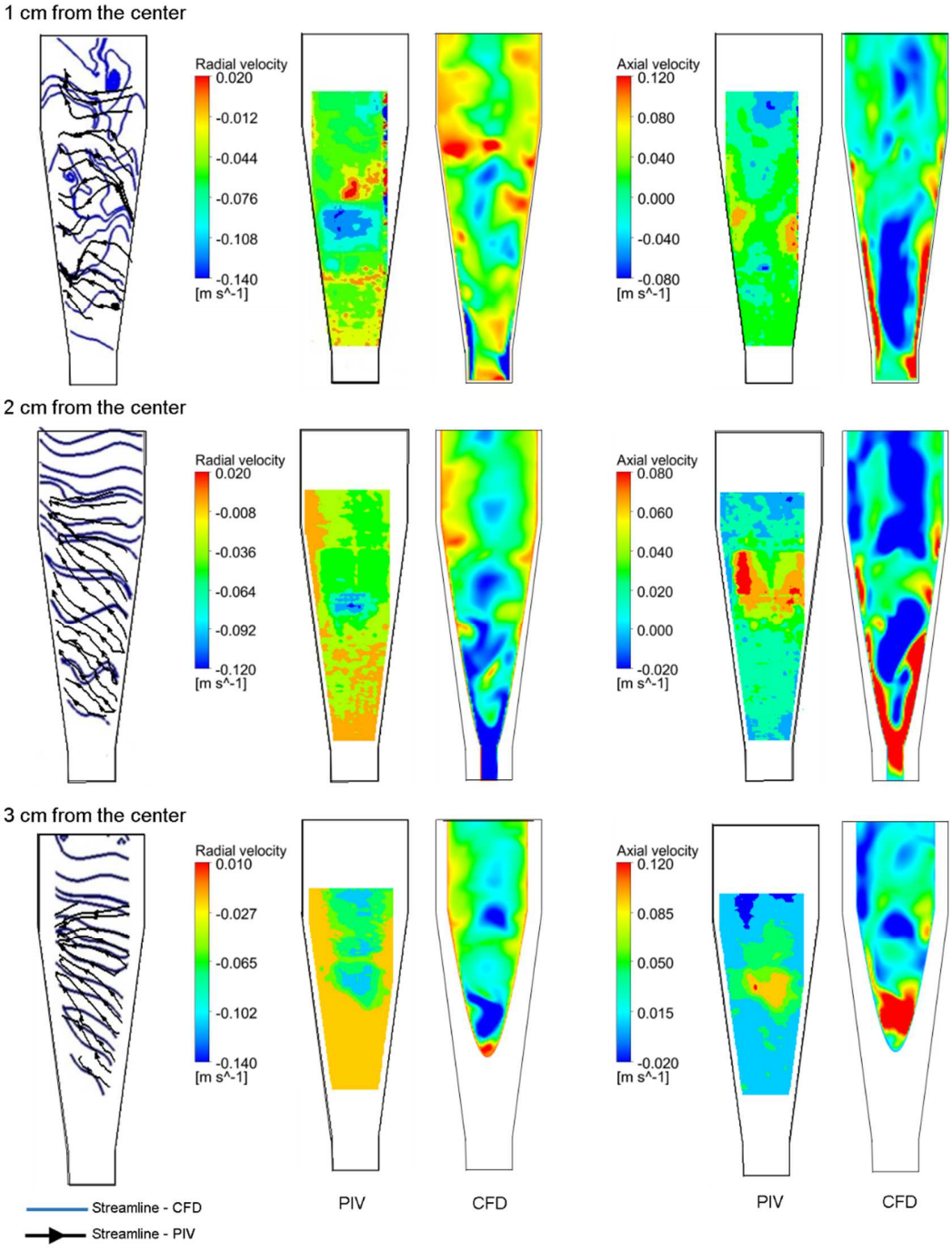

Figure 3.4 PIV and numerical results for flow circulation for the radial (x-direction) and axial (y-direction) mean velocities at the three vertical planes: 1, 2 and 3 cm from the center.

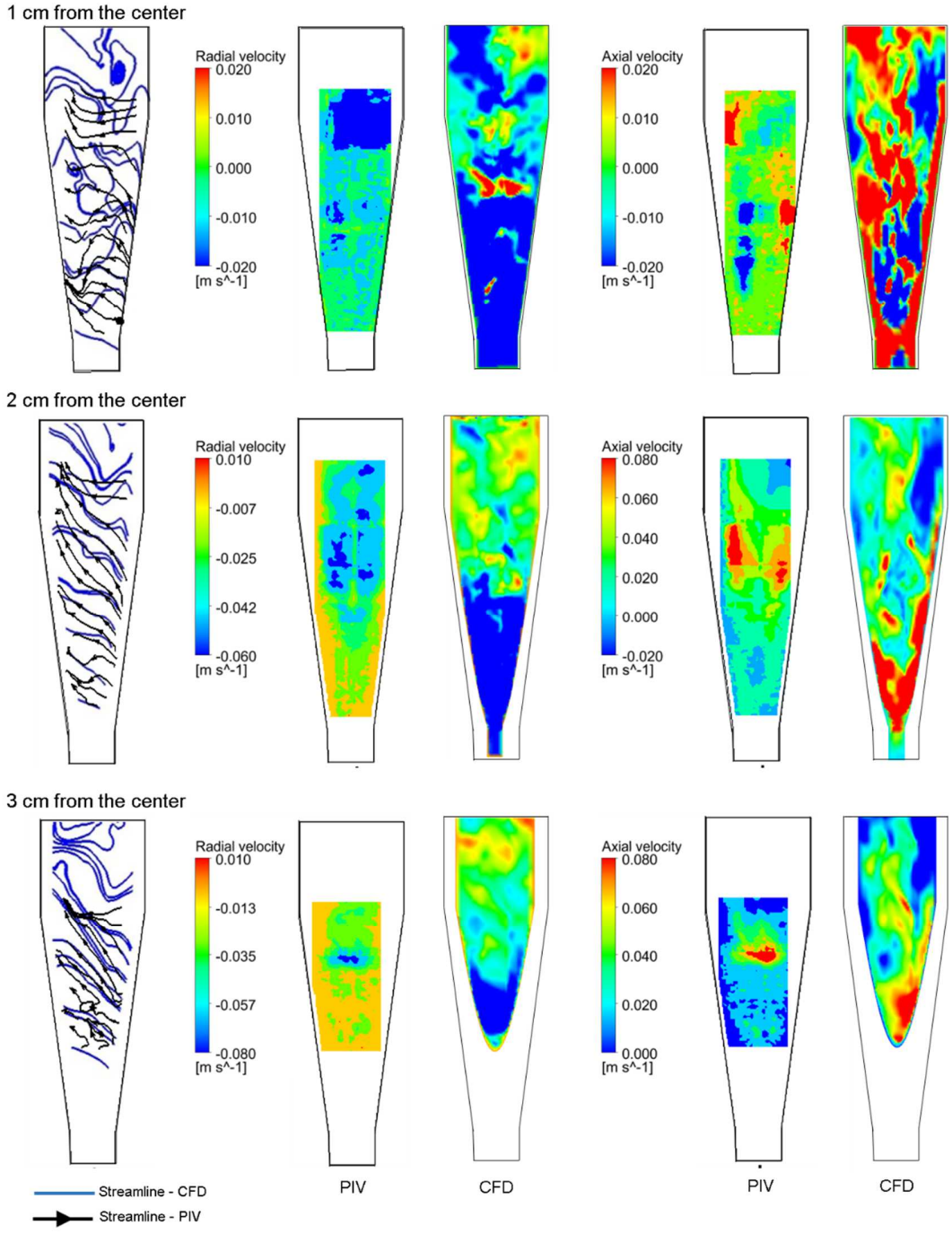

Figure 3.5 PIV and numerical results for flow circulation with the presence of the membrane module for the radial (x-direction) and axial (y-direction) mean velocities at the three vertical planes: 1, 2 and 3 cm from the center.

The insertion of the membrane module to the reactor decreased the turbulence observed in the lowest part of the conical section and increased the energy expenditure to maintain the fluidization. The change of energy expenditure is discussed more in detail below. Good agreement for experimental and numerical results was observed at 2 cm from the center with flow circulation and the membrane module included (Fig. 3.5). The zone including the upper part of the conical section and the cylindrical section shows good agreement between CFD and PIV results. A range of -0.025 to -0.060 m/s for radial velocity and 0.04 to 0.08 m/s for the axial velocity were founded for both experimental and numerical results. Furthermore, the streamlines show a good agreement of flow behavior between both results However, at the down part of the conical section, the numerical results were higher than the results obtained experimentally. The radial velocities obtained experimentally were in a range of -0.025 to -0.042 m/s, while values of -0.06 m/s were determined for numerical results. For axial velocities, values of 0.04 m/s were determined experimentally and 0.08 m/s numerically. In general, the upward flow occurred in the zones close to the reactor walls, starting in the conical section until reaching the cylindrical part of the reactor and the flow that entered in the central part of the reactor acquired downward streams. When the descending flow reached the lower zones of the reactor, it newly started to go upward by the zones close to the walls. This behavior creates swirling fluidization. Numerical results agreed with the experimental data of flow patterns, showing that the RSM model is suitable for modeling the hydrodynamic pattern inside the reactor, which has been used by other authors to simulate the flow pattern in hydrocyclones with good accuracy [152]. At the beginning of the conical section, the velocities were hardly represented; nonetheless, the numerical values obtained agreed with the expected flow behavior inside the reactor.

3.4.2 Granular carbon fluidization

The mean flow velocity contours obtained with GC fluidization are presented in Fig. 3.6. It was observed a modified flow pattern with respect to the results obtained with water circulation without GC particles, mainly related to radial and axial directions. The axial velocity shows an upward flow at the right of the reactor and a descendant flow in the left part of it, both in the conical and cylindrical sections, with velocities of 0.25 m/s at the beginning of the conical section, which was highly decreased to 0.10 - 0.15 m/s in the conical part and reached 0.05 m/s in the cylindrical section. These observations applied for both the upward and downward flow. Meanwhile, the radial flow has two behaviors, it prevailed towards the reactor walls at the external zones and went to the central part of the reactor in the middle of the reactor. The velocities in this direction were lower compared with the axial pattern. Moreover, higher velocities were determined in the conical section, with values close to 0.16 m/s, which decreased to a range of 0.06-0.09 m/s in the middle conical body of the reactor, and finally, the velocity decreased to 0.03 m/s at the cylindrical part. For the tangential velocity (z-direction), the flow behavior was maintained along the height of the reactor and the velocity was gradually decreased from 0.20 to 0.010 at the conical section and further reduced to 0.05 m/s in the cylindrical part (Fig. 3.6(b)).

The flow tangentially entering at the lower part of the conical section suspended the GC particles. The high flow velocities in this zone rose the particles close to the walls of the conical section and then descended until the flow velocity was reduced to a lower value of the minimum velocity of the GC fluidization or when the GC got into a downward stream. During the downward trajectory of the GC, it could enter an upward stream with enough velocity to be newly fluidized. This cycle maintained the particles in constant circulation with swirling trajectories through the reactor; the particle tracking is shown in Fig. 3.7. Fluidization of different sizes and densities allowed the movement of GC particles in the whole reactor covering the membranes, and their distribution was a function of these characteristics. A segregation of GC was observed, with circulation of the higher and medium sizes mainly in the cylindrical section, while particles with the lowest size fluidized in the entire reactor

with a predominant circulation in the cylindrical section. Similar GC size distribution was hypothesized in upward fluidization [105]. The diameter of GC particles has a high influence on the centrifugal force; the outward centrifugal force on the GC particles pushed them towards the walls of the reactor. For large particles, the drag force was lower than the centrifugal intensity. As the GC particles size decreased, the drag force gradually increased, which could be observed in the distribution of the GC sizes along the reactor (see Figures 3.7 and 3.12).

Regarding the density of GC particles, denser GC particles circulated in the conical section, followed by those having medium density, which circulated in the conical section and in part of the cylindrical one, while GC particles with lower density moved throughout the entire reactor (Fig. 3.7). The higher GC velocities were observed with GC particles with density of 0.909 g/ml, followed by those having a density of 1.250 g/mL and 1.666 g/mL, at the lower part of the conical section. The maximum axial GC velocity was 0.21 m/s, 0.15 and 0.13 m/s, for the three GC densities described, respectively. Moreover, the radial velocity was 0.29 m/s, 0.15 m/s, and 0.24 m/s, while the tangential velocity was 0.22 m/s, 0.21 m/s and 0.08 m/s, for the same densities, respectively. This could be explained because drag force depends on the difference of densities between the GC particles and the liquid phase, being higher for the lighter GC particles. This promotes high fluidization of the lighter GC particles, while low distribution occurs for the heaviest GC particles. These velocities were decreased with the height of the reactor; for instance, axial and radial velocities decreased to values lower than 0.15, while tangential velocity decreased to values lower than 0.10 at the end of the conical section. Meanwhile, velocities were lower than 0.06 m/s in the cylindrical section. Flow velocities are therefore higher in the conical section and decrease with the height of the reactor and with the increase of the diameter of the cone. The most remarkable reduction occurred during flow circulation by the cylindrical section. Then, the direction and magnitude of the hit GC-membrane wall depends on the position of the membrane in the reactor and the trajectory of the GC; one particle can hit different membranes in different positions during its circulation through the reactor.

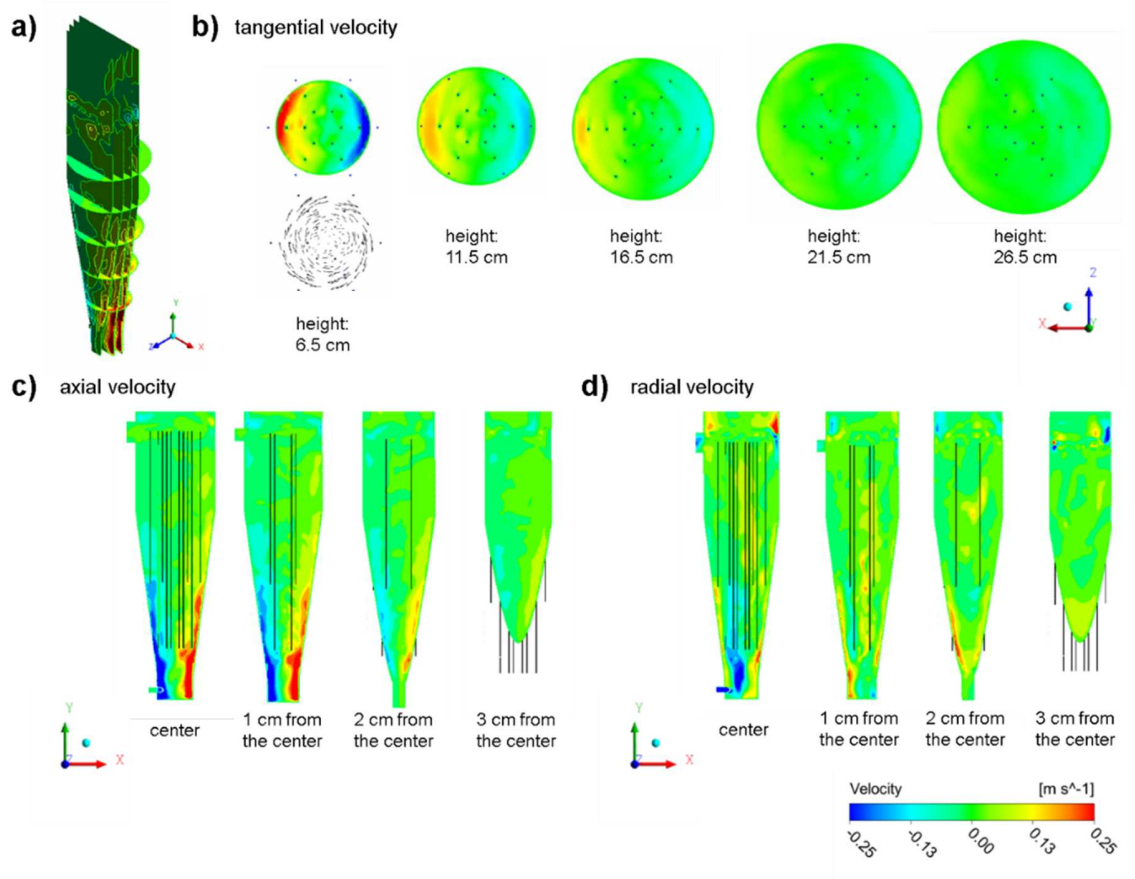

Figure 3.6 Contours of mean flow velocity: a) vertical and horizontal planes; b) tangential velocity to different heights of the reactor; c) axial and d) radial velocities to different depths of the reactor.

In rectangular reactors, GAC particles with sizes from 1.01 to 1.85 mm where fluidized with axial flow velocities from 0.02 to 0.06 m/s [108]. For cylindrical reactors, velocities in the range of 0.0135-0.0407 m/s were used to the fluidization of GAC sizes from 0.15 to 3 mm [87]. These values of axial flow velocities were found in the cylindrical part of the ASMFBR with fluidization of GC sizes lower than 1.68 mm. A variance of this work with the upward fluidization is the difference between the flow velocity and GC particle velocities. Cahyadi et al. [107] reported axial flow velocities with values lower than 0.12 m/s to produce GAC velocities lower than 0.06 m/s, this for sizes between 1.25 and 1.85 mm. In the present work, GC sizes up to 2.3 mm were dragged with axial flow velocity of 0.12 m/s, and the GC acquired approximately the same velocity as the flow velocity. For upward fluidization, the GC are in upward

and downward movement predominantly, while with swirling fluidization, the GC is dragged by the fluid trajectory. The GC mean velocities are presented in Fig 3.8.

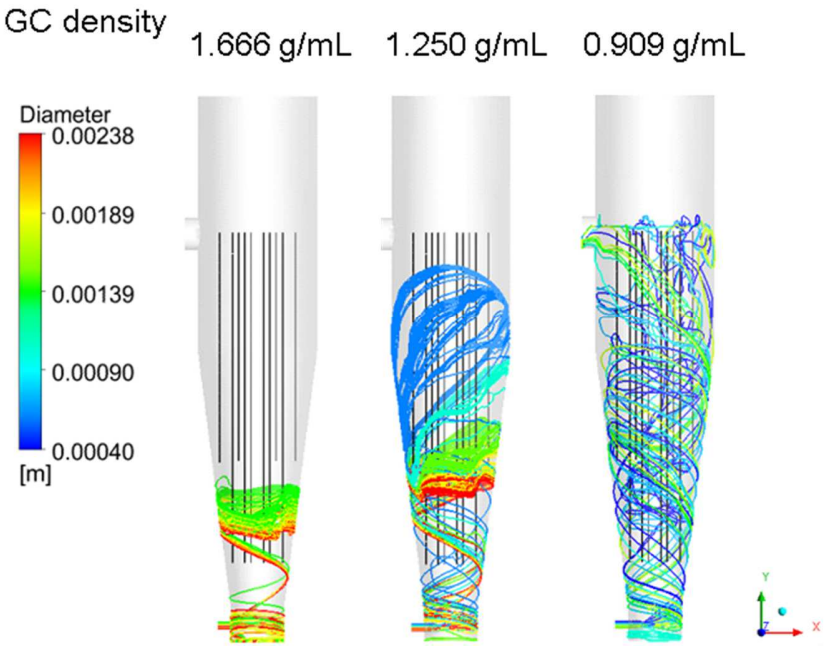

Figure 3.7 Particle tracking for the fluidization of GC particles with different densities and sizes in the ASFMBR.

3.4.3 Water shear stress and particle momentum

The contribution of both water circulation around the membranes and GC fluidization to membrane fouling mitigation can be represented by the water shear stress and the GC momentum [107]. Swirling fluidization produces GC circulation in the entire reactor; however, in agreement with the SMP results found in the membrane surface at different heights of the reactor, foulants were attached to the membrane walls (Fig. 3.9). The water shear stress (τ_w) along the membrane walls was determined by the normal velocity gradient ($\frac{\partial v}{\partial n}$) at the membrane wall, multiplied by the dynamic viscosity of the water (μ) with the following expression [107]:

$$\tau_w = \mu \frac{\partial v}{\partial n} \qquad (3.1)$$

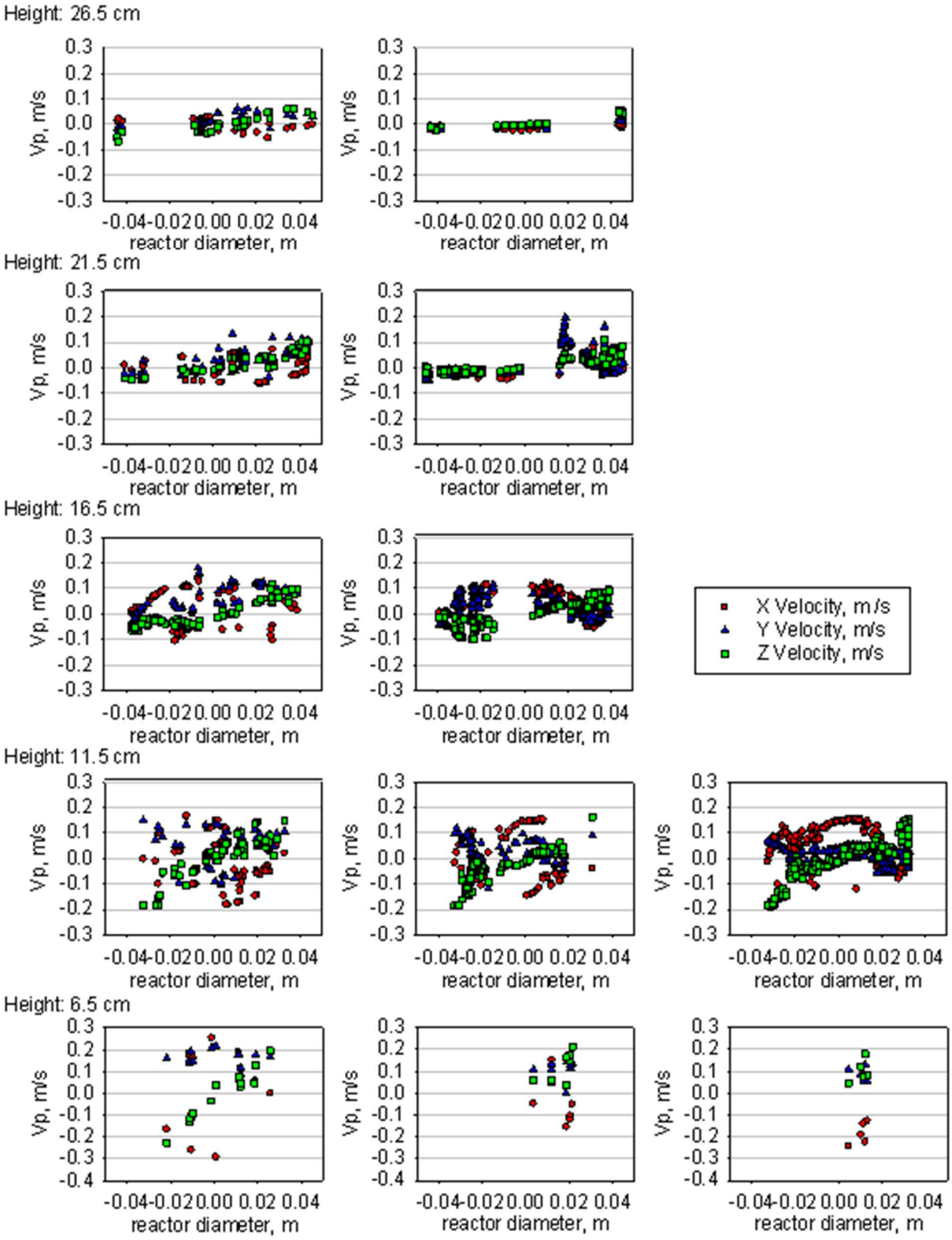

Figure 3.8 GC mean velocities in axial (x-direction), radial (y-direction) and tangential (z-direction) direction at different reactor heights.

SMP deposition was mainly observed at the height of the membranes located in the cylindrical part of the reactor, while lower values of SMPp and SMPc were determined in the conical part, which agrees with the higher water shear stress values obtained by numerical simulation (Fig. 3.10). The maximum stress was obtained in the lower and middle part of the conical section of the reactor and then increased from the center of the reactor to the walls. This is because higher velocities were observed in lower part of the reactor and in the zone close to the reactor walls. At the cylindrical section, the stress decreased because of the loss of flow velocity in this zone, but it was maintained at the external zones, which corresponds to the membrane beyond the center of the reactor, which is due to the axial and tangential velocities that were maintained at this height of the reactor.

The main stress contributions were determined in the tangential direction and at the external membranes of the reactor, which was caused by the tangential inlet that created an important rotational fluidization. The second important contribution was in the axial direction, mainly inward the reactor, where downward flow occurred, whereas low contribution was obtained in the radial direction. The present work has a range of shear stress between 0.09 and 0.14 Pa at the conical section, and between 0.018 and 0.11 Pa at the cylindrical part. For rectangular and cylindrical reactors, the principal shear stress is obtained in axial direction. Cahyadi et al. [107] reported for a rectangular reactor, values lower than 0.010 Pa at the zones close to the reactor walls, and lower than 0.005 Pa in the middle of the reactor. Similar results were obtained in the present work at lower velocities for the axial shear stress in cylindrical section, with values in the range from 0.007-0.090 Pa, in addition to the tangential shear stress contribution. The obtained higher shear stress helped to enhance the back-transport of particle and thus reduce the SMP adherence to the membrane surface.

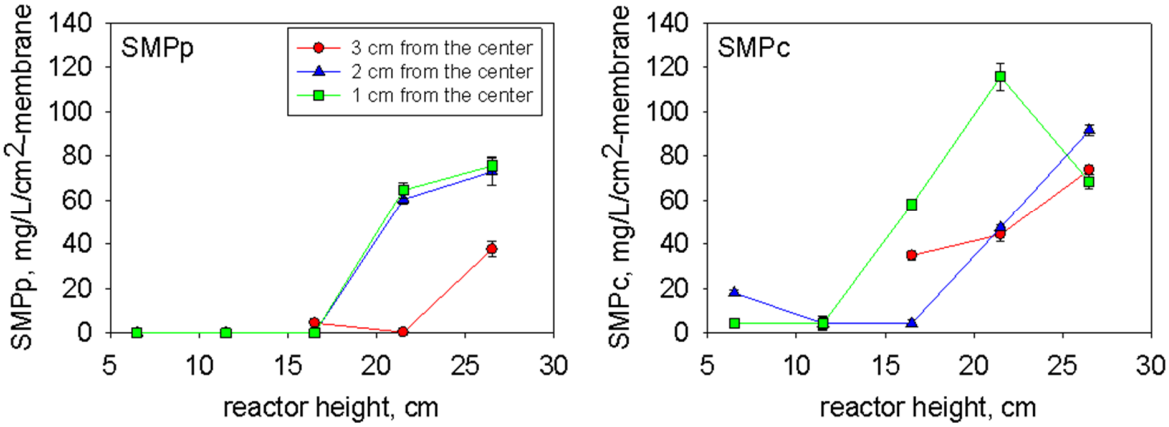

Figure 3.9 SMPp and SMPc deposited on the membrane wall at different heights and depths of the reactor (1,2 and 3 cm from the center of the reactor).

The role of GC fluidization on preventing membrane fouling has been described by means of particle momentum (ρ), which relates the mass (m) and velocity (Vp) of GC particles by the next expression:

$$\rho = mVp \qquad (3.2)$$

Particle momentum transfer has been observed in good agreement with fouling trends [107,108]. This was determined to know the amount of momentum that can be transferred by the hit of GC particles with membrane walls along of the reactor (Fig. 3.11). As previously mentioned, GC fluidization has a stratification in agreement with the GC particles size, but principally by their density. The highest particle momentum was found in the heaviest GC particles, which have poor fluidization. This was obtained in the zones with higher flow velocity, necessary to cause particles fluidization. As a result, maximum momentum values were lower than 4.8×10^{-7} kg m/s. Lighter GC particles, which have a fluidization in the entire reactor, showed the highest momentum in the conical section of the reactor with a maximum value of 3.6×10^{-7} kg m/s. Both GC densities showed high momentum values in the reactor and predominantly in the conical section. Particularly, a GC momentum of 2.6×10^{-7} kg m/s was obtained by GC particles with a diameter of 1.68 mm and a density of 0.909 g/mL at a height of 11.5 cm of the reactor. Likewise, a similar momentum magnitude was obtained by GC particles with density of 1.666 g/mL, diameter of 1.62 mm and at height of 16.5 cm of the reactor. The difference between them was

the velocity of the particle. While the heaviest GC particles have poor fluidization, the lighter GC particles can gain high velocity and offer the same magnitude of momentum at different height. This is due to the higher drag force that cause their movement more easily and give momentum to the GC particles.

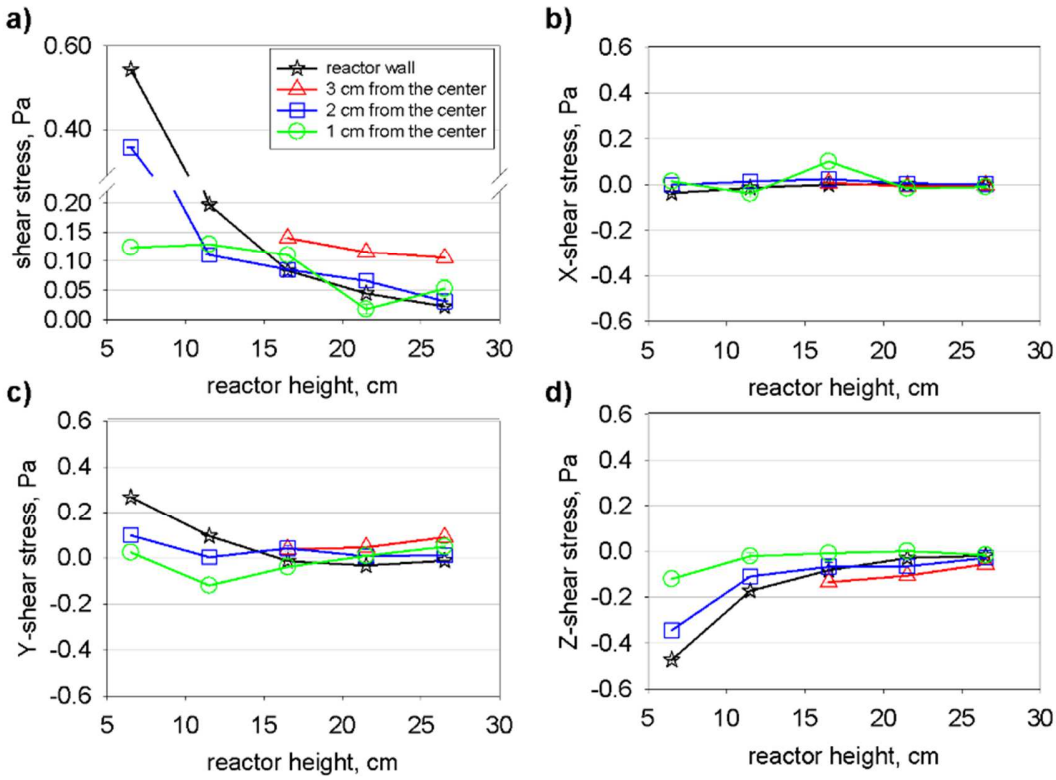

Figure 3.10 Membrane wall shear stress at different heights and depths of the reactor (1,2 and 3 cm from the center of the reactor: a) shear stress; b) X-shear stress; c) Y-shear stress; d) Z-shear stress.

On the other hand, fluidization of GC particles with a density of 1.250 g/mL occurred in the entire reactor; nevertheless, a lower amount of momentum was determined (less than $0.5x10^{-7}$ kg m/s) with respect to the other densities of GC, even when larger GC particles were fluidized. The most remarkable difference was observed in the second height (Fig. 3.11). In contrast, many works showed that higher particle size allowed better scouring effect and higher fouling mitigation [101,102]; although some reports mention that larger GAC particles can cause membrane damage [105] and require more energy to be fluidized [101,107], whereas for lower sizes of

scouring media (less than 0.7 mm) low momentum was determined and some works have been reported that sizes from 0.18 to 0.5 mm could contribute to membrane fouling [87]. However, in the present study, no fouling was observed even with fluidization of particles with low GC sizes, which could be due to the hydraulic conditions promoted by the swirling fluidization.

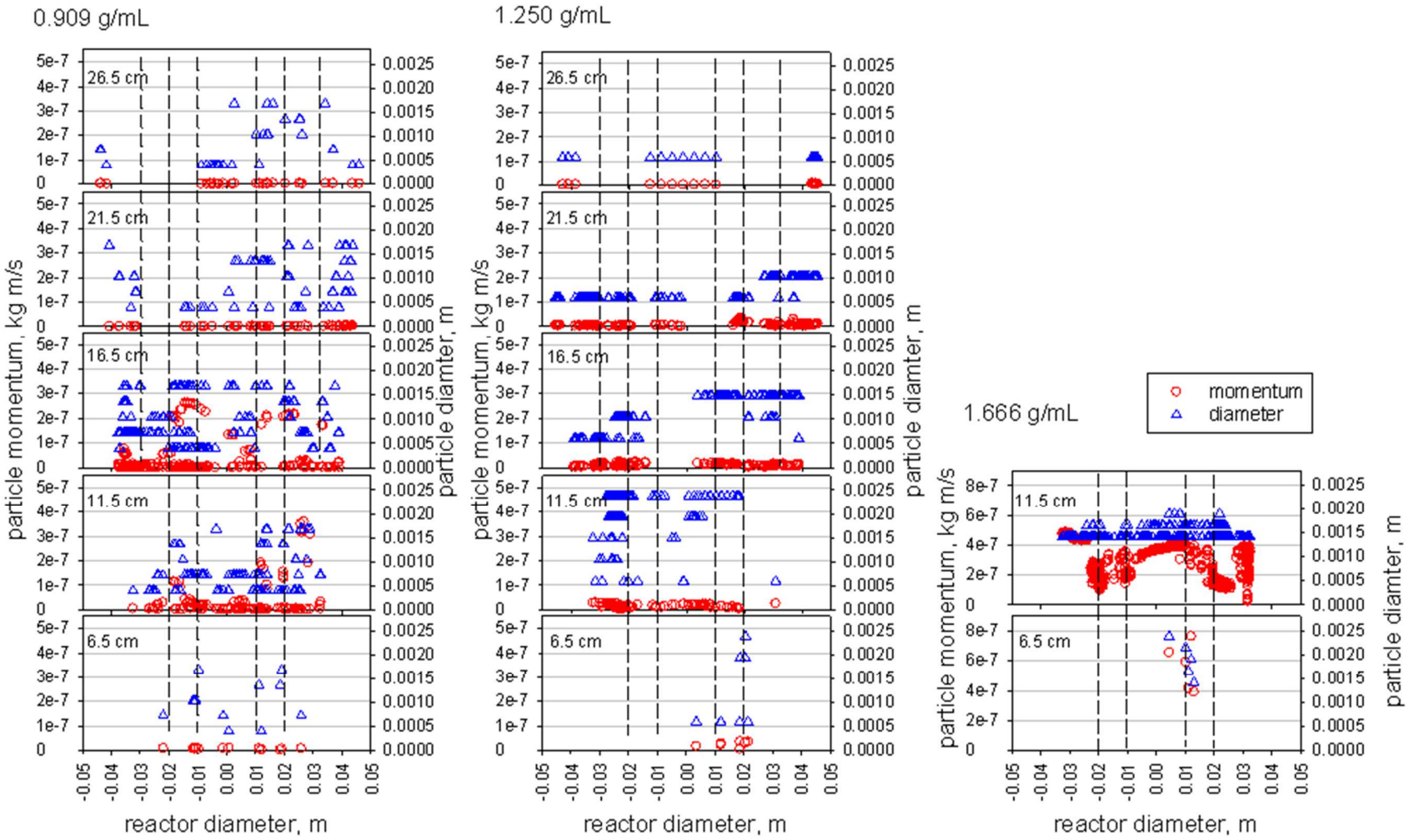

Figure 3.11 Particle momentum and diameter distribution at different heights of the membranes for every GC density. Dash lines represent the membrane position.

Particle momentum contributed over the three directions of the flow (Fig. 3.12). For the heaviest GC particles, the principal momentum occurred in radial and tangential directions, which is reasonable for the low upward fluidization. Meanwhile, for the lighter GC particles, the main momentum contribution occurred in the axial and tangential directions in the conical section and it was maintained in axial direction with the height of the reactor. This explains its contribution at the upper part of the reactor. In general, the obtained values of momentum are: for GC particles with density of 1.250 g/mL and sizes between 0.5-2.4 mm, the momentum was lower to $4x10^{-8}$ kg m/s, while particles of 1.0-2.6 mm and density of 0.999 g/mL showed a particle momentum from $1x10^{-7}$ to $4x10^{-7}$ kg m/s, and lower to $10x10^{-7}$ kg m/s for particle sizes between 0.4 and 0.7 mm. The highest momentum was obtained for GC particles with density of 1.666 g/mL and diameter of 1.4-2.4 mm, with momentum in a range of $4x10^{-7}$ to $7.7x10^{-7}$ kg m/s. The present study obtained lower momentum values than Cahyadi et al. [107]. These authors determined, in a rectangular reactor, momentum values from $1.5x10^{-5}$ to $7x10^{-6}$ kg m/s for GAC sizes from 1.2 to 1.85 mm, whereas, in a cylindrical reactor [87], the values reported were $6.66x10^{-10}$ kg m/s for GAC sizes of 0.18-0.5 mm and $1.50x10^{-7}$ to $7.95x10^{-7}$ kg m/s for sizes between 1.6 mm and 2-3 mm, respectively. These works determined the GAC momentum in agreement with particle concentration, which is obtained at a higher packing ratio than the present study. Moreover, Cahayadi et al. [107] reported that zones of the reactor with maximum values of particle momentum were predominant at lower shear stress and zones with higher shear stress had lower particle momentum. Unlike the present work, both maximum shear stress and GC with the highest motion energy coexist in the same height of the reactor. This could be due to the lower GC concentration and high flow velocities prevailing in this zone, which promoted concomitant high flow velocity (high shear stress) and high particle fluidization. Thus, hydrodynamic engineering can increase the shear stress at the membrane walls and maintaining high particle momentum with stable GC fluidization.

3.4.4 Bioreactor performance

Experimentation was performed in two periods, the first one (days 0-15) was conducted to determine the feasibility to carry out the denitrification process by means of a denitrifying biofilm supported in GC particles under swirling fluidization. At the startup, the bioreactor was supplied with 50 mg $N\text{-}NO_3^-$/L in batch mode at a pH of 7. This initial step was intended to increase the pH through the products generation from denitrification (see equation (3.3)). After reaching a pH close to 8, the acidic metallurgic wastewater was fed to the reactor. The pH was slightly low in the first days of operation, but increased to 8 afterwards, which is satisfactory for a good denitrification performance. Neutralization can be explained by equations 3.4 and 3.5. According to the CO_2 equilibrium, neutralization of citric acid occurs by the formation of bicarbonate or carbonic acid species; the intrinsically produced alkalinity avoids the addition of external neutralizing agents.

$$C_6H_5O_7^{3-} + 3.6NO_3^- + 0.6H^+ + 0.2H_2O \rightarrow 6HCO_3^- + 1.8N_2 \qquad (3.3)$$

$$(H^+)_3(C_6H_5O_7^{3-}) + 3CO_3^{2-} \rightarrow C_6H_5O_7^{3-} + 3HCO_3^- \qquad (3.4)$$

$$(H^+)_3(C_6H_5O_7^{3-}) + 3HCO_3^- \rightarrow C_6H_5O_7^{3-} + 3H_2CO_3 \rightarrow C_6H_5O_7^{3-} + 3CO_2 + 3H_2O \qquad (3.5)$$

During the first days of operation, nitrate removal efficiency was 50% without accumulation of intermediates (Fig 3.13(a)). However, this increased to >90% with marginal accumulation of intermediates. These results show that the denitrification process can be carried out through the swirling fluidization with high nitrate removal, low intermediates generation and intrinsic control of pH by the alkalinity produced from the denitrifying process.

After denitrification reached steady state conditions, the membrane module was installed into the reactor to carry out denitrification and filtration at the same time (days 16-39). To achieve fluidization of the bioreactor, recirculation rate was increased from 2.5 to 3.5 L/min, which was necessary due to the loss of energy caused by friction of flow and GC with the membranes. In the first days of this stage,

nitrate removal efficiency decreased until reaching 60%, but then recovered values above 90% after a few days of operation (Fig. 3.13(a)). The maximum intermediates production observed was 2.4 mg $N\text{-}NO_2^-/L$ and 3.6 mg $N\text{-}N_2O/d$, and the pH remained at an average value of 8.5. Ammonium was not detected during the whole operation period. Thus, the hydrodynamic conditions prevailing in the bioreactor promoted good mass transfer conditions to achieve high denitrifying efficiency.

The VSS content of the biofilm formed on GC particles was measured at the beginning and at the end of the experimentation for GC particles located both at the conical and cylindrical sections during fluidization. At the startup, in the cylindrical and conical parts of the reactor, the VSS content was 7.4 and 4.3 mg VSS/g-support, respectively, while at the end of the test, these values decreased by 17.6 % in GC located in the cylindrical part and 25.6 % in GC that circulated in the conical section. This may be explained by the regimes of GC fluidization in both zones. In the conical section, both the GC velocity and GC momentum are higher compared with the conditions obtained in the cylindrical section. The shear stress exerted between the biofilm and water flow is low because GC is dragged by the flow circulation, which gives a very similar velocity between them and low shear stress; with exception to the heaviest GC that has poor fluidization. Thus, the pounding between GC-biofilm and the membranes could detach the biofilm with lower adherence, while maintaining the stronger biofilm formed. This could reduce the change of density of the biofilm-support caused by the increase of biomass in the support, as has been observed in FBR at denitrifying conditions [155]. Further research is needed to know the effect of the swirling fluidization on biofilm characteristics since hydrodynamic conditions can modify the properties of the biofilm and determine the mass transfer regime. Lakshmi and Setty [156], found that the mass transfer increased with increasing biofilm thickness and decreased with increasing flow rate in a denitrifying fluidized bed reactor. Moreover, even the type of microorganisms attached to the support could change by the shear forces rate in denitrifying fluidized bed reactors [157].

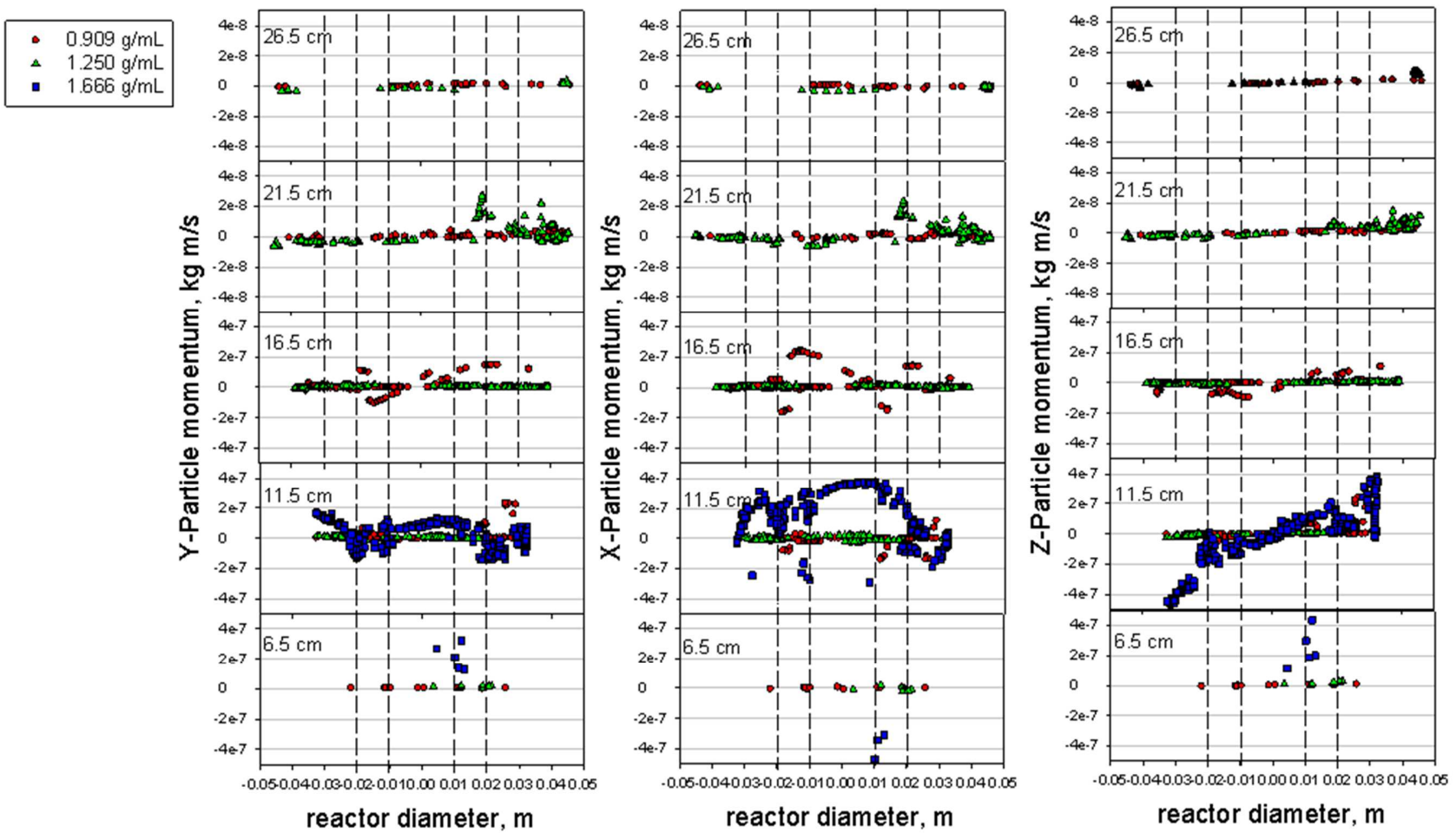

Figure 3.12 Particle momentum at different heights of the reactor for the three densities of GC (0.909 g/mL; 1.250 g/mL and1.666 g/mL) in the three directions of flow: y-direction; x-direction; z-direction.

For the filtration performance, accumulation of solids occurred over time due to biomass generated from the denitrifying process and the solid rejection by the membranes. The degradation of citrate through the denitrification process implies the production of SMP by the microbial growth or subsequent cell decay and lysys, whose presence of proteins and carbohydrates in the medium would make serious contributions to membrane fouling [86,158] due to their interactions with the membrane surface, which are both a hydrodynamic and thermodynamic process [159]. In addition, the composition of the medium in this work could create a conditioning layer which might have promoted attachment of microorganisms to the membranes [160]. The concentrations of SMP in the reactor increased during the operation, and at the end of the operational period, the values obtained for SMPp and SMPc were 156.4 mg/L and 237.01 mg/L, respectively (Fig. 3.13(b)). The average percentage of SMPp and SMPc rejected by the membranes were 87.5 and 91.3%, respectively, while the turbidity was reduced above 99%. Likewise, 91% of TSS was rejected by the membranes and the amount inside the reactor was maintained around 490 mg/L during the entire test. This could be due to the drag of solids to the upper part of the reactor by the swirling fluidization, where the solids can be settling in the traps located in the upper part of the reactor; thus, this fluidization prevents the accumulation of solids in the reactor.

Respect to the SMP deposited at the membrane walls, the higher shear stress and particle momentum are in agreement with the lower amount of carbohydrates and proteins deposited at the membrane walls in the conical section; however, for reactor heights above 15 cm, the shear stress and particle momentum were diminished and the SMPs deposition on the membrane increased. However, no change of suction pressure was observed, which could mean that more permeate flux can be achieve in the membranes without foulants deposition. The highest concentration of SMPc was 115.8 ± 6.2 mg/cm^2, which is lower in comparison with the control experiment (filtration process without fluidization), where suction pressure reached a difference of nearly 20 kPa in 34 h of operation. In this experiment, the cake layer had a concentration of 294.3±10.2 mg/cm^2. In contrast, the SMPp reached a value of 43.3±2.3 mg/cm^2, whereas for the experiment with fluidization, it reached 60 mg/cm^2.

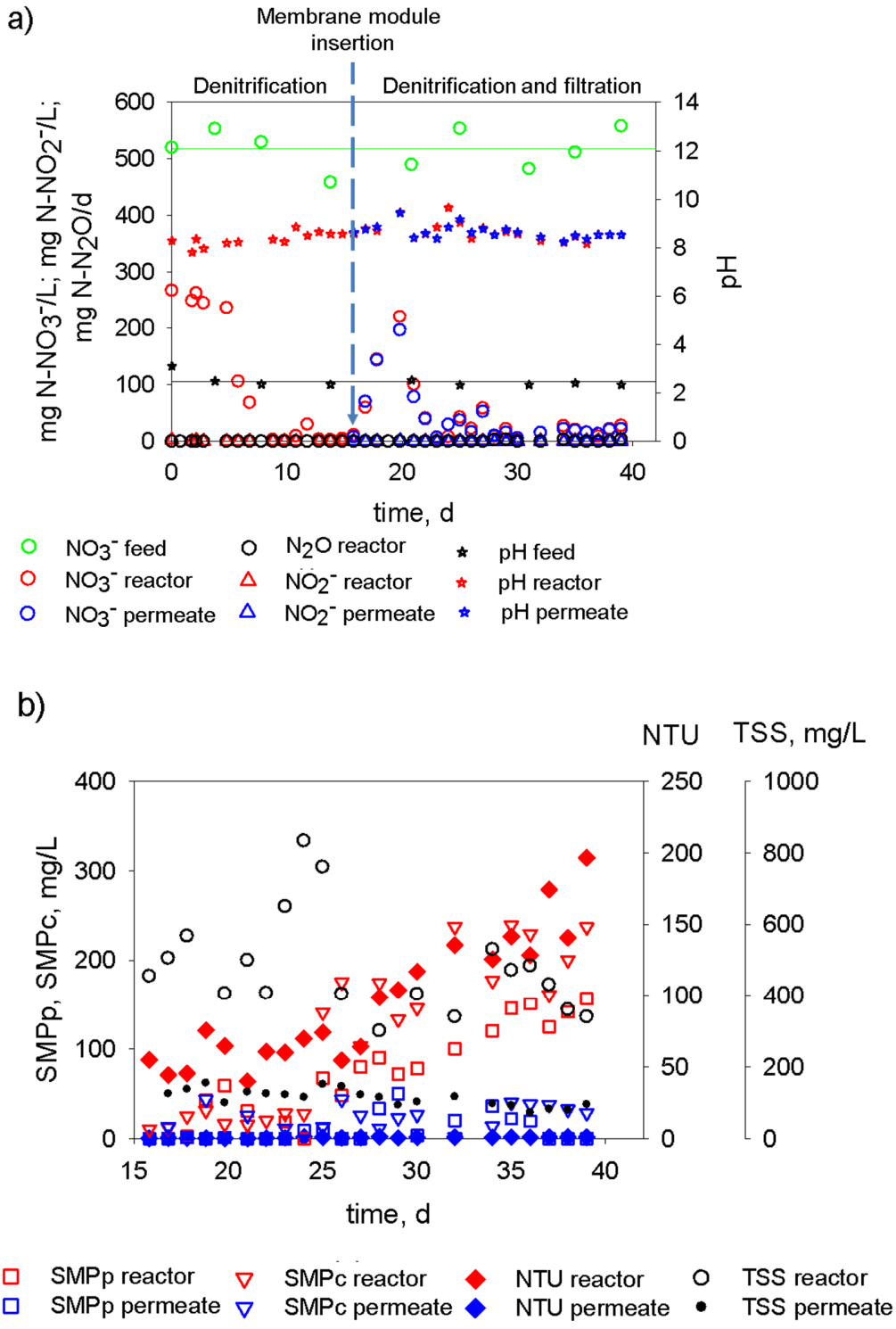

Figure 3.13 (a) denitrification performance with swirling fluidization for the two stages of operation: denitrification, and denitrification with filtration at the same time; (b) monitoring of parameters influencing in filtration performance.

However, no change in the suction pressure was obtained during the operation. The presence of SMPc is in agreement with other studies reporting SMPc as the main cause of membrane fouling [79,86,91,161] and they are hard to remove after chemical and physical cleaning [160]. Despite the accumulation in the reactor by its membrane rejection, no change in suction pressure was observed, which could be due to the swirling fluidization maintaining the solids in constant fluidization. Furthermore, GC fluidization and water shear stress prevented the deposition of foulants on the membrane walls, especially at the conical section where higher shear stress and particle momentum prevailed.

3.4.5 Energies of fluidization and suction extraction

The power required (P_r in kW) to fluidize GC particles is given by:

$$P_r=\Delta P_{bed}Q \quad (3.6)$$

where ΔP_{bed} is the pressure drop across the liquid–solid fluidized bed (kPa) and Q is the volumetric flow rate (m^3/s). The power requirement per permeate unit (Pp) can be obtained by dividing P_r by the permeate flow rate, Q_p (m^3/s), which has units of kWh/m^3 [108]. Energy expenditure in the system, which includes the energy necessary to pump the water through the reactor and for GC fluidization, was determined with the head loss of the system multiply by the recirculation flow. The energy used for fluidization using only water was $6.2x10^{-4}$ kW and increased to $6.8x10^{-4}$ kW with the addition of the membrane module, which represents an increase of 8.43%. Moreover, the energy requirement further increased 12.7% with the addition of the GC particles, resulting in $7.8x10^{-4}$ kW of energy requirements for the whole operation. The low increase of energy fluidization with the addition of GC is due to the low amount of GC added, 9.55 % of packing ratio. This amount is lower compared with other works reporting the use of up to 50% to prevent membrane fouling [88,101,105]; this is because at higher packing ratio there is an increase of the fluidized media to promote shear stress on the membrane surface [88]. However, the energy per unit of permeate (12.96 kWh/m^3) in this study was higher than that

reported in other studies [99,105]. The energy used in the present work could be decreased by increasing the permeate flow rate; nevertheless, this could be adjusted in agreement with the denitrification removal rate because both denitrification and filtration coexist in the same unit. The energy of fluidization for a complete GC fluidization was $4.95x10^{-4}$ kW/L-reactor, which is higher than that obtained by Yoo et al. [162], who reported $1.78x10^{-5}$ kW/L-reactor. However, wastewater treatment system as well as the GC characteristics is different in other reports. Nonetheless, this work has a permeate suction in continuous operation without change in suction pressure, which avoids the use of elements to control the relaxation or backwash flux to diminish membrane fouling. This is important because, unexpectedly, intermittent filtration did not prevent membrane fouling [96] compared with the continuous filtration in AFMBR, which was successful.

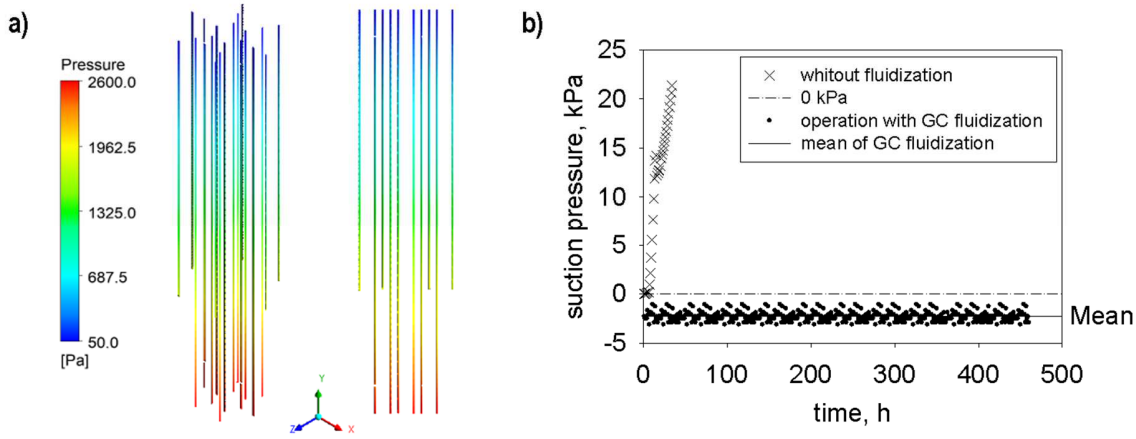

Figure 3.14 Pressure in the suction system: a) static pressure along the membrane walls during the GC fluidization; b) suction pressure in the permeate line.

An important loss of energy in the ASFMBR might be due to the traps located at the upper part of the reactor to retain GC particles. Another important loss of energy might be caused by the tangential inlet created by an elbow, which is known as an important accessory with a significant loss of energy. Other types of tangential inlets can be probed to reduce this loss of energy, such as outer wall tangential, involute, ramped involute ramp, commonly used as hydrocyclone entries. Moreover, it is important the hydrodynamic study with other entries since this can modify the GC

behavior in the reactor and, consequently, the hitting behavior with the membrane walls. On the other hand, the static pressure inside the reactor exerts a positive pressure around the membranes. Higher pressures are obtained at the start of the membranes and gradually decrease with the height of the reactor (Fig. 3.14(a)). This pressure is provided by the pumping of flow to promote fluidization. The pressures obtained in the conical part of the reactor are in the range from 2.6 to 1.32 kPa and diminish in the cylindrical part until 0.05 kPa. Fig. 3.14(b) presents the suction pressure necessary to achieve suction in the permeate line. For the control experiment without fluidization, the suction pressure increased more than 20 kPa in 34 h, whereas the fluidization with DI water filtration resulted in -2.44 kPa. Meanwhile, during the operation with denitrification and filtration, the suction pressure was -2.23 kPa in average. Negative values represent positive pressure. This means that energy is not needed to obtain the permeate flow under the given conditions, whereas fluidization in AFMBR with upward fluidization requires energy to obtain the permeate [162].

3.5 Conclusions

The ASFMBR design developed here promoted a GC swirling fluidization within the reactor. The 3-D hydrodynamic study of GC fluidization showed a stratification in agreement with the GC particles size, but principally depending on their density. The major contribution of water shear stress occurred in the axial and tangential directions, whereas the particle momentum influenced the three directions of flow. The GC density was relevant on the energy of momentum developed during the fluidization through the reactor. The conical geometry of the reactor resulted in a high shear stress and particle momentum capable of maintaining low adherence of SMP on the membrane walls. The particle momentum reached in this reactor has a similar or lower magnitude to other geometries of AFMBR, while the obtained wall stress was higher. The ASFMBR design a suitable configuration to achieve the denitrification of a synthetic metallurgic wastewater. Nitrate removal was ≥90% with

marginal NO_2^- and N_2O production, while the high acidic conditions were intrinsically neutralized by denitrifying byproducts due to the high recirculation established. The low GC packing ratio used, together with the hydraulic conditions established, maintained the suction pressure without change through the continuous operation. This novel reactor configuration could be suitable to design AFMBR for the treatment of industrial effluents.

4. Bio-recovery of metals from a stainless-steal industrial effluent through denitrification performed in a novel anaerobic swirling fluidized membrane bioreactor (ASFMBR)

4.1 Abstract

A novel technology was developed for the treatment of a stainless-steal industrial effluent, which contains a high nitrate concentration (6.8 g N-NO_3^-/L), acidic pH (pH=3.3) and a high concentration of Fe (12.5 g/L), Cr (2.9 g/L), Ni (2.2 g/L), and other elements, which are present at lower concentration. Denitrification was performed in an Anaerobic Swirling Fluidized Bed Membrane Bioreactor (ASFMBR) to treat both synthetic and real metallurgic wastewater. Granular carbon (GC) was used as supporting material for denitrifying biofilm as well as scouring media to prevent membrane fouling. The treatment concept was also integrated by a preliminary precipitation column in which high recirculation of the alkalinity produced from the denitrifying process was introduced to drive the precipitation and recovery of metals present in the industrial wastewater. Two external electron donors (ethanol and citrate) were added to balance the C/N ratio to achieve denitrification.

The novel reactor configuration achieved high nitrate removal (>94 %) with marginal accumulation of intermediates (nitrite and N_2O) with both electron donors tested. Furthermore, the acidic pH was efficiently neutralized in the reactor, by recycling the alkalinity produced from the denitrifying process. The operational strategies also allowed to recover over 40% of the metals present in the industrial wastewater, although the precipitation column needs to be optimized to increase the recovery level. Membrane fouling was avoided by the hydrodynamic regime established in the ASFMBR and GC fluidization. Most metals were recovered in the precipitation column and inside the ASFMBR. The treatment concept is promising to achieve efficient removal of nitrate and recovery of metals, while preserving the membrane filtration by the hydrodynamic conditions prevailing inside the ASFMBR.

This chapter will be submitted for publication as:

J. Ernesto Ramírez, S. Esquivel-Gonzalez, Germán Buitrón, Francisco J. Cervantes, Bio-recovery of metals from a stainless-steal industrial effluent through denitrification performed in a novel anaerobic swirling fluidized membrane bioreactor (ASFMBR), Water Research.

4.2 Introduction

Biological treatment of industrial wastewaters is challenging due to their complex, and sometimes extreme, physicochemical conditions, and because of the presence of toxic or inhibitors components, which negatively affect consortia in bioreactors [71]. Metallurgic effluents are particularly defiant because they are highly acidic, contain large concentrations of heavy metals, as well as nitrate derived from the use of nitric acid as part of the pickling and passivating processes in the stainless-steel production. For food and pharmaceutical industries, citric acid is also used as an extra agent to remove a higher amount of metals due to its chelating capacity. The discharge of this type of effluents, without a previous treatment, causes several environmental risks, such as eutrophication of water bodies by the high nitrogen content [163], and toxicity to aquatic organisms due to heavy metals present at high concentrations [17,164]. The citrate present in these effluents increases metals toxicity risk because it is an organic complex agent that increases metals mobility in the environment due to its chelating capacity. Furthermore, it is difficult the decontamination of wastewaters containing metal complexes.

Denitrification is a cost-effective process widely applied to remove nitrate from wastewaters [12]. During denitrification, nitrate (NO_3^-) is sequentially converted to nitrite (NO_2^-), nitric oxide (NO), nitrous oxide (N_2O) and dinitrogen (N_2) [44]. Heavy metals present in metallurgic effluents could contribute as trace elements to carry out denitrification since denitrifying microorganisms require cofactors, such as Fe, Cu and Mo for the enzymatic conversion of NO_3^- to N_2 [165]. However, heavy metals present at high concentrations can inhibit microbial activities in denitrifying processes, resulting in the accumulation of undesirable intermediates (NO_2^- and N_2O) [55,58,69,166,167]. Production of intermediates in denitrification is of special environmental concern because NO_2^- causes eutrophication of water bodies and triggers the formation of carcinogenic amines [163], while N_2O is a potent greenhouse gas [47]. Likewise, denitrification performance could also be affected by the acidic pH [168] of metallurgic effluents, then the control of the pH to circumneutral values is imperative [48]. Thus, the challenge of the treatment of this type of effluents

includes nitrate removal without accumulation of intermediates, heavy metal removal and pH neutralization.

A strategy to decrease the negative effects of metals to microorganisms could be by means of their precipitation and recovery from the metallurgic wastewater. Recovery of metals from metal-complexes is achieved by ligand destruction, which is commonly carried out by chemical and electrochemical oxidations. After the metals are released, they can be precipitated as insoluble species depending on medium composition [169]. In the last years, biotechnologies have been applied as metals recovery techniques with a high efficiency at low cost and energy requirements [170]. The alkalinity produced in denitrifying processes could be recycled to achieve neutralization of acidic metallurgic effluents, which could also promote the precipitation of heavy metals present in this type of industrial wastewaters. Nevertheless, several mechanisms involved in metals removal in bioreactors should be considered. These mechanisms include physical retention of heavy metals precipitated in sludge flocs; integration, adsorption and complexation of metallic ions with soluble microbial products (SMP); adsorption and diffusivity of metallic ions in biomass particles, as we as precipitation triggered by the alkaline nature of the process or the wastewater [80], or by coprecipitation with other biogenic solids [67].

Citrate present in metallurgic effluents plays an important role in denitrification as an electron donor to carry out the process. At the same time, its complexing capacity modifies the bioavailability of both metals and citrate to microorganisms, affecting the rate of the process. However, citrate biodegradation releases complexed metals, which could in turn be precipitated with denitrification by-products (OH^-, CO_3^{2-}). Previous studies elucidated the mechanisms involved in denitrification with citrate as electron donor in the presence of three of the main metals present in effluents from the stainless-steel industry (Fe(III)/Fe(II), Cr(III), Ni(II)) [167]. However, further studies are demanded to understand the mechanisms involved during the treatment of metallurgic effluents.

Anaerobic Fluidized Bed Reactors (FBR) with a denitrifying biofilm supported on granular activated carbon (GAC) have been used as a promising strategy to

decrease the inhibitory effects of heavy metals by high dilution rates imposed inside of the reactors and by pH neutralization of the acidic feed with denitrification byproducts; additionally, precipitation of heavy metals by products derived from denitrification has also been observed [58,69]. However, despite high nitrate removal and pH neutralization obtained, heavy metals precipitation remains low, yielding an effluent with high metals content [54]. Membrane bioreactors have been used to increase the removal of inorganic components in anaerobic membrane bioreactors (MBR) [74], to comply with environmental regulations. Heavy metals in MBR can be joined to sludge components and be rejected by the membranes [78]. However, heavy metals in MBR have shown negative effects on the biological process, changes in sludge characteristics, as well as membrane fouling by precipitation or incrustation of metals on the membrane surface [79,80]. The study of heavy metals in MBR is limited, particularly for denitrification processes, and they have been focused on two aspects: (a) inhibitory effects of heavy metals on the biological activity; and (b) effect of the heavy metals on membrane fouling.

Table 4.1 Characterization of wastewater generated from a stainless-steel industry.

	mg/L		mg/L		mg/L		mg/L
$N\text{-}NO_3^-$	6864.8 ± 100.2	Fe	12505.7 ± 110.1	K	48.3 ± 3.0	Pb	13.5 ± 2.3
$N\text{-}NO_2^-$	48.15 ± 4.9	Cr	2912.3 ± 111.5	B	45.6 ± 8.8	Cu	12.6 ± 1.0
$N\text{-}NH_4^+$	93.4 ± 6.2	Ni	2211.5 ± 53.7	Co	37.5 ± 0.7	V	12.5 ± 0.4
COD	0.0	Sn	836.5 ± 14.2	Na	33.7 ± 2.0	Mg	5.4 ± 0.1
		Mn	579.5 ± 32.3	P	28.6 ± 1.6		
pH, upH	3.3	Si	243.7 ± 5.4	Ca	26.5 ± 4.4		
ORP, mV	170.0	Mo	87.3 ± 3.7	Al	13.8 ± 0.6		

In the present work, the capacity of a novel Anaerobic Swirling Fluidized Membrane Bed Bioreactor (ASFMBR) to achieve denitrification of synthetic and real metallurgic wastewater was tested. A precipitation column was integrated to the ASFMBR in order to neutralize the metallurgic effluent and to promote metals precipitation. The performance of the ASFMBR was followed in terms of nitrate removal, intermediates accumulation (NO2- and N2O), and neutralization of the acidic feed. Membrane fouling was studied by monitoring membrane suction pressure. The fate of metals

was also studied in the treatment system and the recovered minerals were characterized by X-ray diffraction (XRD).

Table 4.2 Experimental conditions for the coupled system precipitation column - ASFMBR.

Test	Fe	Cr	Ni	Fe-Cr-Ni	Real effluent	Real effluent
electron donor, g C/g N	citrate, 2.26					ethanol, 1.43
N-NO_3^-, mg/d	793.7	756.6	762.6	765.6	854.5	849.2
N-NO_2^-, mg/d	0	0	0	0	4.1	3.1
N-NH_4^+, mg/d	0	0	0	0	33.1	54.9
Fe, mg/d	217.6	0	0	186.2	1755.8	
Cr, mg/d	0	122.5	0	126.9	387.2	
Ni, mg/d	0	0	45.1	44.2	299.0	
pH	2.02	2.10	2.27	2.04	3.16	2.21
HRT, h - precipitation column	8.3				91.7	
HRT, h - ASFMBR	26				287.8	
Membrane flux, L/m^2/h	3.4				0.31	

4.3 Materials and methods

4.3.1 Biofilm formation

Granular carbon of coconut shell with a size between 0.4 and 2.38 mm was used as fluidized media and support of the biofilm, which was formed by mixing clean GC and disintegrated anaerobic granular sludge previously acclimated under denitrifying conditions. The anaerobic granular sludge originated from a wastewater treatment plant treating effluents from a brewery (Cd. Obregón, Mexico). Biofilm formation was performed in two up-flow anaerobic sludge blanket (UASB) reactors with a working volume of 1.1 L. Both reactors were fed with 500 mg N-NO_3^-/L and were supplied with stoichiometric amounts of either ethanol or citrate as electron donors. The columns were operated almost for three months until reaching steady state

conditions. The basal medium had the following composition (mg/L): KH_2PO_4, 300; $MgSO_4 \cdot 7H_2O$, 61.3; $FeSO_4 \cdot 7H_2O$, 17.2; $CaCl_2 \cdot 2H_2O$, 75 and 1 mL/L of trace elements, which composition was as follows (g/L): $MnCl_2 \cdot 4H_2O$, 0.5; H_3BO_3, 0.05; $ZnCl_2$, 0.05; $CuCl_2$, 0.03; $Na_2MoO_4 \cdot 2H_2O$, 0.01; $CoCl_2 \cdot 6H_2O$, 0.5; $NiCl_2 \cdot 6H_2O$, 0.01 Na_2SeO_3, 0.01.

4.3.2 Operational conditions of the treatment system

The ASFMBR was operated both with synthetic and real metallurgic wastewater. Synthetic wastewater contained the main metals present in the real wastewater (Fe(II)/Fe(III), Cr(III), Ni(II)). These metals were tested in individual form and jointly using citric acid as electron donor. The real wastewater used was obtained from a stainless-steel company (Querétaro, Mexico), and its composition is shown in Table 4.1. The treatment of real wastewater was tested with both citric acid and ethanol as electron donors. Table 4.2 shows the experimental design during the operation of the ASFMBR with both synthetic and real wastewater. The treatment concept was integrated by a precipitation column before the ASFMBR in which denitrification and filtration occurred (Fig. 4.1). The precipitation column was of 1.1 L, and the ASFMBR had conical and cylindrical sections with a total volume of 1.57 L. The inlet to the precipitation column was composed of the wastewater of study and a recirculation line coming from the outlet of the ASFMBR, both was feed at the same flow rate. The outlet of the column was fed to the ASFMBR. The ASFMBR was operated with a high recirculation flow (3.8 L/min) to fluidize the GC by a tangential inlet that promote the swirling fluidization. A portion of 150 mL of GC from the column of biofilm formation was added to the ASFMBR, which corresponds to 0.56 g of volatile suspended solids (VSS)/L. The microfiltration module with porous size of 0.1 μm was submerged in the reactor and was composed of 18 hollow fiber membranes of polyvinylidene fluoride (PVDF) with an external diameter of 1.2 mm. The membranes were in vertical position and separated among them to allow the hit of the GC with the membrane walls. The lower part of the membranes was sealed, and all

connected in the other extreme to a peristaltic pump to obtain the permeate. This line worked at continuous operation and was equipped with pressure and flow sensors to monitor membrane fouling. Every testing period was conducted as a new experiment, with a preliminary operational stage in the absence of metals to reach denitrifying steady state conditions before every test. The hydraulic retention time (HRT) during the treatment of real wastewater was adjusted to obtain a similar nitrate load as compared to the experiments performed with synthetic wastewater. The concentration of NO_3^-, NO_2^-, NH_4^+, metals in solution, as well as pH and redox potential (ORP) were measured in the sampling points shown in Fig. 1. Additionally, total suspended solids (TSS), and SMP in terms of carbohydrates (SMPc) and proteins (SMPp) were monitored in the reactor and permeate line. At the upper part of the reactor, gas samples were taken for N_2O measurements. The percentage of metals retained in the precipitation column, ASFMBR, as well as the metals not retained in the system were determined with a mass balance in every treatment unit as follows:

Precipitation column:

$$\%M_P = \frac{\sum\{(Q_{in}M_{in}+Q_{ASFMBR}M_{ASFMBR})-Q_{S/P}M_{S/P}\}}{\sum Q_{in}M_{in}} \times 100 \qquad (4.1)$$

ASFMBR:

$$\%M_{ASFMBR} = \frac{\sum\{Q_{S/P}M_{S/P}-(Q_{out}M_{out}+Q_{ASFMBR}M_{ASFMBR})\}}{\sum Q_{in}M_{in}} \times 100 \qquad (4.2)$$

Metals not retained:

$$\%M_{NR} = \frac{\sum M_{S/P}+\sum M_{ASFMBR}}{\sum Q_{in}M_{in}} \times 100 \qquad (4.3)$$

where M_{in}, M_{ASFMBR}, $M_{S/P}$, and M_{out} correspond to the concentration of metals in the wastewater of study, outlet of the ASFMBR to the precipitation column, outlet of the precipitation column and concentration in the permeate, each of them multiplied by the corresponding flow rate (Q).

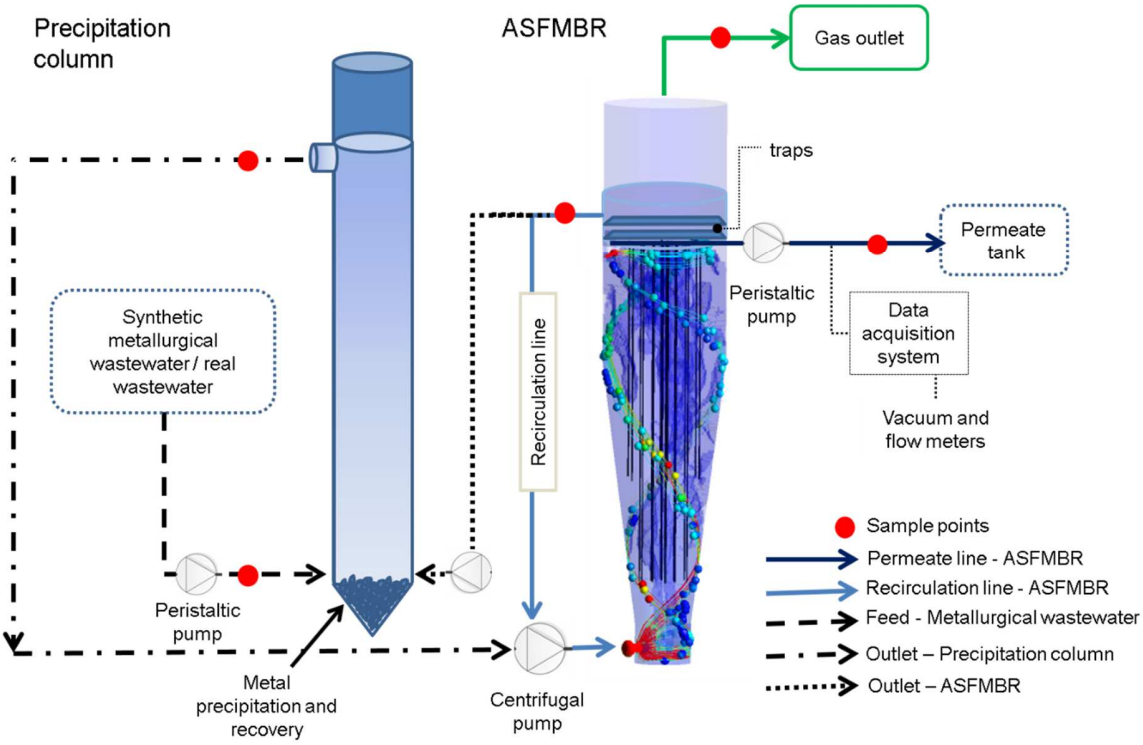

Figure 4.1 Experimental set-up of the couple system precipitation column-ASFMBR.

4.3.3 Analysis

NO_3^-, NO_2^-, NH_4^+, TSS and VSS were measured according to APHA methods [130]. N_2O was monitored by gas chromatography (Agilent 6850 Series GC System) using a thermal conductivity detector at 250 °C, with a column 10' × 1/8" SS packed with HayeSep D 100/120 mesh. The injector temperature was at 250 °C. Nitrogen was the carrier gas at 6 ml/min. Samples of 100 µl were directly injected into the chromatograph. Citrate was measured by capillary electrophoresis. Measurement of pH was done using a pH meter (Thermo Scientific, Orion 4-star). VSS determination of the biofilm supported on GC particles was conducted by detachment of the biofilm of 1 g of GC in 10 mL of distilled water by ultra-sound treatment for 30 min, at the start and at the end of the experiments. The soluble concentration of proteins and carbohydrates were determined by the colorimetric methods of Bradford [153] and Dubois [154], respectively. At the end of the experimentation, samples of GC

circulating from the conical and cylindrical sections of the reactor were taken to determine metals concentration. A section of 1 cm of height of the membrane was cut at different heights of the reactor to determine metal deposition. Metal extraction from GC particles and membranes was accomplished by organic matter oxidation with H_2O_2 and acidic digestion. Samples for heavy metals measurements were filtered through 0.45 μm and analyzed by ICP-OES. Ferrous iron was determined by the ferrozine method [131]. Minerals recovered in the precipitation column and in the ASFMBR were analyzed by XRD.

4.4 Results and discussion

4.4.1 Denitrification performance of the ASFMBR with synthetic and real wastewaters

Denitrification was initially evaluated in the ASFMBR with citrate as electron donor. The effects of the three main heavy metals present in metallurgic wastewater on denitrification were studied. Citrate is frequently found in metallurgic effluents and the stoichiometry to achieve denitrification with this substrate is presented in Eq. (4.1):

$$C_6H_5O_7^{3-} + 3.6NO_3^- + 0.6H^+ + 0.2H_2O \rightarrow 6HCO_3^- + 1.8N_2 \quad (4.1)$$

$$\Delta G^\circ = -1881.0\ kJ\ mol^{-1}$$

4.4.1.1 Effects of Fe(III)/Fe(II)

Iron addition to the ASFMBR resulted in an increase on nitrate and citrate removal efficiencies (Fig. 4.2). This stimulatory effect to the denitrification process was also observed in previous reports [69]. According to the operational conditions prevailing in the ASFMBR, the main iron-citrate species present were [Fe(II)-citrate]$^-$ and [Fe(III)-citrate]. Previous experiments [167] showed that [Fe(II)-citrate]$^-$ is a very

stable complex inhibiting the uptake of citrate for nitrate reduction. The structural characteristics of the metal-citrate complex has a large influence on its biodegradability. Ferric iron has been reported to form a bidentate citrate complex, which is more easily degraded than the tridentate ferrous iron-citrate complex. Thus, degradation of the ferrous iron-citrate complex depends on its oxidation and hydrolysis to form the ferric iron-citrate complex [23]. During the operation of the ASFMBR, the Fe(II) concentration supplied from the precipitation column was removed in the reactor so that its concentration remained below 3 mg/L in the outlet (Fig. 4.3 (a)). This could be due to the precipitation of minerals containing Fe(II), or by Fe(II) oxidation linked to denitrification, with a subsequent precipitation of solids including Fe(II) and Fe(III).

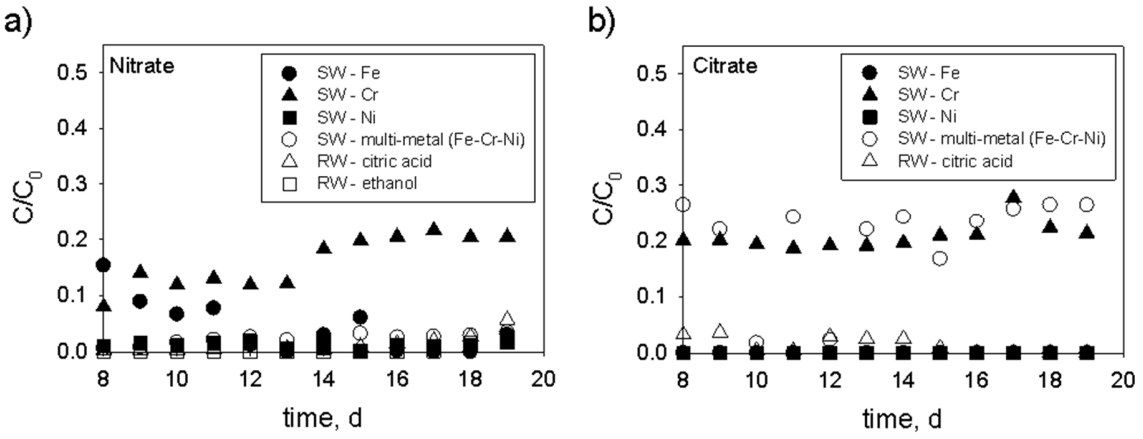

Figure 4.2 (a) Nitrate removal and (b) citrate degradation for the synthetic and real wastewater treatments. SW and RW means synthetic and real wastewater, respectively.

Autotrophic denitrification can be improved by ferrous iron oxidation [61], which has been reported both with pures and enriched mixed cultures using chelating agents to increase the solubility of Fe(II) at circumneutral pH [59]. This is because Fe(II) precipitates at this pH values, affecting denitrification. In the present work, Fe(II) could have improved nitrate removal promoting the release of Fe(III) to be precipitated, contributing with free citrate available to support denitrification. Nevertheless, precipitation of Fe(II) also occurred as $FeCO_3$ in the traps of the reactor, which was evidenced by XRD analysis (Fig. 4.4). Moreover, species

containing Fe(II) can act as reactive solids [171] and contribute to the reduction of N-species by Fe(II) oxidation [61]. Thus, stimulation of denitrification could have occurred by the ferrous iron oxidation both in solution and present in reactive solids.

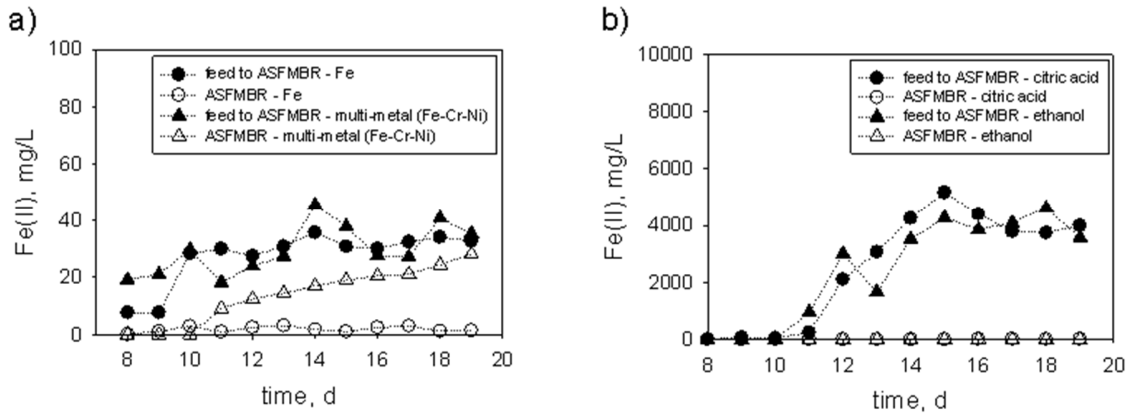

Figure 4.3 Fe(II) concentration both feed to the ASFMBR and maintained in the ASFMBR for the (a) Fe- bearing synthetic wastewater tests, as well as for the (b) real wastewater treatment for both electron donors.

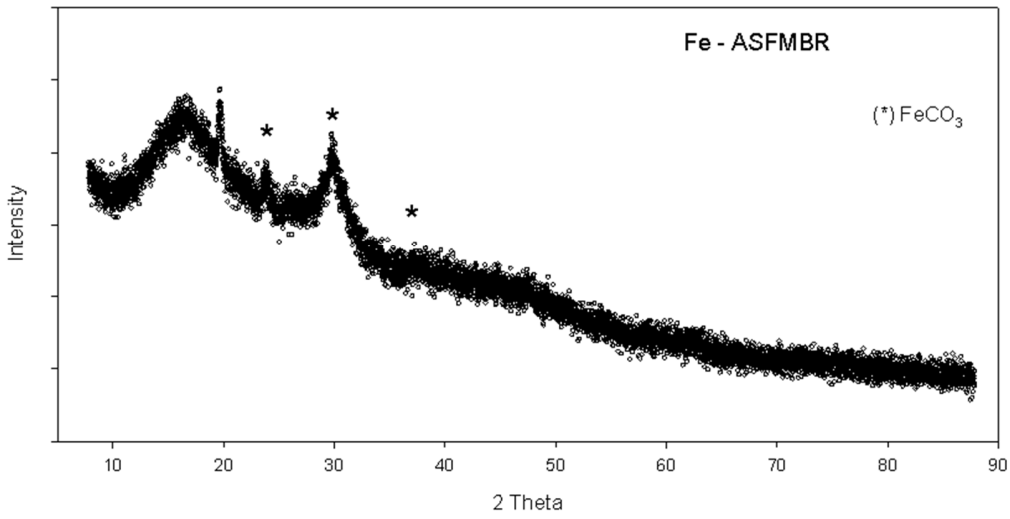

Figure 4.4 XRD diffractogram of the solids founded in the ASFMBR for the synthetic wastewater treatment with Fe addition.

Regarding intermediates accumulation, NO_2^- concentration decreased from 5.2±0.4 to 1.4±0.3 mg N-NO_2^-/d with iron addition. Moreover, N_2O was also produced at a lower concentration of 20.2±2.6 mg N-N_2O/d (only 2 days) as compared to the

reactor performance in the absence of iron. The amount of NO_2^- and N_2O accumulated represent less than 2% of the nitrogen feed. On the other hand, biogas emission decreased with iron addition (data not shown). This could be explained by the formation of insoluble carbonates that decreased CO_2 emissions from the ASFMBR. The decrease of gas emissions was also observed in the other experiments, including the real effluent treatment tests.

4.4.1.2 Effects of Cr(III)

Cr(III) addition to the ASFMBR yielded mild inhibition to the denitrification process both in terms of nitrate removal and citrate degradation. The amount of nitrate and citrate remaining in the treated effluent was ~20% with respect to the added (C_0) concentrations (Fig. 4.2). Similar results were obtained in batch experiments and the inhibition on nitrate removal was attributed to the stable Cr(III)-citrate complexes formed [167]. This stability hinders biodegradation of citrate while linked to Cr(III) (Fig. 4.5(a)). However, a recent study showed the difficulty to precipitate the complex Cr(III)-citrate under alkaline conditions [172], which was possibly associated with a very stable molecular structure formed, which prevailed solubilized even under alkaline conditions. Hydroxides could be incorporated into the structure of Cr(III)-bearing complexes and form polymers thereof. The formation of these complexes could affect Cr(III) recovery and also the bioavailability of citrate for denitrification. Certainly, even though citrate remains solubilized, it could not be taken by denitrifying microorganisms due to the high stability of the complex Cr(III)-citrate, consequently affecting nitrate removal. On the other hand, nitrite reduction was not affected by Cr(III) addition, since its concentration remained in a range of 2 to 17 mg $N\text{-}NO_2^-$/d, while N_2O was produced just during two operational days at 4.4 ± 0.3 and 9.0 ± 0.6 mg $N\text{-}N_2O$/d. Thus, nitrate reduction was the only denitrifying step affected by Cr(III), which is in agreement with results obtained in batch assays [167].

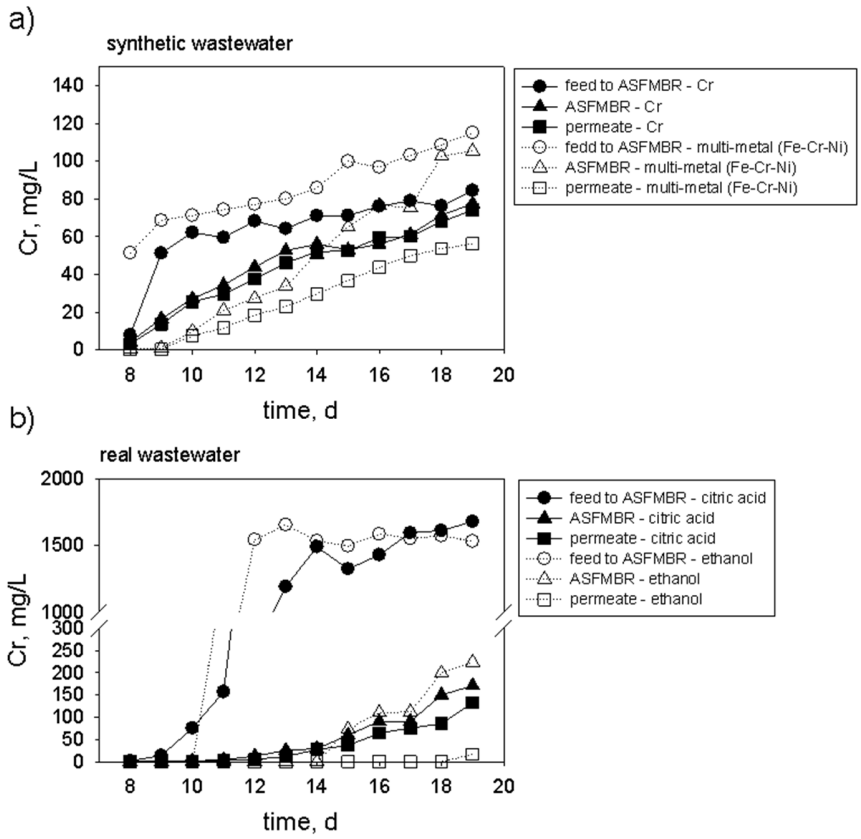

Figure 4.5 Cr concentration for the (a) synthetic and (b) real wastewater treatments in the feed to the ASFMBR, maintained in the ASFMBR and permeate line.

4.4.1.3 Effects of Ni(II)

Nitrate removal efficiency was not affected by Ni(II) addition. These findings contrast with those obtained in batch experiments [167]. In those assays, high inhibition of denitrification and accumulation of intermediates (NO_2^- and N_2O) occurred, while very low effluent NO_2^- concentration (below to 1.7 mg N-NO_2^-/d) and absence of N_2O in the ASFMBR outlet was observed during the operational period in the presence of Ni(II). Further studies report negligible accumulation of nitrate and nitrite by the addition of Ni (5.5 mg Ni/L) to a denitrifying FBR [58]. However, additional works revealed inhibition in nitrate and nitrite removal at a concentration of 60 mg Ni/L [54], although no accumulation of denitrification intermediates was observed at a high Ni

concentration (500 mg/L) when the reactor was operated at a HRT (5.4 h). This suggests that the hydrodynamic conditions prevailing in the FBR and the low HRT imposed (low contact time of Ni(II) with microorganisms), together with the insoluble Ni(II) species formed, could have alleviated the inhibitory effects of Ni(II). In the present work, the ASFMBR was operated at a higher HRT (26 h) without an apparent inhibition of the denitrification process. In fact, high Ni(II) precipitation was observed during the operation of the ASFMBR in the presence of this metal (Fig. 4.6), which could have prevented the inhibitory effects of Ni(II) to denitrifying microorganisms. Likewise, Ni(II) toxicity could have been mitigated by the formation of Ni complexes with dissolved organic matter. The production of SMPp increased with Ni addition after several days of operation (Fig. 4.18(a)). This result could be due to cellular damage and release of proteins [160] as a mechanism of cellular protection [173]. The release of SMP has been reported under anaerobic conditions and these SMP showed the capacity to form stable complexes with Ni [174]. The formation of these complexes could explain the absent of negative effects on the denitrification driven by Ni addition to the ASFMBR. Moreover, the hydrodynamic conditions established in the reactor could also have played an important role on mitigating the effects of metals. The hydrodynamic study of the ASFMBR (Ref. ASFMBR) revealed a dragging of particles with small size to the upper part of the reactor, in which they were retained in the traps located in this zone. This retention mechanism prevented the accumulation of precipitates onto the biomass that could have triggered inhibition to the denitrification process.

4.4.1.4 Joined effects of Fe, Cr and Ni

Addition of the three studied heavy metals altogether to the ASFMBR resulted in some differences with respect to the individual tests. During these experiments, iron precipitated to a lower extent than the experiments exploring its individual addition. Meanwhile, Cr(III) and Ni(II) showed partial and high precipitation, respectively, during the joined addition assays. The amount of Fe(II)/Fe(III) and Cr(III) maintained

in solution (Fig. 4.6) limited citrate bioavailability (Fig. 4.2). Nevertheless, nitrate removal efficiency was maintained (Fig. 4.2), suggesting that the negative impact of Cr(III) was counteracted by the positive effects driven by Fe and Ni addition. Autotrophic denitrification promoted by Fe(II) could have also contributed to the denitrification performance observed. Unlike experiments conducted with Fe alone, the concentration of Fe(II) decreased to a lower extent in experiments performed with the three metals. In fact, Fe(II) was almost completely removed in the individual test (Fig. 4.3(a)). This difference could be due to inhibition of autotrophic denitrification caused by the presence of Cr(III) and Ni(II), which prevented Fe(II) oxidation with a subsequent precipitation. Kiskira et al. Kiskira et al. (2018) reported certain effect of Ni on Fe(II)-driven autotrophic denitrification. However, further research is necessary to clarify the effect of Cr(III) on this process. Similar to experiments conducted with individual addition of Fe, it was observed precipitation of solids containing Fe(II) during the operation of the reactor with all metals evaluated. Certainly, minerals containing both Fe(II) and Fe(III) and recovered from the treatment system include $FeCO_3$, Fe_3O_4, hematite and ferrihydrite (Fig. 4.7). Biogenic production of ferrihydrite in autotrophic denitrification has been observed as a result of a rapid oxidation of Fe(II) or by the presence of $FeCO_3$ [61]. Thus, Fe(II) oxidation could have contributed to sustain high nitrate removal efficiency, even when citrate was less bioavailable due to prevalence of metal-complexes, mainly including Fe(II) (Fig. 4.3(a)) and Cr(III) (Fig. 4.5(a)).

Regarding accumulation of denitrification intermediates, a maximum production of 1.7 mg $N\text{-}NO_2^-$/d occurred, while N_2O was not detected in the biogas. These levels of intermediates production were lower than those obtained in individual tests. Similar results were observed in batch assays previously conducted [167]. In these tests, iron addition stimulated the denitrification process alleviating the inhibitory effects of Ni(II) and Cr(III). However, in batch assays, N_2O was only detected in incubations with Ni(II), while it was produced in the Fe and Cr tests in the present study. This discrepancy could be due to the hydrodynamic conditions prevailing in the ASFMBR.

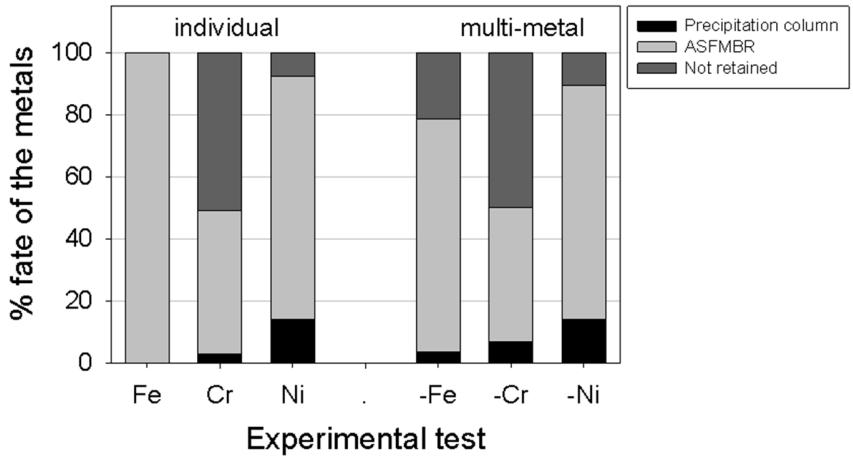

Figure 4.6 Metals balance in the system precipitation column-ASFMBR for the synthetic wastewater experiments.

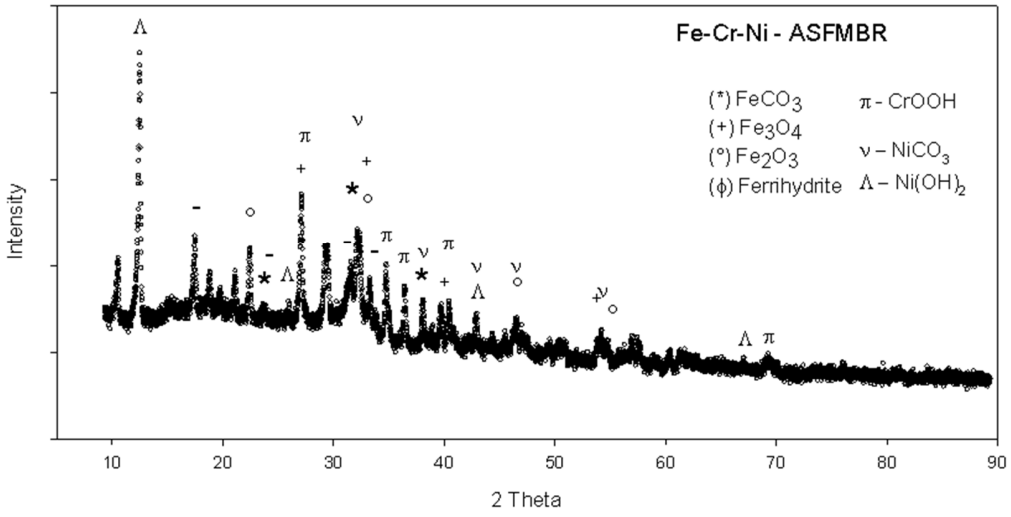

Figure 4.7 XRD diffractogram of the solids founded in the ASFMBR for the synthetic wastewater treatment with multi-metal addition.

4.4.1.5 Performance of the ASFMBR treating real wastewater from a stainless-steel industry

Denitrification of wastewater originated from a stainless-steel industry was evaluated in the ASFMBR with both citrate and ethanol as electron donors. The stoichiometry of denitrification with ethanol is described in Eq. (4.5):

$$C_2H_5OH + 2.4NO_3^- \rightarrow 2HCO_3^- + 1.2N_2 + 0.4OH^- + 1.8H_2O \quad (4.5)$$

$$\Delta G^\circ = -1230.7 \text{ kJ mol}^{-1}$$

High nitrate removal was achieved in the ASFMBR with both electron donors tested (Fig. 4.2(a)). Efficient denitrification could be accomplished despite the chelating properties of citrate, which form complexes with different metals decreasing its bioavailability to serve as electron donor. Considering that this industrial effluent contained high iron concentration, it is plausible that autotrophic denitrification driven by Fe(II) significantly contributed to nitrogen removal as it was observed in the synthetic wastewater tests. In fact, Fe(II) concentration fed to the ASFMBR reached ~4 g/L, which drastically decreased to values lower than 20 and 11 mg/L for the tests with citrate and ethanol, respectively, Fig 4.3 (b). During the experiments with citrate, it was difficult to detect Fe-bearing minerals by XRD analysis. However, for experiments conducted with ethanol, the main solids recovered include akaganeite β-FeOOH, Fe_3O_4 and $Fe(OH)_2$ (Fig. 4.8). Akaganeite is a product of Fe(III) precipitation, while magnetite could be formed via Fe(II) oxidation [175].

Regarding intermediates formation during the treatment of the industrial effluent, ethanol supply yielded very high nitrogen removal so that lower intermediates production occurred as compared to the operational period performed with citrate. NO_2^- was produced in a range of 12.4 to 37.4 mg/d with citrate, while experiments performed with ethanol did not show accumulation of this intermediate. Furthermore, N_2O was not detected during the treatment of the industrial effluent regardless the type of substrate supplied. Ethanol was a better electron donor than citrate to achieve denitrification of the stainless-steel industry wastewater, while a higher denitrification efficiency was obtained with citrate in previous batch assays [167].

This discrepancy could be due to the hydrodynamic conditions established in the ASFMBR, which were different to the mixing conditions prevailing in batch incubations by orbital shaker. However, further research must be conducted to clarify the effects of shear stress on denitrification performance with different carbon sources. Ammonium was detected in very low concentrations in the reactor and permeate line for both electron donors tested, suggesting that it was consumed to support microbial growth in the ASFMBR.

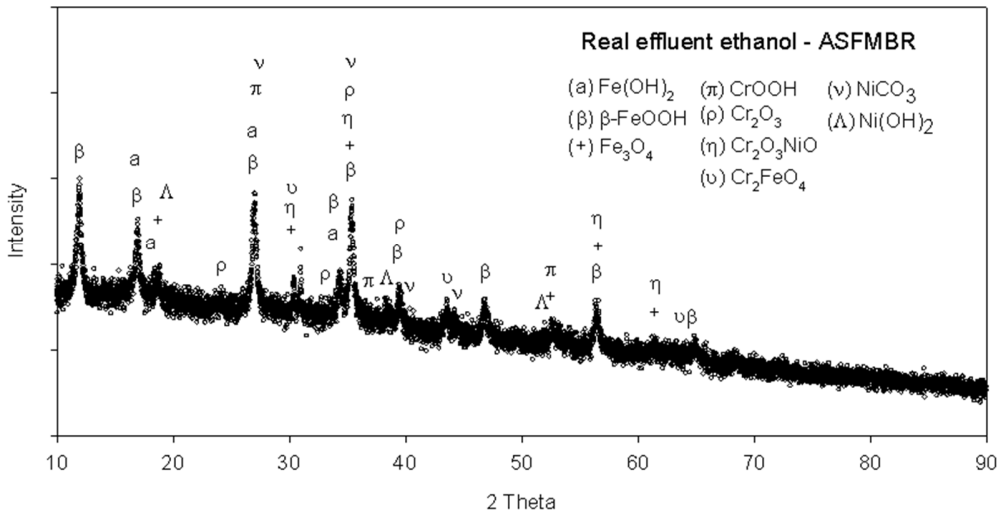

Figure 4.8 XRD diffractogram of the solids founded in the ASFMBR for the real wastewater.

Previous studies have reported inhibitory effects to denitrification by different metals that are present in the industrial effluents studied. Cu has been reported to affect nitrate removal rate and promote NO_2^- accumulation, while a deficient concentration could increase N_2O production [55]. Nevertheless, long term exposure to Cu in bioreactors can decrease its inhibitory effects as compared to short-term tests [57]. Co has also been shown to cause nitrite accumulation in batch assays [58]. High Ca concentrations decreased microbial growth and denitrification rate in a Sequential Batch Reactor (SBR) [8]. In the present work, a fraction of Cu was recovered in the precipitation column, while a higher fraction was retained in the ASFMBR, maintaining a low concentration in solution (Fig. 4.9). Thus, no inhibitory effects were expected for this metal. Similar results were obtained with Co. Meanwhile, Ca was

hardly removed in the precipitation column, but it was significantly retained in the ASFMBR (63.9% and 79% removal for citrate and ethanol experiments (Fig. 4.9), respectively). The large fraction of metals, which precipitated in the treatment system evaluated might have decreased the expected inhibitory effects.

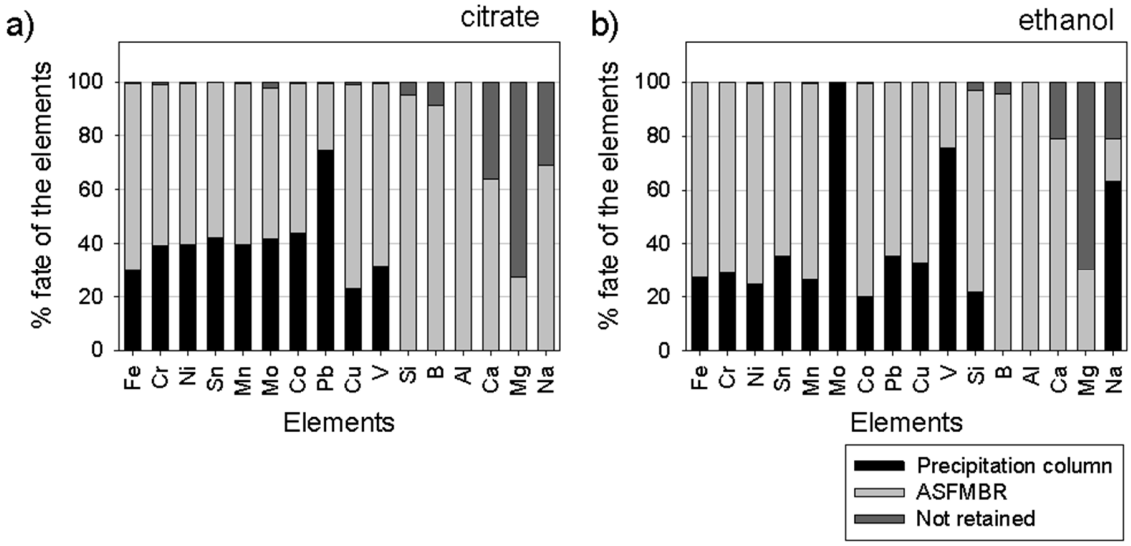

Figure 4.9 Metals balance in the system precipitation column-ASFMBR for the real wastewater experiments with (a) citrate and (b) ethanol as electron donors.

4.4.2 Recovery of mineral in the treatment system and their characterization

4.4.2.1 Synthetic wastewater tests

4.4.2.1.1 Precipitation column

The precipitation column was fed with both a recirculation line from the ASFMBR and the acidic synthetic medium. Before metals addition, this column was maintained in a pH close to 6 (Fig. 4.10(a)). Addition of Fe(II)/Fe(III) and Cr(III) decreased the pH just after the first days of metals addition, but increased to 6 afterwards. For the tests performed with nickel and the three metals together, the pH of the column was controlled without important affectation in a range between 7 and 8. According to the

CO_2 equilibrium, neutralization of citric acid occurs by the formation of bicarbonate or carbonic acid species.

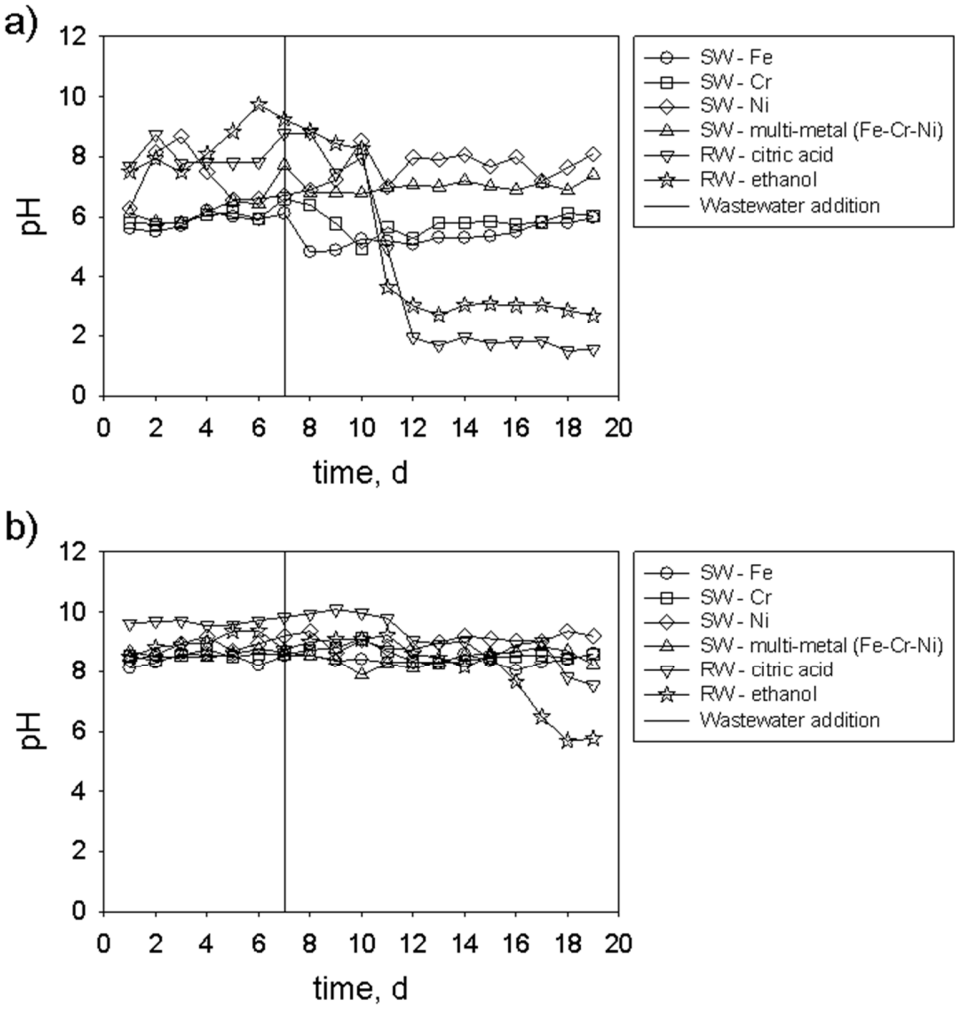

Figure 4.10 Values of the pH in the (a) precipitation column and (b) ASFMBR for the synthetic and real wastewater experiments. SW and RW means synthetic and real wastewater, respectively.

Poor iron retention was achieved in this column, while only 3% and 14% of Cr(III) and Ni(II) fed, respectively, was retained. However, metals retention increased in the multi-metals experiments to 3.6%, 6.9% and 14.1% for Fe, Cr and Ni, respectively. This could be caused by the higher metals concentrations that could have decreased the metal-citrate stability complex, and also due to metals co-precipitation. The strong stability of citrate-metal complexes, even when the pH was neutralized, might

have affected metals recovery. According to chemical speciation analysis obtained in previous assays [167], the [Fe(II)-citrate]$^{-}$ complex is maintained at alkaline pH, while the concentration of the [Fe(III)-citrate] complex decreased. The same pattern occurred for the complexes [Ni(II)-citrate$_2$]$^{4-}$ and [Cr-citrate$_2$]$^{4-}$. Iron-bearing minerals were difficult to identify by XRD, while Cr was found as $Cr(OH)_3{\cdot}3H_2O$ and chromium oxides, such as CrO_2 and Cr_2O_3. Ni was recovered as $NiCO_3$ and $Ni_3(PO_4)_2$ (Fig. 4.11). Thus, acidic metallurgic effluents can be neutralized with denitrifying by-products promoting precipitation and recovery of metals; however, the stability of metals-citrate complexes challenges metals recovery efficiency.

4.4.2.1.2 ASFMBR

The outlet of the reactor is just composed by the line of permeate flow. This allows the saturation of the chemical species, their precipitation, and rejection by the membranes. Metals bio-recovery from complexed species was accomplished after destroying ligands and forming insoluble compounds, which depended on metals-complexes stability. Citrate degradation conducted by denitrifying microorganisms in the ASFMBR released metals promoting their precipitation with denitrification by-products. pH was maintained above pH 8 in the ASFMBR during the whole operational period with synthetic wastewater (Fig. 4.10(a)), even when a higher precipitation of metals was obtained as compared to the precipitation column. Iron was almost completely precipitated during the experiments with this metal. Nevertheless, its precipitation decreased 24.9% for the tests assessing the effects of the three metals together (Fig. 4.6). Individual addition of iron resulted in precipitation and/or oxidation of Fe(II), as previously discussed in section 4.4.1.1. Citrate degradation together with Fe(II) oxidation triggered iron precipitation in the individual metal addition tests. However, for experiments conducted with the three metals together, residual Fe(II) was obtained in the reactor (Fig. 4.3(a)). Thus, as mentioned in section 4.4.1.4, Fe(II) oxidation and its subsequent precipitation could be affected by the presence of the other metals studied (Cr and Ni). Another

explanation is that the three metals added competed for the denitrifying by-products available to become precipitated. Thus, the stability of the Fe(II)-citrate complex was less affected so that Fe(II) was maintained in solution. $FeCO_3$ was detected during the individual addition of Fe, and additional iron-bearing minerals were recovered during the multi-metals experiments, such as Fe_3O_4, hematite and ferrihydrite. Thus, Fe(II) could have been oxidized followed by its subsequent precipitation in these minerals. This mechanism has previously been reported, in which citrate degradation occurred through an oxidation of $[Fe(II)\text{-citrate}]^-$ (log K~4.4) to a lesser hydrolyzed complex $[Fe(III)(OH)_2\text{-citrate}]^{2-}$ (log K~1.9-2.6) [23]. This could have promoted high nitrate removal efficiency despite a lower consumption of citrate, as found in the multi-metals experiments (Fig. 4.2(b)).

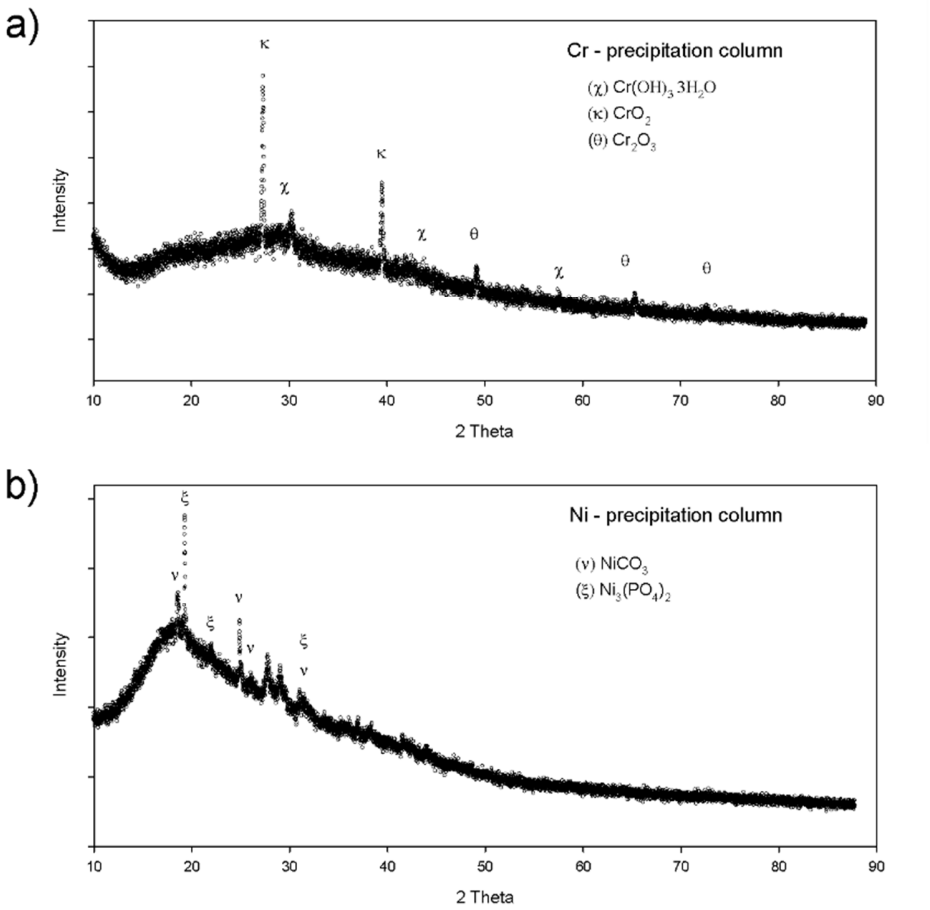

Figure 4.11 XRD diffractogram of the solids founded in the precipitation column for the synthetic wastewater with (a) Cr and (b) Ni addition.

Regarding Cr(III) and Ni(II), their retention occurred at the same level both in individual and multi-metals experiments. Cr(III) was poorly removed (≤50%) because hydroxides produced from denitrification would have been incorporated into the structure of Cr(III)-bearing complexes, which are difficult to precipitate [172]. This limited Cr(III) bio-recovery and led to a large amount of residual Cr(III) in the permeate line. Cr(III) could be recovered as $Cr(OH)_3 \cdot 3H_2O$ as evidenced by XRD analysis (Fig. 4.12(a)) during Cr(III) individual supply, while it was recovered as CrOOH when the three metals were jointly tested (Fig. 4.7). For experiments conducted with Ni(II), a recovery of up to 90% of this metal was accomplished. The predominant species in solution of Ni(II) at the pH of the reactor operation were [Ni-citrate]$^-$ (pK~5.19) [31] and $[Ni(citrate)_2]^{4-}$ (pK~2.1) [29]. In previous batch experiments, Ni(II) was complexed and maintained in solution [167]. The higher Ni(II) bio-recovery achieved in the present work in comparison with the batch assays could be caused by the higher dilution and alkalinity present in the reactor that saturated the insoluble Ni species and promoted their precipitation.

Neutralization of an acidic feed in a denitrifying FBR with ethanol as electron donor was reported by Papirio et al. (2014). Afterwards, addition of $NiSO_4$ resulted in a pH decrease in the FBR [58]. The authors assumed precipitation of Ni(II) as NiS with by-products derived from sulfate reduction, as well as acidification according the next reaction: $Ni^{2+} + H_2S \rightarrow NiS_{(s)} + 2H^+$. Subsequently, XRD analysis showed precipitation of Ni(II) as $Ni_3(PO)_2$ and chemical speciation analysis further predicted other precipitates like hydroxides and carbonates [54]. In the present work, Ni was recovered as $Ni_3(PO)_2$ and $NiCO_3$ in individual studies (Fig. 4.12(b)). Furthermore, it was precipitated as $Ni(OH)_2$ when the three metals were added simultaneously to the ASFMBR (Fig. 4.7). The presence of carbonates and hydroxides of nickel for this work compared with other studies could be explained by the higher HRT applied in the present study, which might have allowed reaching equilibrium among these species to be precipitated. In addition, a metallic color was observed on GC particles inside the ASFMBR. A report indicates the capacity of *Pseudomonas sp*. to reduce Ni(II) to Ni(0) as a detoxifying mechanism in denitrification [52]. During the operational tests, the redox potential was maintained at reductive conditions,

reaching ORP values of up to -0.17 V (Fig. 4.13), which could have promoted the reduction of Ni(II) to Ni(0). However, the reduction potential of Ni(II) to Ni(0) is -0.26 V and Ni(0) could not be detected by XRD analysis.

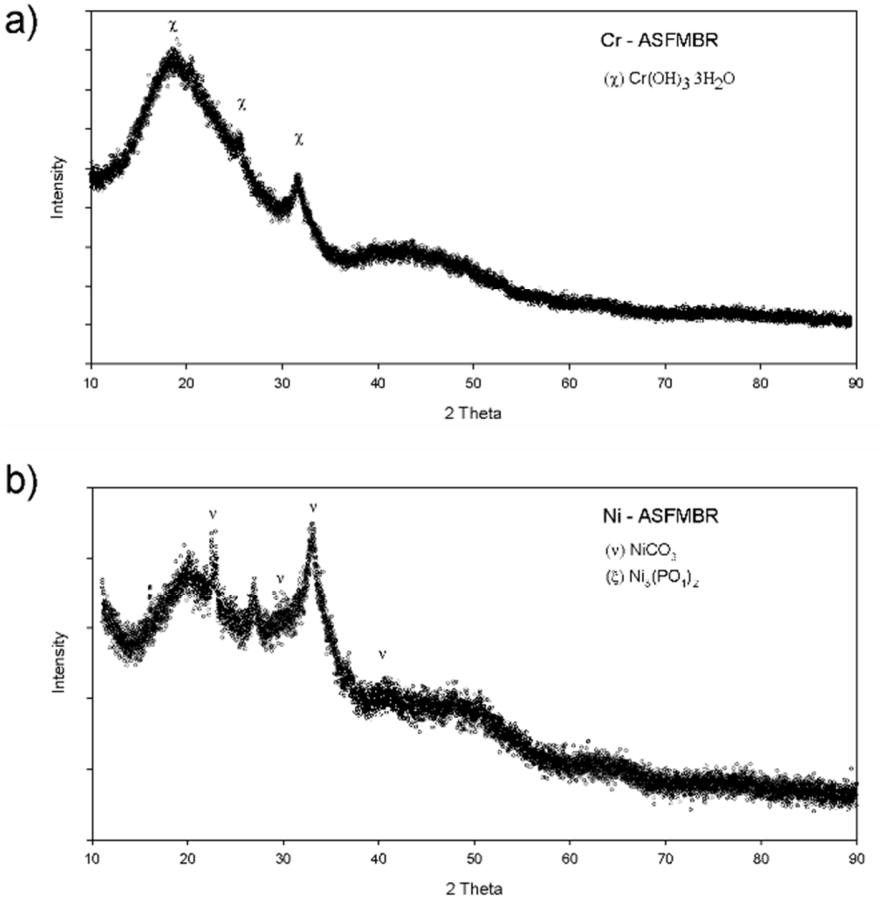

Figure 4.12 XRD diffractogram of the solids founded in the ASFMBR for the synthetic wastewater with (a) Cr and (b) Ni addition.

A fraction of metals was deposited on GC particles that circulated both at the conical and cylindrical-traps sections of the ASFMBR (Table 4.3). Metals precipitation on GC particles could be obtained with active denitrifying microorganisms, which have been observed to promote bio-mineralization [66]. VSS content measured on the biofilm supported on GC particles circulating in the upper part of the reactor was higher than that found in solids circulating in the conical section of the ASFMBR (Fig. 4.14). Likewise, metals concentration on GC particles collected from the cylindrical-traps section was higher than in solids circulating at the conical part of the reactor.

The hydrodynamic conditions of the reactor (Chapter 3, section: 3.4.1 and 3.4.2) could also have determined the higher metals concentration obtained in the upper part of the reactor by sending the lower particles sizes to the upper reactor zone, which has a lower flow velocity allowing a higher metal settling. However, it is also interesting to note metals deposition on GC particles circulating in the conical section of the ASFMBR. This zone of the reactor has a high flow velocity, thus the contact time between the flow dragging (containing metals and denitrifying by-products) with GC particles is low. On the other hand, the amount of heavy metals precipitated on GC particles agree with the amount of metals precipitated in the ASFMBR, which is related to the heavy metal-citrate complex stability, following the trend Fe>Ni>Cr. For the multi-metals experiment, minerals recovery was generally lower than the individual experiments. Ni precipitation in a FBR working under denitrifying and sulfate-reducing conditions has been reported using granular activated carbon (GAC) as supporting material for denitrifying biofilm [54].

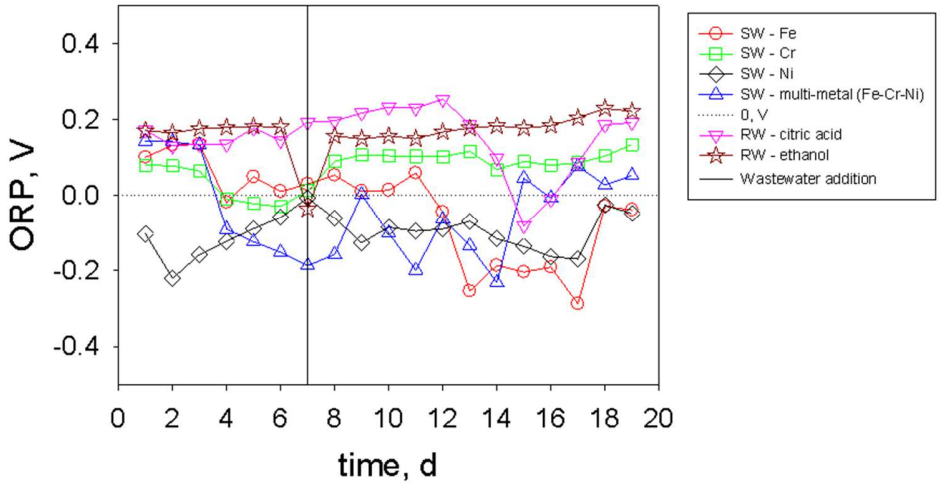

Figure 4.13 Redox potential in the ASFMBR for the synthetic and real wastewaters treatments. SW and RW means synthetic and real wastewater, respectively.

Table 4.3 Elements precipitated on GC both synthetic wastewater and real wastewater treatments for the GC circulating in the conical and cylindrical section of the ASFMBR. SW and RW means synthetic and real wastewater, respectively.

Test -SW		individual addition		multi-metal (Fe-Cr-Ni)	
	Section	Conical	cylindrical	conical	cylindrical
mg/g-GC	Fe	2.58	3.58	0.92	4.17
	Cr	0.72	0.99	0.18	0.47
	Ni	1.16	1.53	0.48	1.25
Test-RW	e^- donor	citric acid	ethanol	citric acid	ethanol
	GC	conical section		cylindrical section	
mg/g-GC	Fe	2.4	2.78	2.58	3.66
	Si	1.3	2.48	0.05	0.66
	K	0.69	0.8	1.24	0.72
	Cr	0.44	0.65	0.64	0.87
	Ni	0.35	0.47	0.5	0.7
	P	0.35	0.26	0.41	0.45
	Ca	0.14	0.22	0.39	1.01
	Mn	0.1	0.1	0.13	0.2
	Al	0.02	0.07	0.04	0.3
	Mg	0.01	0.06	0.03	0.21
µg/g-GC	Mo	20.88	12.63	11.42	12.66
	Zn	9.17	10.17	10.21	16.32
	Co	4.63	8.41	7.97	13.97
	Na	27.93	6.99	44.57	22.29
	V	1.49	1.88	2.09	3.36
	Cu	4.25	1.38	13.06	4.64
	Li	0.25	0.24	0.19	0.54
	Pb	0.69	0	0.57	1.42
	Sn	0.15	0	0.02	0

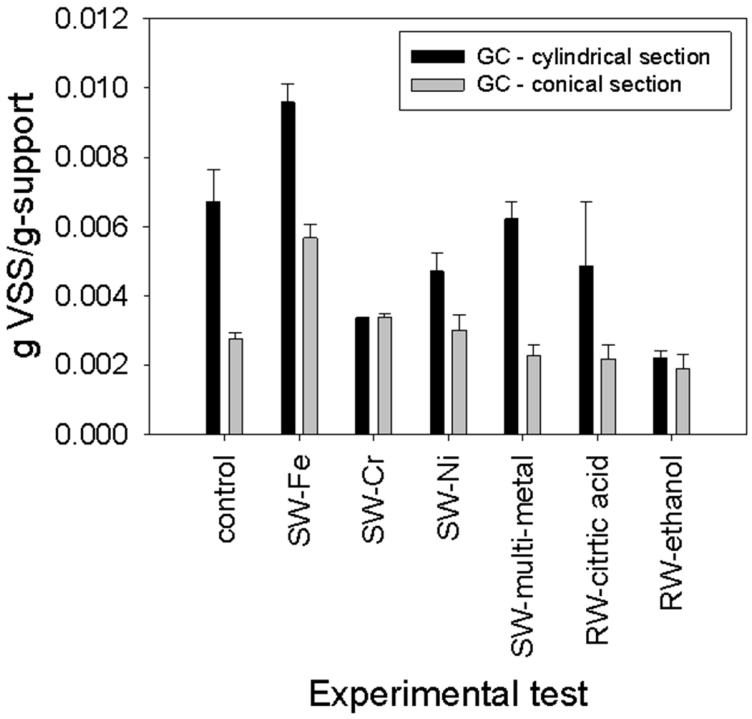

Figure 4.14 Volatile suspended solids of the biofilm supported on GC circulating in the conical and cylindrical section of the reactor for the synthetic and real wastewater experiments. SW and RW means synthetic and real wastewater, respectively.

4.4.2.2 Real wastewater tests

4.4.2.2.1 Precipitation column

This treatment unit showed the capacity to retain significant amounts of Fe, Cr, Ni, Sn, Mn, Mo, Co, Pb, Cu and V for experiments performed with both carbon sources during the treatment of real stainless-steel industry wastewater (Fig. 4.9). However, B, Al, Ca and Mg were poorly recovered here. Additional elements were obtained during the operation with ethanol, such as Si and Na, while Mo was completely recovered. The higher metal removal achieved with ethanol as compared to citrate was probably due to the absence of metals-complexes formation, which allowed high metals precipitation. For both carbon sources, less than 40% of metals present in

the industrial effluent was retained in the precipitation column. The acidic feed was neutralized in this column after a few days of operation. Nevertheless, the pH was drastically decreased to values around 3 and 2 for ethanol and citrate experiments, respectively. This may be explained by high metals precipitation occurring and deficient recirculation of the alkalinity from the ASFMBR to the column. However, a higher amount of metals was retained in the column as compared to experiments performed with synthetic medium. This could be explained by the higher HRT applied during the treatment of real wastewater, which allowed saturation and precipitation of a larger amount of insoluble species. Thus, further work should be conducted to optimize the precipitation column to increase metals recovery.

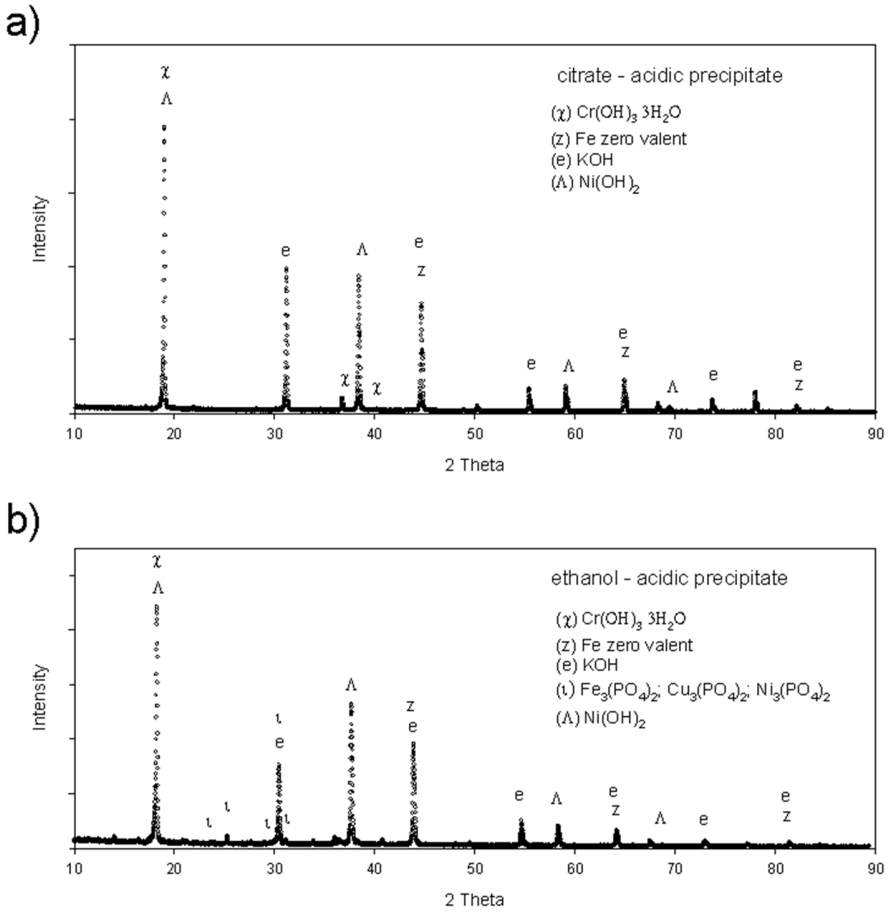

Figure 4.15 XRD diffractogram of the solids founded before the inlet of the precipitation column at acidic conditions for the citrate (a) and ethanol (b) treatments in the real wastewater experiments.

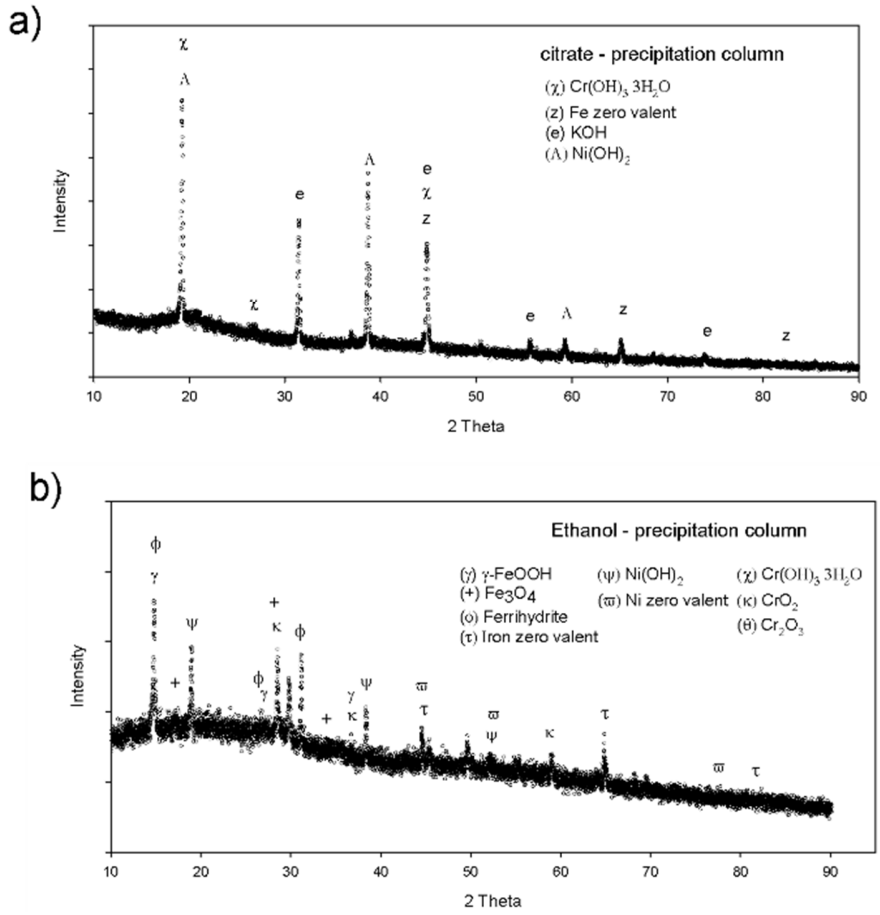

Figure 4.16 XRD diffractogram of the solids founded in the precipitation column for the real wastewater treatment with (a) citrate and (b) as electron donors.

Some studies have reported that citrate and heavy metals can be jointly precipitated both at acidic and alkaline pH values [169,176,177]. Nevertheless, for the present study, crystalline solids were obtained for both electron donors under acidic pH previous to the precipitation column, while citrate was not detected by XRD analysis. Minerals detected by XRD under acidic pH include $Cr(OH)_3 \cdot 3H_2O$, Fe(0), K(OH) and $Ni(OH)_2$ for both electron donors tested (Fig. 4.15). Additional picks related to phosphates of Fe, Cu and Ni were also detected by XRD for the ethanol test, which agrees with the presence of phosphorus in the wastewater studied. The same solids obtained under acidic pH were settled in the precipitation column for the citric acid test (Fig 4.16(a)). Additional species were recovered for the ethanol experiment, such as lepidocrocite (γ-FeOOH), which could be formed by the oxidation of green

rust [175]. Other precipitated minerals include Fe_3O_4, ferrihydrite, Fe(0), Ni(0), CrO_2 and Cr_2O_3 (Fig. 4.16(b)).

4.4.2.2.2 ASFMBR

The pH in the ASFMBR gradually decreased from 9 to 7.5 for experiments with citrate, while it could be maintained above 8 for most experimental period with ethanol; although the pH dropped to 5.5 for the last days of operation with the latter substrate (Fig. 4.10). The better control of pH with citrate (Eq. 4.4) could be due to higher alkalinity produced as compared with ethanol (Eq. 4.5). pH decrease could be related to the amount of metals forming species with denitrifying by-products. All elements were removed above 90% in the ASFMBR with both electron donors, except for Na and Ca with a retention below 80%, and Mg with precipitation lower than 30%. For the remaining elements, the amount of metals retained in the reactor for citrate tests (≥90%) by citrate residual concentration in the ASFMBR was lower than that obtained in ethanol experiments (≥99%) (Fig. 4.9). Ethanol can be considered as a suitable electron donor to achieve high nitrate removal, but the pH can also be decreased affecting the denitrification performance, which is also reflected in deficient alkalinity production, thus shrinking metal precipitation and pH control of the ASFMBR. On the other hand, citrate maintains an adequate pH, but the metals-citrate complexes formed were hardly removed. Complexes of citrate with Sn(II)[34], Sn(IV)[35], Mg(II)[36,37], Ca(II)[36,37], Co(II)[31,32], Mn(II)[31,32], Mo(VI) [38], Zn(II)[32], Cu(II)[24,30,31], Al(III)[39], Pb(II)[22], Na[37], K[37], and V[40] can also be found, in addition to the main metals studied (Fe, Cr and Ni). Ethanol does not form any complex with the metals, but a low fraction of Ni, Mn, Si B and Co crossed the permeate line, and thus were detected in the effluent. The main minerals recovered in the ASFMBR during its operation with ethanol were $Fe(OH)_2$, akageneite (β-FeOOH), Fe_3O_4, CrOOH, $Ni(OH)_2$, $NiCO_3$ and possible co-precipitation as Cr_2O_3NiO, Cr_2FeO_4 and Cr_2O_3 (Fig. 4.8). For experiments performed with citric acid, it was difficult to identify the species precipitated.

Similar to the results obtained with synthetic wastewater, the amount of elements precipitated on GC particles circulating at the superior traps of the reactor was higher than those prevailing in the conical section, except for Si. The formation of metals-citrate complexes decreases metal precipitation on GC particles, which can be observed with the higher concentration of metals for ethanol experiments (Table 4.3). The amount of metals precipitated on GC particles showed the following trend Fe>Si>K>Cr>Ni>P>Ca>Mn for elements with ≥ 0.1 mg/g-GC. Interestingly, Si was present at high concentration on GC particles and characterized as SiO_2 by XRD analysis (Fig. 4.17); however, it was hardly found in other solids analyzed. Dai and Hu (2015) reported that a surface of quartz particles can be affected by the presence of ions, such as Cr(III), which change their charge, consequently inhibiting the precipitation of iron hydroxide on quartz. However, further investigation must be performed to clarify these aspects. Additional elements, such as Mn, Al, Mg, Mo, Zn, Co, Na, V, Cu, Li, Pb and Sn were detected at trace concentrations. Precipitation of metals in a FBR under denitrifying and sulfate-reducing conditions has also been reported using GAC as supporting material for biomass, obtaining the precipitation of Ni, Fe, Ca, Mg, Mn, S and P, being Ni the principal metal of study [54].

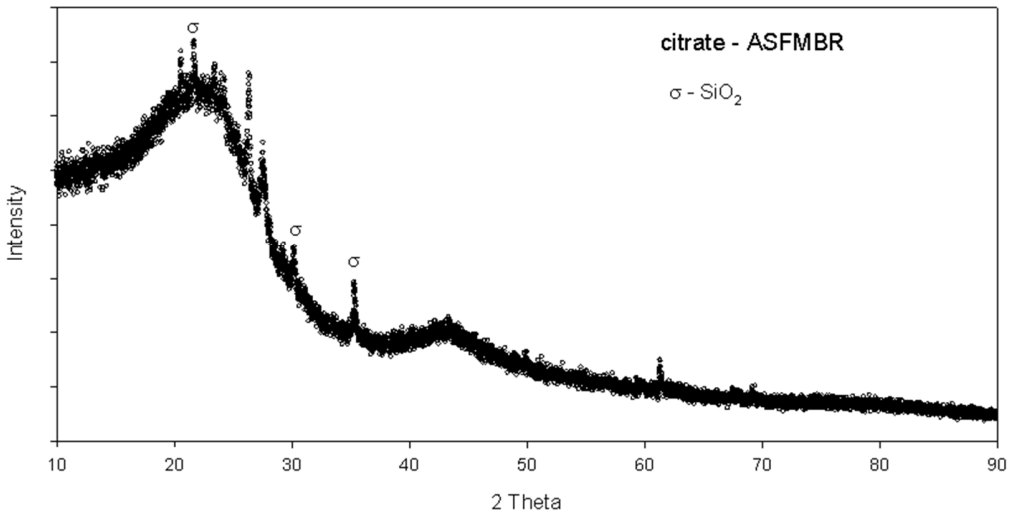

Figure 4.17 XRD diffractogram of the GC in the ASFMBR for the real wastewater treatment with citrate as electron donor.

4.4.3 Filtration performance in the ASFMBR

Degradation of citrate and ethanol through denitrification implies the production of SMP linked to microbial growth, cells decay and lysis. Additionally, SMP production could also be associated to protection of microorganisms against toxic effects of some metals [173]. This could contribute to the organic-inorganic membrane fouling by metal deposition [79]. Besides, metal precipitation with by-products or dissolved organic matter increases the content of TSS, which can also contribute to membrane fouling. During the reactor operation, SMPp gradually increased for the tests with individual Cr(III) addition and with the supply of the three metals together. Similar results were also observed in experiments performed in the absence of metals (Chapter 3, section: 3.4.3), which was triggered by the reactor design promoting accumulation of solids rejected by the membrane. For experiments run with iron addition, SMPp concentration decreased, while the opposite happened during Ni(II) addition (Fig. 4.18(a)). Despite this considerable increase, the suction pressure of the permeate line remained unaltered (Fig. 4.19). Nevertheless, a report indicates a link between SMP and Fe(III)/Fe(II) [179] and the co-precipitation between SMP and Fe(III) [180]. This co-precipitation could prevent membrane fouling. The addition of the three metals together resulted in a gradual and slow increase on the SMPp in the reactor. The negative effect of Ni(II) on high SMPp production could have been decresed by the positive effect of iron on SMPp production. An important decrease on SMPp was observed during the treatment of real metallurgic wastewater, perhaps due to the high Fe concentration fed, which precipitated with the proteins. This might have had an effect on the production of SMPp.

Despite the decrease observed on SMPp with the addition of iron, an increase in the suction pressure was detected during this experiment (Fig. 4.19), indicating some membrane fouling. This was the unique case with this behavior observed. According to the SMPc concentration in the reactor (Fig. 4.18(b)), addition of metals resulted in a gradual increase, except for the iron tests, where a high production of SMPc was obtained. Likewise, the TSS concentration was higher with iron addition than with the other metals, which may be related to the high iron precipitation obtained (Fig.

4.20). Therefore, membrane fouling could be explained by the higher SMPc and TSS concentrations reached in the ASFMBR. The higher attribution of SMPc with respect to SMPp on membrane fouling has previously been reported [160] and the insertion of heavy metals resulted in an increase on SMP, concomitant to membrane fouling, which was attributed to the attachment of SMPc to the membrane surface during the treatment of domestic wastewater [79]. The concentration of SMP on the cake layer formed over the membrane was found to be higher for carbohydrates (294.3±10.2 mg/cm^2) than for proteins (43.3±2.3 mg/cm^2) in a previous test conducted without fluidization in the ASFMBR (Chapter 3, section: 3.4.3). This implies an affinity of carbohydrates to be adhered on the membrane. However, the concentrations of SMPc and TSS reached in the reactor during the experiments with Fe were similar than those obtained in a previous experiment performed without heavy metals addition, in which not fouling was observed (Chapter 3, section: 3.4.3 and 3.4.5).

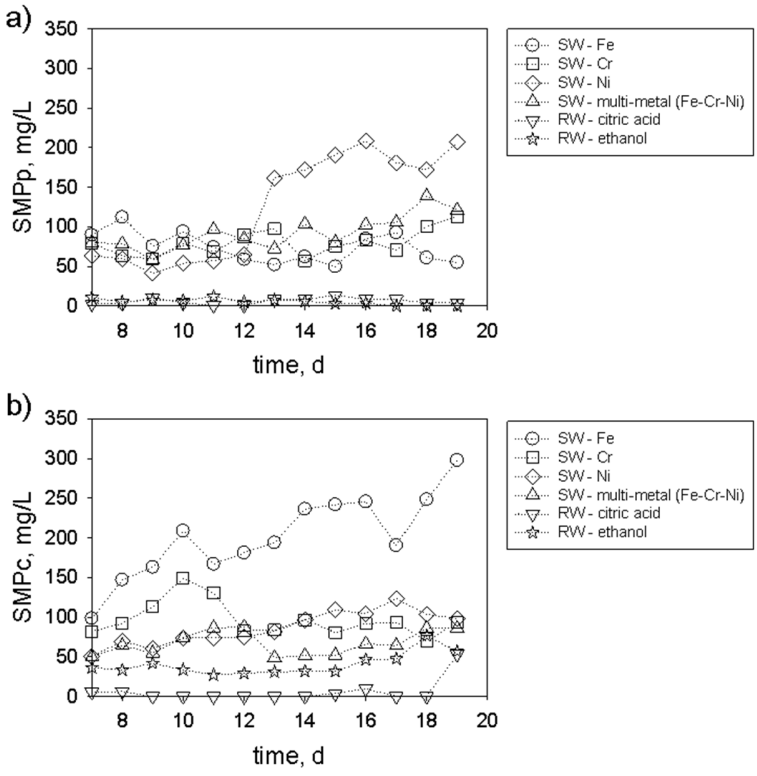

Figure 4.18 Soluble microbial products in terms of (a) proteins and (b) carbohydrates for the synthetic and real wastewater treatments. SW and RW means synthetic and real wastewater, respectively.

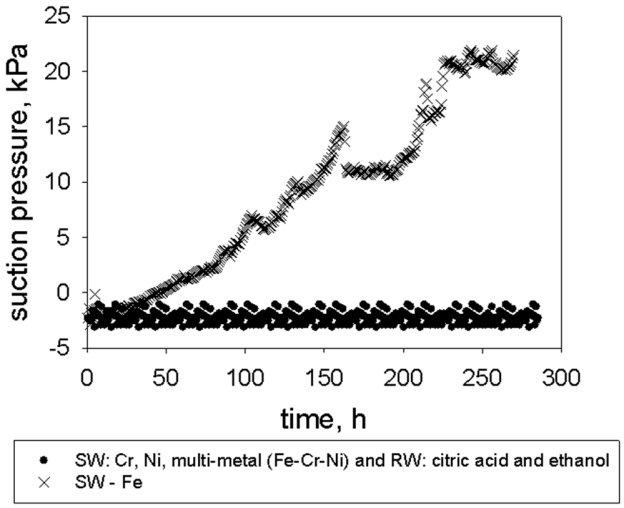

Figure 4.19 Suction pressure at the permeate line for the synthetic and real wastewater experiments. SW and RW means synthetic and real wastewater, respectively.

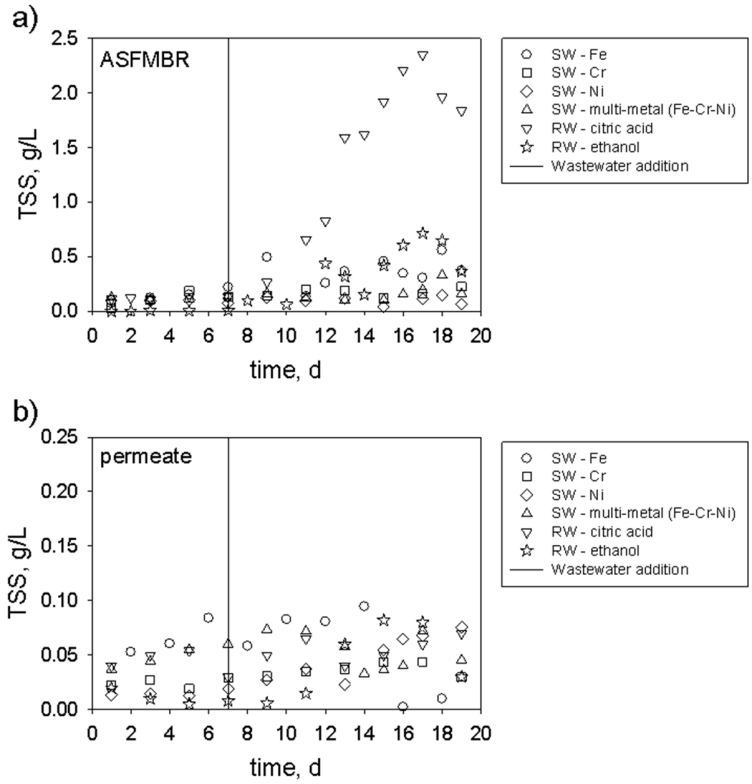

Figure 4.20 Total suspended solids for the synthetic and real wastewater experiments in the (a) ASFMBR and (b) permeate line.

Metal precipitation could have also caused membrane fouling. Concentrations of Cr and Ni on the membranes were low for the experiments with citric acid (Fig. 4.21(a) and (b)). This happened even at the higher metal rejection obtained on the real wastewater treatment compared with synthetic experiments. Meanwhile, for Fe-addition experiments, the Fe concentration on membranes was in agreement with the concentration of Fe added. A previous hydrodynamic study of the reactor revealed that higher shear stress and particle momentum was obtained at the lower part of the reactor (Chapter 3, section: 3.4.3). Low shear stress and particle momentum on the membrane are related to higher SMP deposition. Similar metals concentration on the membrane was observed for the experiments with synthetic wastewater. Metals concentration on the membrane increased with the height of the reactor where the shear stress and particle momentum are low, excepting for Fe experiments. However, lower amount of metals was detected at the highest zone of the reactor. This could be explained because, at this height of the reactor, the adherence of SMP was higher due to deficient GC particles fluidization and low shear stress obtained in this zone of the reactor (Chapter 3, section: 3.4.3). SMP covered membrane surface, thus avoiding metals deposition thereafter. The presence of heavy metals, such as Zn(II), Cu(II), Pb(II) and Cd(II), in cake layer has been reported in MBR [79]. Another aspect is that, due to the accumulation of SMP on the membrane at the upper part of the reactor, porous were covered and thus it is expected that filtration was mainly carried out in membranes located in the lower part of the ASFMBR, where low concentration of SMP were found.

The high HRT applied during the treatment of real wastewater promoted large solids precipitation and, as a consequence, high metals rejection by the membrane. The Fe concentration on the membrane for the citrate experiments (≤0.16 mg/cm^2-membrane) was higher than that obtained in synthetic tests (≤0.04 mg/cm^2-membrane). However, the concentration greatly increased to 0.76 mg/cm^2-membrane for the experiment with ethanol. Therefore, the Fe-citrate complex moved the iron through the membrane and decreased its precipitation thereafter, obtaining iron in the permeate line. Despite the high precipitation of metals, especially Fe, on the membrane during the treatment of real wastewater, suction pressure remained

unaltered (Fig. 4.19). A remarkable difference in concentration among the metals studied occurred at different reactor heights (Fig. 4.21(b)). The lowest concentrations were detected in the upper part of the reactor, which could be related to the high amount of SMP deposited on this zone of the ASFMBR (Chapter 3, section: 3.4.3) preventing metals deposition on the membrane. The concentration of TSS in the reactor (≤0.72 g/L) was lower when ethanol was supplied as electron donor than that produced with citrate (≤1.96 g/L). This could be explained by the high metals concentration maintained in solution due to the metals-citrate complexes formed, which avoided metals precipitation. These solids are suspended and rejected by the membrane, which can be observed by the amount of TSS measured in the permeate line, reaching values ≤0.10 g/L for all the experiments (Fig. 4.20).

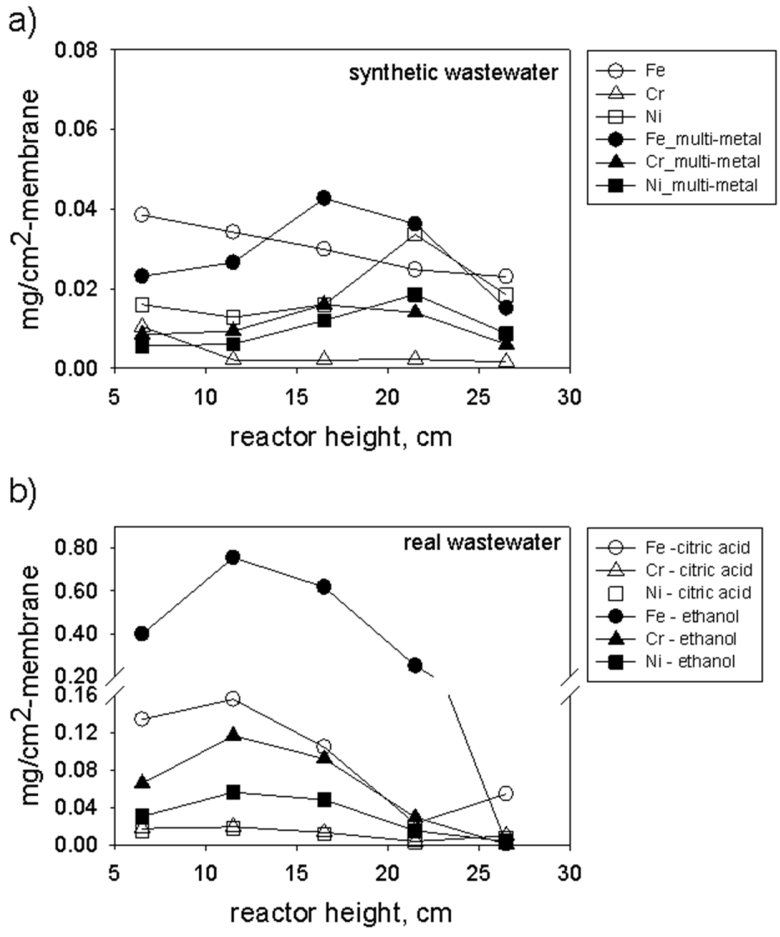

Figure 4.21 Principal metals on membrane surface at different heights of the reactor for the (a) synthetic wastewater and (b) real wastewater treatments.

The swirling fluidization of GC particles can decrease cake layer growth on the membrane surface; however, internal fouling of the membrane can occur. The presence of iron in MBR has resulted in amorphous ferric oxyhydroxides particles and gelatinous assemblages containing Fe(III) bound to polysaccharides responsible for irreversible membrane fouling [181]. For the present study, difference iron-bearing minerals were identified during the operation of the ASFMBR. Siderite (green color) was deposited in different zones of the reactor during the operation with iron, while additional iron-containing solids (brown color, characteristic for ferric oxides and hydroxides) were also detected in the remaining experiments. This was confirmed by XRD analysis. Similar colored minerals were observed on the membranes at the end of the experimentation. Siderite precipitation could have caused membrane fouling in experiments performed with iron, while deposition of iron oxides and hydroxides in the other experiments could occur without affecting membrane filtration. Thus, the prevalence of different iron minerals may affect the half-life of the membrane.

4.5 Conclusions

The ASFMBR introduced in the present study showed high nitrate removal efficiency during the treatment of synthetic and real metallurgic wastewater with negligible production of NO_2^- and N_2O. The acidic pH was efficiently neutralized by high recirculation of denitrifying by-products. This strategy also allowed precipitation and recovery of a large amount of metals present in the metallurgic effluent, although further studies should be conducted to optimize the recovery of metals. Membrane fouling was prevented by the hydrodynamic conditions prevailing in the ASFBMR promoting appropriate GC particles fluidization. The treatment concept is promising to achieve efficient removal of nitrate and recovery of metals, while preserving the membrane module by the hydrodynamic conditions prevailing inside the ASFMBR.

5. General discussion and recommendations

5.1 Introduction

The characteristics of stainless-steel effluents demand their efficient treatment before discharge to fulfil environmental regulations. The treatment of this type of industrial effluent has the challenge to remove high nitrate concentrations, neutralize the acidic pH, and remove high amounts of metals. The applied treatment must be robust to resist the complex composition of the effluent and to accomplish the high requirements of discharge. Denitrification is a cost-effective process to remove nitrate [42] at high concentrations [9,43]. However, neutralization of the pH is required to fulfil regulations [10] and to obtain good denitrification performance[48]. This can be achieved by mixing the acidic inlet with denitrifying by-products[58,69], which reduce the need of external neutralizing agents. In addition, denitrifying by-products can precipitate with metals in the form of oxides, hydroxides and carbonates, reducing metals concentration in solution. Carbonates formation reduces the emission of CO_2, which is an important gas that contributes to the greenhouse effect. Referring to the content of metals in metallurgic effluents, some of them are trace elements, which are essential for denitrification, such as Fe, Ni, Mn, Mo, B, Co, Na, P, Ca, Cu, Mg. Moreover, Fe(II) can serve as electron donor in autotrophic denitrification [61]. However, high metals concentration can affect microbial activities in denitrifying processes, resulting in the accumulation of undesirable intermediates (NO_2^- and N_2O) [55,58,69]. These intermediates are of special environmental concern [47,163]. Moreover, the presence of citrate has two different effects. Firstly, metals complexation promoted by citrate reduces metals precipitation. Secondly, citrate can act as an electron donor for denitrification. Thus, the presence of citrate in metallurgic effluents has strong influence on the denitrification efficiency.

The aforementioned processes must be conducted in an adequate treatment system. Denitrification of synthetic wastewater with heavy metals has effectively

been performed in FBR in terms of nitrate reduction, pH neutralization and prevention of negative effects exerted by some metals. This has been achieved through high recirculation of alkalinity produced by denitrification in the reactor [54,58,69]. However, the outlet of the FBR contains a high amount of solids and metals. The use of membrane technology offers good solids rejection that can resolve the effluent of FBR with high solid content. Membrane bioreactor wastewater treatment technology is a combination of a membrane separation unit and a biological treatment process to obtain good retention of microorganisms (long SRT), which can allow the operation of the system at short HRT with excellent solids retention. However, membrane fouling is a major obstacle for the widespread use of MBR in many applications. For submerged membrane bioreactor, many studies indicate that membrane fouling is caused by particles deposition on the membrane surface. Thus, it is necessary to optimize the reactor design to prevent membrane fouling. During the last years, the confidence in the use of MBR for industrial wastewater treatment has increased, even when several challenges are present [71,72]. The presence of metals in industrial effluents during the application of biological treatment systems and membrane filtration has resulted in metals accumulation in sludge components [78]. Additional effects include inhibition of the biological process, change in the sludge characteristics, and inorganic fouling by precipitation or incrustation of minerals on the membrane surface [79,80]. In industrial wastewater, it has been reported that Cr and Pb intensify membrane fouling [81]. Thus, the main challenges for stainless-steel wastewater treatment are maintaining a good biological activity, joined to high metals retention toward avoiding membrane fouling.

The development of the anaerobic fluidized membrane bed bioreactor has resulted in a promising antifouling technique. Several studies have been focused on evaluating factors, such as size of media, carrier dosage, adsorbing media capacity and process configuration [96,101–103]. AFMBR has even been probed at pilot scale [104]. Some problems associated to this type of reactor include bioreactor size limitations due to the height-to-diameter ratio, high energy requirements due to high recycle ratios, and long start-up period for biofilm formation, as well as membrane

fouling after certain time of operation. However, this technology has hydrodynamic characteristics promoting excellent mixing, which enable high-rate environmental and industrial applications [68]. Manipulation of hydrodynamic conditions around membrane surfaces to avoid membrane fouling has not been explored, becoming an important area of research [74]. In the present work, a novel Anaerobic Swirling Fluidized Membrane Bioreactor (ASFMBR) was developed and tested for the treatment of the stainless-steel effluent. In this chapter, the relevant results obtained during the treatment of this effluent will be discussed. The discussion focuses on the effect of metal-citrate complexes on denitrification process. Moreover, this chapter also discusses the feasibility of GC particles fluidization with a swirling fluidization on denitrification performance and membrane fouling mitigation. Likewise, the test of the treatment both synthetic and real stainless-steel effluent through the ASFMBR is also discussed.

5.2 Chemical aspects driving denitrification of wastewater in the presence of metals and citrate

Chapter 2 describes the use of citrate as electron donor on denitrification, which yielded a better performance in comparison with ethanol, which is commonly used in denitrifying processes. However, the interaction of citrate with the metals present in the synthetic metallurgic wastewater resulted in different effects depending on the stability of the metal-citrate complexes. These effects include both inhibition and stimulation denitrification. For instance, citrate limits metals precipitation and the complexes formed affect the bio-availability of both citrate and metals to microorganisms. Citrate experiments also elucidated chemical species promoting inhibition of the denitrifying process. $[Fe\text{-}cit]_{(aq)}$ was readily biodegraded, while ferrous citrate complex, $[Fe\text{-}cit]^{-}$, was resistant to biodegradation. Nickel formed strong complexes, such as $[Ni\text{-}cit_2]^{4-}$ and $[Ni\text{-}cit]^{-}$. Predominant chromium species like $[Cr\text{-}cit_2]^{4-}$ caused denitrification inhibition and a simpler form of this species. Citrate decreases the effects of Ni on denitrifying microorganisms, supporting higher metals concentrations than those observed in medium lacking this complexing

agent. Chemical speciation analysis showed that $[Ni\text{-}cit_2]^{4-}$ is a stable complex that affects denitrification rate, whereas the ionic form of Ni affects nitrate reduction to nitrite. In general, iron and chromium inhibited the overall process (based on N_2 production rate), while nickel suppressed all denitrification steps. Furthermore, for both electron donors tested, it was observed an accumulation of nitrite and N_2O with the oversaturation of $NiCO_3$ and $Ni(OH)_2$, respectively. Another interesting aspect is that the multi-metals system showed milder inhibitory effects than individual metals systems. Positive effects promoted by Fe(II) on denitrification decreased the inhibition caused by Cr and Ni. This is a relevant aspect since real metallurgic effluents contain large iron concentrations. The information obtained from these batch assays is relevant to predict and understand the effects of metals, commonly found in metallurgic effluents, on denitrification performance, as well as the interaction between metals and denitrifying by-products.

5.3 Swirling fluidization in ASFMBR

Granular carbon fluidization in AFMBR has two main objectives, one of them is to serve as supporting material of microorganisms to carry out biological process, and the other one is to prevent the formation and growth of cake layer on the membrane walls by scouring effect. Different problems associated with the operation of FBR does emphasis on exploring a different type of fluidization. Fluidization in FBR usually occurs in one direction (upward and downward), whereas with swirling fluidization the movement of flow prevails in three special directions. The use of granular carbon as an antifouling technique has prevented cake layer growth on membranes surface. The hydrodynamic conditions established in the ASFMBR take relevance in the use of this technique, which depends on several factors, such as flow velocity, particle velocity, particle characteristics, material and geometry of the membrane, hardness and sizes of the particles, diffusers or distributers of the flow and reactor geometry. The proposal of the present dissertation was to design a novel reactor by changing the reactor geometry, the inlet flow pattern, and the membrane

module design. Collectively, these aspects created a swirling fluidization inside the ASFMBR for both the liquid phase and granular carbon particles, which has not been reported in fluidized bed reactors. In this work, higher water shear stress was obtained in comparison with other reactor configurations, while and for particle momentum similar and lower values were obtained; these at lower packing ratio. This is important to decrease the operational costs and to increase the fluidization around the membranes. Furthermore, the hydraulic conditions promoted inside the ASFMBR avoid dead zones. However, important attachment of SMP occurred in the upper part (cylindrical section) of the reactor, where low shear stress and particle momentum prevailed. Nevertheless, the suction pressure remained unaltered during the whole operation period. Thus, swirling fluidization created hydraulic conditions, which prevented membrane fouling during denitrification of synthetic metallurgic wastewater.

Another challenge for the swirling fluidization was to produce an adequate fluidization without the loss of biomass on GC particles, which could be detached by the collision of GC particles with membranes and by the shear stress caused by the GC fluidization. For swirling fluidization, GC was dragged by the flow circulation, then the difference in velocities between flow and GC was low, which decreases shear stress and maintains the biofilm. Through biomass measurement (VSS content) at the end of the experimentation, it was observed that biofilm supported on small particles of GC was better preserved. This is because smaller GC particles collided the membranes to a lower extent as compared to bigger GC particles. Denitrification was successfully carried out with high nitrate removal efficiency and low intermediates production. Thus, it could be concluded that swirling fluidization maintained good mixing conditions to avoid mass transfer limitations in the denitrifying process. Another important aspect was pH neutralization. The alkalinity generated through denitrification and the high recirculation established in the reactor could neutralize the acidic pH feed, which is highly convenient for the treatment of metallurgical wastewater. These favorable results emphasize that the ASFMBR is a suitable technology to treat this type of industrial effluents.

5.4 Application of the ASFMBR to achieve denitrification and metals bio-recovery from metallurgic wastewater

5.4.1 Treatment of synthetic metallurgic wastewater

Addition of the principal metals found in stainless-steel effluents (Fe, Cr, and Ni) to the ASFMBR showed different aspects on denitrification and on the filtration performance, as well as on metals bio-recovery. Denitrification efficiency was increased with Fe(II)/Fe(III) addition, which agrees with previous results obtained in batch assays (Chapter 1). This is because Fe(II) oxidation, in solution or precipitated, contributes to reduce NOx species. Cr(III) yielded mild inhibition to the denitrification process by the stable complex formed, whereas Ni(II) did not show negative effect on denitrification as expected. Joint addition of the three metals studied counteracted negative Cr(III) effects, so that high nitrate removal was obtained. As observed in batch assays, the positive effect of iron offset the adverse effects of Cr and Ni.

A precipitation column was placed before the ASFMBR to promote precipitation and recovery of metals. However, poor metals recovery was achieved with synthetic wastewater, which could have been due to insufficient alkalinity recycled from the ASFMBR to the precipitation column, as well as to the high stability of the metals-citrate complexes. A higher precipitation was obtained in the ASFMBR, where the microbial degradation of citrate and the denitrifying by-products generated promoted metals precipitation. Metal precipitation was higher for the studies conducted with the three metals together as compared with individual assays, which could be due to co-precipitation and/or reduction of metal-citrate complexes stability by saturation.

The outlet of the reactor was constituted only by the line of permeate flow. This allowed saturation of chemical species, their precipitation, and rejection by the membranes. Metals were mainly precipitated at the traps of the ASFMBR and another fraction on GC particles. Previous works report XRD analysis revealing Ni(II) precipitation as $Ni_3(PO)_2$ in a FBR under denitrifying conditions [54], but chemical speciation analysis further predicted precipitates, such as hydroxides and carbonates of Ni(II), as well as a large amount of Ni(II) in solution. In the present

work, Ni was recovered as $Ni_3(PO)_2$ and $NiCO_3$ in studies with individual addition of metals. Furthermore, Ni was precipitated as $Ni(OH)_2$ when the three metals were added simultaneously to the ASFMBR. The higher HRT applied in the present work, through the reactor design, allowed a higher metal retention in the reactor and allowed to reach the equilibrium of diverse species to be precipitated.

Membrane fouling was mitigated by GC fluidization, except for the experiment with iron addition in individual form. The important parameters that have influence on membrane fouling, such as SMPp, SMPc and TSS where determined. Among them, SMPp concentration decreased with iron addition, whereas SMP and TSS concentrations were higher than those observed with the other metals studied. This could explain the cause of membrane fouling; however, the values of solids reached were similar to those measured in previous control experiments without metals addition (Chapter 3, section: 3.4.3). This indicates that membrane fouling could not be explained only with these parameters. Another parameter determined was the concentration of metals on the membrane, in which higher concentration of iron was obtained in comparison with the other metals. However, for experiments performed with real wastewater, a higher iron concentration on the membranes was detected. However, the suction pressure remained unaltered for these experiments. An important difference observed was the amount of iron precipitated. For experiments with individual addition of Fe, predominant amorphous $FeCO_3$ precipitated, whereas for the other experiments, iron oxides and hydroxides were principally precipitated. Amorphous ferric oxyhydroxides bound to polysaccharide have been reported as a responsible factor for irreversible membrane fouling [181]. Thus, the prevalence of different iron minerals may affect the clogging porous of the membrane. For this case, the presence of other metals, in addition to iron, resulted favorable to decrease $FeCO_3$ precipitation, which was observed in experiments conducted with individual iron addition.

5.4.2 Real metallurgic wastewater

High denitrification and filtration efficiencies were accomplished during the treatment of real metallurgic wastewater. The high Fe(II)/Fe(III) concentration present in this effluent supported high nitrate removal efficiency and scarce intermediates production. Likewise, the high precipitation of metals obtained in the precipitation column and in the ASFMBR alleviated their negative effects on denitrification. An interesting aspect is that ethanol promoted a better performance as electron donor as compared to citric acid. This was contradictory to the results obtained in batch assays. This discrepancy could be due to the hydrodynamic conditions established in the ASFMBR, which were different to the mixing conditions prevailing in batch incubations by orbital shaker. Likewise, the amount of solids maintained in suspension was lower for experiments conducted with ethanol than that observed with citric acid. This is important to take into account because scaling of the process from batch assays to full scale could result in different responses. Filtration was performed without any change in suction pressure, even though high metals rejection occurred. Interestingly, Cr and Ni were poorly attached to the membrane, in contrast to iron, which accumulated at an important level. This indicates that the nature of the minerals formed has influence on the interaction with the membranes, with some of them being dragged by the circulating flow prevailing in the reactor, while others being attached to the membrane surface.

As expected, the amount of metals precipitated was higher for ethanol tests than that obtained in citrate experiments. Likewise, minerals produced during the experiments with ethanol showed high settling capacity. Membranes can efficiently reject the solids formed inside the ASFMBR; however, settling of the solids must be achieved with additional strategies. Characterized minerals, recovered from the treatment system, include oxides, hydroxides and carbonates. Regarding metals precipitation on GC particles, this occurred with both carbon sources tested and recovered minerals showed predominant elements, such as Fe, Si, K, Cr, Ni, P, Ca, and Mn, being higher their concentration in zones with low flow velocity (upper part of the ASFMBR). However, Si was an exception because its concentration was higher in

GC particles circulating in the zone with high flow velocity in the reactor (conical part). This could indicate that hydrodynamic conditions can affect attachment of metals on GC particles. An additional aspect was the precipitation under acidic conditions, in which production of minerals with a higher crystallinity occurred as compared to minerals recovered under alkaline conditions.

Table 5.1 Limit of discharge established by the Mexican legislation (NOM-001-SEMARNAT-1996 and values obtained for treated real wastewater (RW) with citric acid and ethanol as electron donors.

Parameters	Limit of discharge	RW treated with citric acid	RW treated with ethanol
mg Total-N/L	≤ 35	24-62	0-1.5
pH	6.5-8.5	8.33-9.77	5.7-9.2
COD, mg/L	≤ 210	600-800	0-53.2
TSS, mg/L	≤ 84	40-70	5-82
Cu, mg/L	≤ 6	0.01-0.14	0-0.03
Cr, mg/L	≤ 1.5	0.35-132.8	0-0.06
Ni, mg/L	≤ 4	0.12-61.28	0.13-0.74
Pb, mg/L	≤ 0.4	0-0.18	0-0
Zn, mg/L	≤ 20	0-0	0-0

Mexican legislation establishes the maximum concentration of contaminants allowed in discharged wastewaters [10]. Table 1 shows a comparison of these parameters with those obtained in the treated wastewater in the system precipitation column-ASFMBR. Total nitrogen concentration achieved through the treatment concept was within an acceptable discharge level when ethanol was used as electron donor, whereas for citrate the level obtained was slightly higher. This could be due to the metals-citrate complexes formed, which limited the availability of this electron donor, but this limitation could be overcome by supplying an additional electron donor. The acidic pH can be neutralized by the alkalinity generated denitrification. However, for experiments performed with ethanol, high metal precipitation decreased the pH.

Thus, it is necessary to add an external neutralizing agent to maintain the pH under favorable values for denitrification.

A problem with the presence of citrate, as chelating agent of metals, is that it is difficult to be degraded, thus metals remain complexed with citrate reducing their precipitation. This implies that metals can be transported through the wastewater treatment system to the discharge, as occurred with Cr and Ni, so that their concentration exceeded the limit of discharge. Likewise, the COD obtained was higher because citrate was not fully degraded. The addition of an external electron donor must be handled carefully since an excess can lead to high COD concentration in the discharge. Thus, automatization of the process is required. On the other hand, filtration showed a good performance as the concentration of solids was constant and below to the limit of discharge. Another important aspect to control is Fe(II) oxidation, which contributes to reduce nitrate. However, the prevalence of autotrophic denitrification with Fe(II) decreases the uptake of citrate or ethanol, thus a residual concentration is obtained, increasing the outlet COD. Therefore, the porous size used was adequate to obtain a discharge fulfilling legislation standards. Lower size of porous in the membrane could be tested to increase metals retention when citrate is used as electron donor during the treatment of metallurgic wastewater.

5.5 Concluding remarks

The effects of chemical speciation of metal-citrate complexes on denitrification performance was studied. Fe(II) improved nitrate removal, while Ni(II) affected the reduction of NO_3^-, NO_2^- and N_2O. Cr(III) only inhibited the nitrate reduction step. Swirling fluidization of granular carbon in the AFMBR is suitable to carry out denitrification and mitigate the growth of cake layer over membranes surface. In continuous studies performed in the ASFMBR, it was observed that addition of metals decreases the negative effects of Ni(II) on denitrification. Fe(II) stimulated the process possibly by promoting autotrophic denitrification, and Cr(III)-citrate

complexes were difficult to break. The ASFMBR concept showed to be a suitable technology for the treatment of spent pickling baths discharged in the stainless-steel production. Negligible production of denitrification intermediates, efficient neutralization of acidic pH and high metals recovery with denitrifying by-products could be achieved in the ASFMBR. Furthermore, the hydraulic conditions established in the bioreactor together with the collision of the membranes driven by GC particles prevented membrane fouling. Nevertheless, the precipitation column needs to be optimized to increase the recovery of metals. For the treatment of effluents in the presence of citrate, it will be necessary to implement an additional strategy for the recovery of metals from metallurgic wastewater.

5.6 Recommendations for future research

For the first part of the project, through chemical speciation analysis, it was observed that Ni(II) in ionic form affected the step of nitrate reduction to nitrite. Moreover, accumulation of nitrite and N_2O was linked to oversaturation of $NiCO_3$ and $Ni(OH)_2$, respectively. Further research must be performed to clarify the relation between the species precipitated and the production of the denitrification intermediates. The improvement of denitrification performance with Fe(II)/Fe(III) addition must be clarified to understand the contribution of Fe(II) oxidation, both with Fe(II) in solution and with Fe-bearing minerals. The effects of other metals in the denitrifying process should also be assessed. Regarding the ASFMBR, the study of several aspects related to reactor design can be considered with the aim to optimize the collision of particles with the membrane and to increase the shear stress. One parameter of design is the inlet to the ASFMBR, which has relevance in the trajectories of particles developed around the membranes. The objective of the study could be the determination of the higher values of both particle momentum and water shear stress varying the size, geometry, and angle of the inlet with the fewer energy requirements. Particle characteristics, such as sizes, hardness, density and form factor, as well as the packing ratio, also have an influence on particle trajectories. Therefore, a study

involving different conditions with these characteristics for evaluating particle momentum and shear stress at the lower energy requirements can be useful to improve the filtration. Membrane module can also be improved with the increase of membranes to produce a higher permeate flux. In addition, membranes can be positioned in different configurations with the aim to increase GC particles collision with the membrane surface, which depends on particle trajectories and membrane location. Likewise, the conical section of the ASFMBR has a good performance, however, the cylindrical section has low efficiency in avoiding the attachment of solids to the membranes. All these aspects of the design can be tested with computational fluid dynamics to reduce the costs and time for reactor optimization. In addition, the inadequate hit of GC particles with membrane walls can affect the integrity of the membrane walls. Thus, further research should be directed for evaluating membrane integrity at long-term operation periods. Another interesting aspect was the contradictory effect on denitrification performance obtained between batch assays and those performed with the ASFMBR, possibly due to the shear stress applied. Besides, the content of solids maintained in solution was lower in experiments conducted with ethanol. Thus, it is interesting to decipher the effects of shear stress on denitrification and filtration performance with different carbon sources.

Precipitation of metals under acidic conditions can be a favorable option for metal recovery. Hence, key aspects involved in precipitation can be studied, improving the recovery of metals. Iron minerals formed during precipitation of this metal with denitrifying by-products must be understood and controlled to avoid the prevalence of amorphous solids, which could promote the membrane fouling. In addition, the hydrodynamic effects on metals precipitation on GC particles is interesting to study with the aim to determine the flow velocity at which metals recovery can be optimized. The physical properties of GC must be considered because the change of GC density can yield a higher particle momentum. However, the increase of hardness of the GC by metals precipitation over it can affect the integrity of the membranes. Then a study of different GC hardness and the effect on membrane

integrity must be performed. Minerals recovered from metallurgic effluents should also be tested in the future as catalysis in environmental applications [182].

References

[1] J.S. Noh, N.J. Laycock, W. Gao, D.B. Wells, Effects of nitric acid passivation on the pitting resistance of 316 stainless steel, Corros. Sci. 42 (2000) 2069–2084. doi:10.1016/S0010-938X(00)00052-4.

[2] W.E. Mckee, W.F. Hamilton, Analysis of Hydrofluoric-Nitric Acid Stainless Steel Pickling Bath, Ind. Eng. Chem. 17 (1945) 310–312.

[3] C. Frías, O. Pérez, Recuperación de ácidos y metales en baños agotados del decapado de aceros inoxidables, Rev. Metal. 34 (1998) 427–431. doi:10.3989/revmetalm.1998.v34.iExtra.786.

[4] N. Sato, Basics of Corrosion Chemistry, in: S.K. Sharma (Ed.), Green Corros. Chem. Eng. Oppor. Challenges, First Edit, Wiley-VCH Verlag GmbH & Co. KGaA, 2012.

[5] R. Crookes, Decapado y Pasivado del acero inoxidable, 2004.

[6] American Iron and Steel Institute, Cleaning an descaling stainless steels, in: A Des. Handb. Ser. No. 9001, American Iron and Steel Institute, Washington, DC 20005, U.S.A., 1982.

[7] M. Maanonen, Steel Pickling in Challenging Conditions, 2014.

[8] Y. Fernández-Nava, E. Marañón, J. Soons, L. Castrillón, Denitrification of wastewater containing high nitrate and calcium concentrations, Bioresour. Technol. 99 (2008) 7976–7981. doi:10.1016/j.biortech.2008.03.048.

[9] Y. Fernández-Nava, E. Marañón, J. Soons, L. Castrillón, Denitrification of high nitrate concentration wastewater using alternative carbon sources, J. Hazard. Mater. 173 (2010) 682–688. doi:10.1016/j.jhazmat.2009.08.140.

[10] SEMARNAT, NOM-001-semarnat-1996, Límites máximos permisibles de contaminantes en las descargas de aguas residuales en aguas y bienes nacionales, 1996.

[11] D. 91/271/EEC, Council Directive 91/271/EEC of 21 May 1991 on urban waste water treatment, 1991.

[12] EPA, Nitrogen Control, (1993).

[13] A. Wood, M. Blackhurst, T. Hawkins, X. Xue, N. Ashbolt, J. Garland, Cost-effectiveness of nitrogen mitigation by alternative household wastewater management technologies, J. Environ. Manage. 150 (2015) 344–354. doi:10.1016/j.jenvman.2014.10.002.

[14] E.V.S.P. Rao, K. Puttanna, Nitrates , agriculture and environment, 79 (2000).

[15] WHO, Trace elements in human nutrition and health, Switzerland: Geneva, 1996.

[16] P.B. Tchounwou, C.G. Yedjou, A.K. Patlolla, D.J. Sutton, Heavy Metals Toxicity and the Environment, Natl. Inst. Heal. (2014) 1–30. doi:10.1007/978-3-7643-8340-4.

[17] A. Kumar, N. Singh, R. Pandey, V.K. Gupta, B. Sharma, Biochemical and Moleccular Targets of Heavy Metals and Their Actions, in: M. Rai, A.P. Ingle, S. Medici (Eds.), Biomed. Appl. Met., Springer Intrnational Publishing AG, 2018. doi:10.1007/978-3-319-74814-6.

[18] B. Dhal, H.N. Thatoi, N.N. Das, B.D. Pandey, Chemical and microbial remediation of hexavalent chromium from contaminated soil and mining/metallurgical solid waste: A review, J. Hazard. Mater. 250–251 (2013) 272–291.

[19] F. Fu, Q. Wang, Removal of heavy metal ions from wastewaters: A review, J. Environ. Manage. 92 (2011) 407–418. doi:10.1016/j.jenvman.2010.11.011.

[20] U.S. Army, Engineering and Design. PRECIPITATION / COAGULATION / FLOCCULATION, 2001.

[21] J.L. Pierre, I. Gautier-Luneau, Iron and citric acid: A fuzzy chemistry of ubiquitous biological relevance, Biometals. (2000) 91–96.

[22] C. Chu, K. Darling, R. Netusil, R.P. Doyle, J. Zubieta, Synthesis and structure of a lead(II)–citrate: $\{Na(H_2O)_3\}[Pb_5(C_6H_5O_7)_3(C_6H_6O_7)(H_2O)_3]_{9.5}H_2O$, Inorganica Chim. Acta. 378 (2011) 186–193. doi:10.1016/j.ica.2011.08.054.

[23] A.J. Francis, C.J. Dodge, Influence of complex structure on the biodegradation of iron-citrate complexes, Appl. Environ. Microbiol. 59 (1993) 109–113.

[24] T.B. Field, J.L. Mccourt, M.W.A. E, Composition and Stability of Iron and Copper Citrate Complexes in Aqueous Solution, Can. J. Chem. 52 (1974) 3119–3127.

[25] Y.Z. Hamada, N. Bayakly, A. Peipho, B. Carlson, Accurate Potentiometric Studies of Chromium-Citrate and Ferric-Citrate Complexes in Aqueous Solutions at Physiological and Alkaline pH Values, Synth. React. Inorg. Met. Nano-Metal Chem. 36 (2006) 469–476. doi:10.1080/15533170600777960.

[26] A.M.N. Silva, X. Kong, M.C. Parkin, R. Cammack, R.C. Hider, Iron (III) citrate speciation in aqueous solution, Dalt. Trans. 40 (2009) 8616–8625. doi:10.1039/b910970f.

[27] P. Vukosav, M. Mlakar, V. Tomiˇ, Revision of iron(III)–citrate speciation in aqueous solution . Voltammetric and spectrophotometric studies, Anal. Chim. Acta. 745 (2012) 85–91. doi:10.1016/j.aca.2012.07.036.

[28] C. Gabriel, C.P. Raptopoulou, A. Terzis, V. Tangoulis, C. Mateescu, A. Salifoglou, pH-Specific Synthesis , Spectroscopic , Structural and Magnetic Studies in Relevance to Aqueous Cr(III)-Citrate System, Inorg. Chem. 46 (2007) 2998–3009.

[29] G.R. Hedwig, J.R. Liddle, R.D. Reeves, Complex formation of nickel(II) ions with citric acid in aqueous solution: A potentiometric and spectroscopic study, Aust. J. Chem. 33 (1980) 1685–1693. doi:10.1071/CH9801685.

[30] S. Rode, C. Henninot, M. Matlosz, Complexation Chemistry in Nickel and Copper-Nickel Alloy Plating from Citrate Baths, J. Electrochem. Soc. 152 (2005) C248–C254. doi:10.1149/1.1869980.

[31] A.S. Bastug, S. GÖKTÜRK, T. Sismanoglu, 1:1 Binary Complexes of Citric Acid with Some Metal Ions: Stability and Thermodynamic Parameters, Asian J. Chem. 20 (2008) 1269–1278.

[32] D. Wyrzykowski, L. Chmurzyn, Thermodynamics of citrate complexation with Mn2+, Co2+, Ni2+ and Zn2+ ions, J. Therm. Anal. Calorim. 102 (2010) 61–64. doi:10.1007/s10973-009-0523-4.

[33] O.Y. Zelenin, Interaction of the Ni2+ ion with citric acid in an aqueous solution, Russ. J. Coord. Chem. 33 (2007) 355–359.
doi:10.1134/S1070328407050065.

[34] P.R. Deacon, M.F. Mahon, K.C. Molloy, P.C. Water, Synthesis and characterisation of tin(II) and tin(IV) citrates, J. Chem. Soc., Dalt. Trans. (1997) 3705–3712.

[35] L.C. Bichara, M.V. Fiori Bimbi, C.A. Gervasi, P.E. Alvarez, S.A. Brandán, Evidences of the formation of a tin(IV) complex in citric–citrate buffer solution: A study based on voltammetric, FTIR and ab initio calculations, J. Mol. Struct. 1008 (2012) 95–101. doi:10.1016/j.molstruc.2011.11.032.

[36] T. Hirokawa, Y. Kiso, Complex-forming equilibria in isotachophoresis. II. Evlauation of stability constants of tartrate and citrate complexes, J. Chromatogr. 248 (1982) 341–362.

[37] M. Walser, Ion association. V. Dissociation constants for complexes of citrate with sodium, potassium, calcium, and magnesium ions, J. Phys. Chem. 65 (1961) 159–161. doi:10.1021/j100819a045.

[38] N.W. Alcock, Complexation between Molybdenum(VI) and citrate: structural charcaterisation of a Tetrameric Complex, $K_4[(MoO_2)_4O_3(cit)_2]_6H_2O$, J. Chem. Soc., Dalt. Trans. (1990) 707–711.

[39] O. Happel, A. Seubert, Characterization of stable aluminium-citrate species as reference substances for aluminium speciation by ion chromatography, J. Chromatogr. 1108 (2006) 68–75. doi:10.1016/j.chroma.2005.12.100.

[40] Z.-H. Zhou, H. Zhang, Y.-Q. Jiang, D.-H. Lin, H.-L. Wan, K.-R. Tsai, Complexation between vanadium(V) and citrate: spectroscopic and structural characterization of a dinuclear vanadium (V) complex, Transit. Met. Chem. 24 (1999) 605–609.

[41] K. Blomqvist, E.R. Still, Solution Studies of Systems with Polynuclear Complex Formation. 4 . Heteronuclear Copper(II) Citrate Complexes with Nickel(II) or Magnesium(II), Inorganica Chim. Acta. 82 (1984) 141–144.

[42] EPA, Wastewater Treatment Fact Sheet: External Carbon Sources for Nitrogen Removal, (2013).

[43] P.B. Dhamole, R.R. Nair, S.F. D´Souza, S.S. Lele, Denitrification of high strength nitrate waste, Bioresour. Technol. 98 (2007) 247–252.

[44] W.G. Zumft, Cell Biology and Molecular Basis of Denitrification, Microbiol. Mol. Biol. Rev. 61 (1997) 533–616.

[45] N. Adouani, T. Lendormi, L. Limousy, O. Sire, Effect of the carbon source on N2O emissions during biological denitrification, Resour. Conserv. Recycl. 54 (2010) 299–302. doi:10.1016/j.resconrec.2009.07.011.

[46] I.C. Anderson, J.S. Levine, Relative rates of nitric oxide and nitrous oxide production by nitrifiers, denitrifiers, and nitrate respirers, Appl. Environ. Microbilogy. (1986) 938–945.

[47] S. Solomon, D. Qin, M. Manning, Z. Chen, M. Marquis, K.B. Averyt, M. Tignor, H.L. Miller, Climate Change 2007: The Physical Science Basis, Contribution of Working Group I to the Fourth Assessment Report of the Intergovernmental Panel on Climate Change, in: IPCC, Cambridge University Press, Cambridge, United Kingdom and New York, NY, USA, 2007: p. 996.

[48] G. González-Blanco, R. Beristain-Cardoso, F. Cuervo-López, F.J. Cervantes, J. Gómez, Denitrification applied to wastewater treatment: processes regulation and ecological aspects, in: N. Savaglio, R. Puopolo (Eds.), Nova Science Publishers, Inc., 2011.

[49] N.S. Srinu, Y.P. Setty, Biological denitrification of wastewater-A Mini Review on Carbon Source, in: Int. Conf. Chem. Environ. Sci. Eng., 2012: pp. 47–51.

[50] P. Gikas, Kinetic responses of activated sludge to individual and joint nickel (Ni(II)) and cobalt (Co(II)): An isobolographic approach, J. Hazard. Mater. 143 (2007) 246–256. doi:10.1016/j.jhazmat.2006.09.019.

[51] S. Anne, Implications of Microbial Heavy Metal Tolerance in the Environment, Rev. Undergrad. Res. 2 (2003) 1–6.

[52] G. Zhan, D. Li, L. Zhang, Aerobic bioreduction of nickel (II) to elemental nickel with concomitant biomineralization, Environ. Biotechnol. 96 (2012) 273–281. doi:10.1007/s00253-011-3827-9.

[53] K.E. Giller, E. Witter, S.P. McGrath, Heavy metals and soil microbes, Soil Biol. Biochem. 41 (2009) 2031–2037. doi:10.1016/j.soilbio.2009.04.026.

[54] G. Zou, S. Papirio, E.D. Van Hullebusch, J.A. Puhakka, Fluidized-bed denitrification of mining water tolerates high nickel concentrations, Bioresour. Technol. 179 (2015) 284–290.

[55] G. Wu, X. Zhai, C. Jiang, Y. Guan, Denitrifying kinetics and nitrous oxide emission under different copper concentrations., Water Sci. Technol. 69 (2014) 746–54. doi:10.2166/wst.2013.769.

[56] F. Cervantes, O. Monroy, J. Gomez, Accumulation of intermediates in a denitrifying process at different copper and high nitrate concentrations, 20 (1998) 959–961.

[57] H. Chen, Q.-Q. Chen, X.-Y. Jiang, H.-Y. Hu, M.-L. Shi, R.-C. Jin, Insight into the short- and long-term effects of Cu(II) on denitrifying biogranules, J. Hazardos Mater. 304 (2016) 448–456.

[58] G. Zou, S. Papirio, A. Ylinen, F. Di Capua, A.M. Lakaniemi, J.A. Puhakka, Fluidized-bed denitrification for mine waters. Part II: Effects of Ni and Co, Biodegradation. 25 (2014) 417–423. doi:10.1007/s10532-013-9670-1.

[59] K. Kiskira, S. Papirio, E.D. Van Hullebusch, G. Esposito, Influence of pH , EDTA/Fe (II) ratio, and microbial culture on Fe(II)-mediated autotrophic denitrification, Env. Sci Pollut Res. 24 (2017) 21323–21333. doi:10.1007/s11356-017-9736-4.

[60] K. Kiskira, S. Papirio, C. Fourdrin, E.D. Van Hullebusch, G. Esposito, Effect of Cu , Ni and Zn on Fe (II)-driven autotrophic denitrification, J. Environ. Manag. 218 (2018) 209–219. doi:10.1016/j.jenvman.2018.04.050.

[61] K. Kiskira, S. Papirio, E.D. Van Hullebusch, G. Esposito, Fe (II)-mediated autotrophic denitrification: A new bioprocess for iron bioprecipitation/biorecovery and simultaneous treatment of nitrate-containing wastewaters, Int. Biodeterior. Biodegradation. 119 (2017) 631–648. doi:10.1016/j.ibiod.2016.09.020.

[62] Y.. Chen, Q. Lin, Y.. Luo, Y.. He, S.. Zhen, Y.. Yu, G.. Tian, M.. Wong, The role of citric acid on the phytoremediation of heavy metal contaminated soil, Chemosphere. 50 (2003) 807–811. doi:10.1016/S0045-6535(02)00223-0.

[63] A.J. Francis, G.A. Joshi-Tope, C.J. Dodge, Biodegradation of Nickel-Citrate and Modulation of Nickel Toxicity by Iron, Environ. Sci. Technol. 30 (1996) 562–568.

[64] C.J. Dodge, A.J. Francis, Biotransformation of Binary and Ternary Citric Acid Complexes of Iron and Uranium, Environ. Sci. Technol. 31 (1997) 3062–3067. doi:10.1021/es961058+.

[65] R.A. Thomas, A.J. Beswick, G. Basnakova, R. Moller, L.E. Macaskie, Growth of naturally occurring microbial isolates in metal–citrate medium and bioremediation of metal–citrate wastes, J. Chem. Technol. Biotechnol. 75 (2000) 187–195.

[66] R. Singh, H. Yoon, R.A. Sanford, L. Katz, B.W. Fouke, C.J. Werth, Metabolism-Induced $CaCO_3$ Biomineralization During Reactive Transport in a Micromodel: Implications for Porosity Alteration, Environ. Sci. Technol. 49 (2015) 12094–12104. doi:10.1021/acs.est.5b00152.

[67] S.H. Ahoranta, M.E. Kokko, S. Papirio, B. Özkaya, J.A. Puhakka, Arsenic removal from acidic solutions with biogenic ferric precipitates, J. Hazard. Mater. 306 (2016) 124–132.

[68] B. Ozkaya, A. Kaksonen, E. Sahinkaya, J.A. Puhakka, Fluidized bed bioreactor for multiple environmental engineering solutions, Water Res. 150 (2019) 452–465. doi:10.1016/j.watres.2018.11.061.

[69] S. Papirio, a. Ylinen, G. Zou, M. Peltola, G. Esposito, J. a. Puhakka, Fluidized-bed denitrification for mine waters. Part I: Low pH and temperature operation, Biodegradation. 25 (2014) 425–435. doi:10.1007/s10532-013-9671-0.

[70] W. Soedel, Handbook of membrane reactors Volume 2: Reactor types and industrial applications, Woodhead Publishing Limited, 2013. doi:10.1201/9781420006445.bmatt1.

[71] H. Lin, W. Gao, F. Meng, B. Liao, K. Leung, L. Zhao, J. Chen, H. Hong, Membrane Bioreactors for Industrial Wastewater Treatment : A Critical Review, 2012. doi:10.1080/10643389.2010.526494.

[72] S.J. Judd, The status of industrial and municipal effluent treatment with membrane bioreactor technology, Chem. Eng. J. 305 (2016) 37–45.

[73] Q. Dong, W. Parker, M. Dagnew, Long term performance of membranes in an anaerobic membrane bioreactor treating municipal wastewater, Chemosphere. 144 (2016) 249–256.

[74] B.-Q. Liao, J.T. Kraemer, D.M. Bagley, Anaerobic Membrane Bioreactors: Applications and Research Directions, Crit. Rev. Environ. Sci. Technol. 36 (2006) 489–530. doi:10.1080/10643380600678146.

[75] J. Busch, A. Cruse, W. Marquardt, Modeling submerged hollow-fiber membrane filtration for wastewater treatment, J. Memb. Sci. 288 (2007) 94–111. doi:10.1016/j.memsci.2006.11.008.

[76] I.-S. Chang, P. Le Clech, B. Jefferson, S. Judd, Membrane Fouling in Membrane Bioreactors for Wastewater Treatment, J. Environ. Eng. 128 (2002) 1018–1029. doi:10.1061/(ASCE)0733-9372(2002)128:11(1018).

[77] F. Meng, S. Zhang, Y. Oh, Z. Zhou, H.-S. Shin, S.-R. Chae, Fouling in membrane bioreactors: An updated review, Water Res. 114 (2017) 151–180. doi:10.1016/j.watres.2017.02.006.

[78] J. Arévalo, L.M. Ruiz, J. Pérez, B. Moreno, M.A. Gómez, Removal performance of heavy metals in MBR systems and their influence in water reuse, Water Sci. Technol. (2013) 894–901.

[79] B. Feng, Z. Fang, J. Hou, X. Ma, Y. Huang, L. Huang, Effects of heavy metal wastewater on the anoxic/aerobic-membrane bioreactor bioprocess and membrane fouling, Bioresour. Technol. 142 (2013) 32–38. doi:10.1016/j.biortech.2013.05.019.

[80] E. Katsou, S. Malamis, M. Loizidou, Performance of a membrane bioreactor used for the treatment of wastewater contaminated with heavy metals., Bioresour. Technol. 102 (2011) 4325–4332. doi:10.1016/j.biortech.2010.10.118.

[81] B. Aftab, S.J. Jamal, T. Maqbool, N.P. Hankins, Heavy metals removal by osmotic membrane bioreactor (OMBR) and their effect on sludge properties, Desalination. 403 (2017) 117–127.

[82] M.F.R. Zuthi, W. Guo, H. Hao, D. Long, F.I. Hai, S. Xia, J. Li, J. Li, Y. Liu, New and practical mathematical model of membrane fouling in an aerobic submerged membrane bioreactor, Bioresour. Technol. 238 (2017) 86–94.

[83] D. Jeison, J.B. van Lier, Cake formation and consolidation: Main factors governing the applicable flux in anaerobic submerged membrane bioreactors (AnSMBR) treating acidified wastewaters, Sep. Purif. Technol. 56 (2007) 71–78. doi:10.1016/j.seppur.2007.01.022.

[84] H.J. Lin, K. Xie, B. Mahendran, D.M. Bagley, K.T. Leung, S.N. Liss, B.Q. Liao, Sludge properties and their effects on membrane fouling in submerged anaerobic

membrane bioreactors (SAnMBRs), Water Res. 43 (2009) 3827–3837. doi:10.1016/j.watres.2009.05.025.

[85] W.J. Gao, H.J. Lin, K.T. Leung, H. Schraft, B.Q. Liao, Structure of cake layer in a submerged anaerobic membrane bioreactor, J. Memb. Sci. 374 (2011) 110–120. doi:10.1016/j.memsci.2011.03.019.

[86] M. Aslam, P.H. Lee, J. Kim, Analysis of membrane fouling with porous membrane filters by microbial suspensions for autotrophic nitrogen transformations, Sep. Purif. Technol. 146 (2015) 284–293. doi:10.1016/j.seppur.2015.03.042.

[87] A. Charfi, M. Aslam, G. Lesage, M. Heran, J. Kim, Macroscopic approach to develop fouling model under GAC fluidization in anaerobic fluidized bed membrane bioreactor, J. Ind. Eng. Chem. 49 (2017) 219–229. doi:10.1016/j.jiec.2017.01.030.

[88] A. Charfi, M. Aslam, J. Kim, Modelling approach to better control biofouling in fluidized bed membrane bioreactor for wastewater treatment, Chemosphere. 191 (2018) 136–144. doi:10.1016/j.chemosphere.2017.09.135.

[89] B. Verrecht, T. Maere, I. Nopens, C. Brepols, S. Judd, The cost of a large-scale hollow fibre MBR, Water Res. 44 (2010) 5274–5283. doi:10.1016/j.watres.2010.06.054.

[90] H. Lin, J. Chen, F. Wang, L. Ding, H. Hong, Feasibility evaluation of submerged anaerobic membrane bioreactor for municipal secondary wastewater treatment, Desalination. 280 (2011) 120–126. doi:10.1016/j.desal.2011.06.058.

[91] T. Kurita, K. Kimura, Y. Watanabe, The infl uence of granular materials on the operation and membrane fouling characteristics of submerged MBRs, 469 (2014) 292–299.

[92] F. Zamani, J.W. Chew, E. Akhondi, W.B. Krantz, A.G. Fane, Unsteady-state shear strategies to enhance mass-transfer for the implementation of ultrapermeable membranes in reverse osmosis: A review, Desalination. 356 (2015) 328–348. doi:10.1016/j.desal.2014.10.021.

[93] B.D. Shoener, C. Zhong, A.D. Greiner, W.O. Khunjar, P.Y. Hong, J.S. Guest, Design of anaerobic membrane bioreactors for the valorization of dilute organic carbon waste streams, Energy Environ. Sci. 9 (2016) 1102–1112. doi:10.1039/c5ee03715h.

[94] M. Aslam, A. Charfi, G. Lesage, M. Heran, J. Kim, Membrane bioreactors for wastewater treatment : A review of mechanical cleaning by scouring agents to control membrane fouling, Chem. Eng. J. 307 (2017) 897–913. doi:10.1016/j.cej.2016.08.144.

[95] O.T. Iorhemen, R.A. Hamza, J.H. Tay, Membrane fouling control in membrane bioreactors (MBRs) using granular materials, Bioresour. Technol. 240 (2017) 9–24. doi:10.1016/j.biortech.2017.03.005.

[96] B. Wu, Y. Wang, W. Lim, J. Wei, A.G. Fane, Enhanced performance of submerged hollow fibre micro filtration by fluidized granular activated carbon, 499 (2016) 47–55. doi:10.1016/j.memsci.2015.10.050.

[97] A.G. Fane, Ultrafiltration of suspensions, J. Memb. Sci. 20 (1984) 249–259. doi:10.1016/S0376-7388(00)82002-5.

[98] J. Wang, B. Wu, Y. Liu, A.G. Fane, J.W. Chew, Effect of fluidized granular activated carbon (GAC) on critical flux in the microfiltration of particle foulants, J. Memb. Sci. 523 (2017) 409–417.

[99] J. Kim, K. Kim, H. Ye, E. Lee, C. Shin, P.L. McCarty, J. Bae, Anaerobic Fluidized Bed Membrane Bioreactor for Wastewater Treatment, Environ. Sci. Technol. 45 (2011) 576–581.

[100] M.A. Johir, S. Shanmuganathan, S. Vigneswaran, J. Kandasamy, Performance of submerged membrane bioreactor (SMBR) with and without the addition of the different particle sizes of GAC as suspended medium, Bioresour. Technol. 141 (2013) 13–18. doi:10.1016/j.biortech.2013.03.032.

[101] M. Aslam, P.L. McCarty, J. Bae, J. Kim, The effect of fluidized media characteristics on membrane fouling and energy consumption in anaerobic fluidized

membrane bioreactors, Sep. Purif. Technol. 132 (2014) 10–15. doi:10.1016/j.seppur.2014.04.049.

[102] J. Wang, B. Wu, S. Yang, Y. Liu, A.G. Fane, Characterizing the scouring ef fi ciency of Granular Activated Carbon (GAC) particles in membrane fouling mitigation via wavelet decomposition of accelerometer signals, 498 (2016) 105–115.

[103] B. Wu, Y.P. C, A.G. Fane, The potential roles of granular activated carbon in anaerobic fluidized membrane bioreactors: effect on membrane fouling and membrane integrity, Desalin. Water Treat. 53 (2015) 1450–1459. doi:10.1080/19443994.2014.943057.

[104] C. Shin, P.L. McCarty, J. Kim, J. Bae, Pilot-scale temperate-climate treatment of domestic wastewater with a staged anaerobic fluidized membrane bioreactor (SAF-MBR), Bioresour. Technol. 159 (2014) 95–103. doi:10.1016/j.biortech.2014.02.060.

[105] C. Shin, K. Kim, P.L. McCarty, J. Kim, J. Bae, Integrity of hollow-fiber membranes in a pilot-scale anaerobic fluidized membrane bioreactor (AFMBR) after two-years of operation, Sep. Purif. Technol. 162 (2016) 101–105. doi:10.1016/j.seppur.2016.02.019.

[106] M.Y. Jaffrin, Hydrodynamic Techniques to Enhance Membrane Filtration, Annu. Rev. Fluid Mech. 44 (2012) 77–96. doi:10.1146/annurev-fluid-120710-101112.

[107] A. Cahyadi, S. Yang, J. Wei, CFD study on the hydrodynamics of fluidized granular activated carbon in AnFMBR applications, 178 (2017) 75–89.

[108] J. Wang, F. Zamani, A. Cahyadi, J. Yuan, S. Yang, B. Wu, Y. Liu, A.G. Fane, J. Wei, Correlating the hydrodynamics of fl uidized granular activated carbon (GAC) with membrane-fouling mitigation, 510 (2016) 38–49.

[109] J. Wang, B. Wu, S. Yang, Y. Liu, A.G. Fane, J.W. Chew, Characterizing the scouring efficiency of Granular Activated Carbon (GAC) particles in membrane

fouling mitigation via wavelet decomposition of accelerometer signals, J. Memb. Sci. 498 (2016) 105–115. doi:10.1016/j.memsci.2015.09.061.

[110] H. Prieske, L. Böhm, A. Drews, M. Kraume, Optimised hydrodynamics for membrane bioreactors with immersed flat sheet membrane modules, Desalin. Water Treat. 18 (2010) 270–276. doi:10.5004/dwt.2010.1784.

[111] X. Liu, Y. Wang, T.D. Waite, G. Leslie, Numerical simulations of impact of membrane module design variables on aeration patterns in membrane bioreactors, J. Memb. Sci. 520 (2016) 201–213. doi:10.1016/j.memsci.2016.07.011.

[112] B.G. Fulton, P.R. Bérubé, Optimizing the sparging condition and membrane module spacing for a ZW500 submerged hollow fiber membrane system, Desalin. Water Treat. 42 (2012) 8–16. doi:10.1080/19443994.2012.682962.

[113] a. Manipura, J.R. Duncan, H.J. Roman, J.E. Burgess, Potential Biological Processes Available for Removal of Nitrogenous Compounds from Metal Industry Wastewater, Process Saf. Environ. Prot. 83 (2005) 472–480. doi:10.1205/psep.04271.

[114] S. Rajakumar, P.M. Ayyasamy, K. Shanthi, P. Thavamani, P. Velmurugan, Y.C. Song, P. Lakshmanaperumalsamy, Nitrate removal efficiency of bacterial consortium (Pseudomonas sp. KW1 and Bacillus sp. YW4) in synthetic nitrate-rich water., J. Hazard. Mater. 157 (2008) 553–63. doi:10.1016/j.jhazmat.2008.01.020.

[115] M.O. Rivett, S.R. Buss, P. Morgan, J.W.N. Smith, C.D. Bemment, Nitrate attenuation in groundwater: a review of biogeochemical controlling processes., Water Res. 42 (2008) 4215–32. doi:10.1016/j.watres.2008.07.020.

[116] R.M. Sterrit, J.N. Lester, Interactions of heavy metals with bacteria, Sci. Total Environ. 14 (1980) 5–17.

[117] A. Kapoor, T. Viraraghavan, Nitrate removal from drinking water-review, J. Environ. Eng. 123 (1997) 371–380.

[118] M.K. Firestone, E.A. Davidson, Microbiologial Basis of NO and N20 production and consumption in soil, Exch. Trace Gases between Terr. Ecosyst. Atmos. (1989) 7–21. doi:10.1017/CBO9781107415324.004.

[119] L. Wegrelius, B. Sjödén, Passivation treatment of stainless steel, Acom - Outo Kumpu “A Corros. Manag. Appl. Eng. Magaxine.” (2004) 1–10.

[120] M. Izquierdo, C. Gabaldón, P. Marzal, Interference of EDTA in the treatment of metal plating wastewater by biosorption, J. Chem. Technol. Biotechnol. 88 (2013) 606–614. doi:10.1002/jctb.3872.

[121] F. Cecen, N. Semerci, A.G. Geyik, Inhibitory effects of Cu , Zn , Ni and Co on nitrification and relevance of speciation ¸ e G ul, J. Chem. Technol. Biotechnol. 85 (2010) 520–528. doi:10.1002/jctb.2321.

[122] S.S. Adav, D.J. Lee, J.Y. Lai, Enhanced biological denitrification of high concentration of nitrite with supplementary carbon source, Appl. Microbiol. Biotechnol. 85 (2010) 773–778. doi:10.1007/s00253-009-2265-4.

[123] S.G. dos Santos, M.B. Amâncio Varesche, M. Zaiat, E. Foresti, Comparison of Methanol, Ethanol, and Methane as Electron Donors for Denitrification, Environ. Eng. Sci. 21 (2004) 313–320. doi:10.1089/109287504323066950.

[124] Y. Peng, Y. Ma, S. ying Wang, Denitrification potential enhancement by addition of external carbon sources in a pre-denitrification process, J. Environ. Sci. 19 (2007) 284–289. doi:10.1016/S1001-0742(07)60046-1.

[125] D. Martin, J.M. Salminen, R.M. Niemi, I.M. Heiskanen, M.J. Valve, P.P. Hellstén, T.H. Nystén, Acetate and ethanol as potential enhancers of low temperature denitrification in soil contaminated by fur farms: A pilot-scale study, J. Hazard. Mater. 163 (2009) 1230–1238. doi:10.1016/j.jhazmat.2008.07.092.

[126] A. Devi, A. Singhal, R. Gupta, A review on spent pickling liquor, Ipublishing.Co.In. 4 (2013) 284–295. doi:10.6088/ijes.2013040300007.

[127] C. Glass, J. Silverstein, Denitrification of high-nitrate, high-salinity wastewater, Water Researcch. 33 (1999) 223–229.

[128] W. Zhao, Y. Wang, S. Liu, M. Pan, J. Yang, S. Chen, Denitrification activities and N2O production under salt stress with varying COD/N ratios and terminal electron acceptors, Chem. Eng. J. 215–216 (2013) 252–260.

[129] M.H. Zwietering, I. Jongenburger, F.M. Rombouts, K. Van, Modeling of the Bacterial Growth Curve, Appl. Environ. Microbilogy. 56 (1990) 1875–1881.

[130] APHA, Standard Methods for the Examination of Water and Wastewater, 20th Edition, APHA American Public Health Association, 1998.

[131] L.L. Stookey, Ferrozine - a new spectrophotometric reagent for iron, Anal. Chem. 42 (1970) 779–781. doi:10.1021/ac60289a016.

[132] T. Arbel, N. Assulin, N. Sharon, J. Laffay, Parameters influencing Nitrite generation in drinking water MBBR Denitrification, Portland Oregon, 2010.

[133] H.B. Cheng, M. Kumar, J.G. Lin, Interpretation of redox potential variation during biological denitrification using linear non-equilibrium thermodynamic model, Int. Biodeterior. Biodegrad. 67 (2012) 28–39. doi:10.1016/j.ibiod.2011.11.010.

[134] D. Karadag, J.A. Puhakka, Enhancement of anaerobic hydrogen production by iron and nickel, Int. J. Hydrogen Energy. 35 (2010) 8554–8560. doi:10.1016/j.ijhydene.2010.04.174.

[135] K. Abu-Shandi, F. Al-Wedian, Estimation of composition, coordination model, and stability constant of some metal/phosphate complexes using spectral and potentiometric measurements, Chem. Pap. 63 (2009) 420–425. doi:10.2478/s11696-009-0027-5.

[136] J. Monhemius, Precipitation diagrams for metal hydroxides, sulfides, arsenates and phosphates, Trans. Inst. Min. Metall. 86 (1977) C202–C206. https://www.researchgate.net/publication/266137129_Precipitation_diagrams_for_metal_hydroxides_sulfides_arsenates_and_phosphates.

[137] O. Van Cleemput, W.H. Patrick, R.C. McIlhenny, Formation of chemical and biological denitrification products in flooded soil at controlled pH and redox potential, Soil Biol. Biochem. 7 (1975) 329–332.

[138] S.R. Pedada, S. Bathula, S.S.R. Vasa, K.S. Charla, G.N. R., Micellar effect on metal-ligand complexes of Co(II), Ni(II), Cu(II) and Zn(II) with citric acid, Bull. Chem. Soc. Ethiop. 23 (2009) 347–358.

[139] C.E. Barrera-díaz, V. Lugo-Lugo, B. Bilyeu, A review of chemical, electrochemical and biological methods for aqueous Cr(VI) reduction, J. Hazard. Mater. 223–224 (2012) 1–12.

[140] D. He, M. Zheng, T. Ma, C. Li, J. Ni, Interaction of Cr(VI) reduction and denitrification by strain Pseudomonas aeruginosa PCN-2 under aerobic conditions, Bioresour. Technol. 185 (2015) 346–352. doi:10.1016/j.biortech.2015.02.109.

[141] Y. Ma, P.S. Hooda, Chromium, Nickel and Cobalt, in: P.S. Hooda (Ed.), Trace Elem. Soil, John Wiley & Sons, Ltd, Chichester, UK, 2010: pp. 461–480.

[142] D.L. Parker, P. Borer, R. Bernier-Latmani, The response of Shewanella oneidensis MR-1 to Cr(III) toxicity differs from that to Cr(VI), Front. Microbiol. 2 (2011) 1–14. doi:10.3389/fmicb.2011.00223.

[143] G. Farabegoli, A. Carucci, M. Majone, E. Rolle, Biological treatment of tannery wastewater in the presence of chromium, 71 (2004) 345–349. doi:10.1016/j.jenvman.2004.03.011.

[144] J.P. Gustafsson, I. Persson, A.G. Oromieh, J.W.J. Van Schaik, C. Sjostedt, D.B. Kleja, Chromium(III) Complexation to Natural Organic Matter: Mechanisms and Modeling, Environ. Sci. Technol. 48 (2014) 1753–1761.

[145] Y. Tang, F.M. Michel, L. Zhang, R. Harrington, J.B. Parise, R.J. Reeder, Structural Properties of the Cr(III)-Fe(III) (Oxy)hydroxide Compositional Series: Insights for a Nanomaterial “Solid Solution,” Chem. Mater. 22 (2010) 3589–3598. doi:10.1021/cm1000472.

[146] F. Zamani, J. Wei, E. Akhondi, W.B. Krantz, A.G. Fane, Unsteady-state shear strategies to enhance mass-transfer for the implementation of ultrapermeable membranes in reverse osmosis: A review, Desalination. 356 (2015) 328–348.

[147] C. Shin, P.L. McCarty, J. Kim, J. Bae, Pilot-scale temperate-climate treatment of domestic wastewater with a staged anaerobic fluidized membrane bioreactor (SAF-MBR), Bioresour. Technol. 159 (2014) 95–103. doi:10.1016/j.biortech.2014.02.060.

[148] A. Charfi, N. Thongmak, B. Benyahia, M. Aslam, J. Harmand, N. Ben Amar, G. Lesage, P. Sridang, J. Kim, M. Heran, A modelling approach to study the fouling of an anaerobic membrane bioreactor for industrial wastewater treatment, Bioresour. Technol. 245 (2017) 207–215. doi:10.1016/j.biortech.2017.08.003.

[149] X. Du, Y. Wang, G. Leslie, G. Li, H. Liang, Shear stress in a pressure-driven membrane system and its impact on membrane fouling from a hydrodynamic condition perspective: a review, J. Chem. Technol. Biotechnol. 92 (2017) 463–478. doi:10.1002/jctb.5154.

[150] E.E. Rios-Del Toro, N.E. López-Lozano, F.J. Cervantes, Up-flow anaerobic sediment trapped (UAST) reactor as a new configuration for the enrichment of anammox bacteria from marine sediments, Bioresour. Technol. 238 (2017) 528–533. doi:10.1016/j.biortech.2017.04.087.

[151] Ronald J. Adrian, Particle-Imaging Techniques for Experimental Fluid Mechanics, Annu. Rev. Fluid Mech. 23 (1991) 261–304. doi:10.1146/annurev.fl.23.010191.001401.

[152] B.Y. Cui, D.Z. Wei, S.L. Gao, W.G. Liu, Y.Q. Feng, Numerical and experimental studies of flow field in hydrocyclone with air core, Trans. Nonferrous Met. Soc. China. 50 (2014) 2642–2649. doi:10.1016/S1003-6326(14)63394-X.

[153] M.M. Bradford, A rapid and sensitive method for the quantitation of microgram quantities of protein utilizing the principle of protein-dye binding, Anal. Biochem. 72 (1976) 248–254. doi:10.1016/0003-2697(76)90527-3.

[154] M. Dubois, K.A. Gilles, J.K. Hamilton, P.A. Rebers, F. Smith, Colorimetric Method for Determination of Sugars and Related Substances, Anal. Chem. 28 (1956) 350–356. doi:10.1021/ac60111a017.

[155] C.F. Alves, L.F. Melo, M.J. Vieira, Influence of medium composition on the characteristics of a denitrifying biofilm formed by Alcaligenes denitrificans in a fluidised bed reactor, Process Biochem. 37 (2002) 837–845. doi:10.1016/S0032-9592(01)00282-5.

[156] L.P. Lakshmi, Y.P. Setty, Liquid-solid mass transfer in a two phase fluidized bed bioreactor, Chem. Eng. J. 135 (2008) 135–140. doi:10.1016/j.cej.2007.04.020.

[157] H. Sich, J. Van Rijn, Scannig electron microscopy of biofilm formation in denitrifying, fluidised bed reactors, 31 (1997) 733–742.

[158] Y. Tian, L. Chen, S. Zhang, S. Zhang, A systematic study of soluble microbial products and their fouling impacts in membrane bioreactors, Chem. Eng. J. 168 (2011) 1093–1102. doi:10.1016/j.cej.2011.01.090.

[159] H. Lin, M. Zhang, F. Wang, F. Meng, B.Q. Liao, H. Hong, J. Chen, W. Gao, A critical review of extracellular polymeric substances (EPSs) in membrane bioreactors: Characteristics, roles in membrane fouling and control strategies, J. Memb. Sci. 460 (2014) 110–125. doi:10.1016/j.memsci.2014.02.034.

[160] C. Li, Y. Yang, S. Ding, L. Hou, Dynamics of biofouling development on the conditioned membrane and its relationship with membrane performance, J. Memb. Sci. 514 (2016) 264–273. doi:10.1016/j.memsci.2016.04.066.

[161] H.P. Chu, X. Li, Membrane Fouling in a Membrane Bioreactor (MBR): Sludge Cake Formation and Fouling Characteristics, Biotechnol. Bioeng. Bioeng. 90 (2005) 323–331. doi:10.1002/bit.20409.

[162] R. Yoo, J. Kim, P.L. McCarty, J. Bae, Anaerobic treatment of municipal wastewater with a staged anaerobic fluidized membrane bioreactor (SAF-MBR) system., Bioresour. Technol. 120 (2012) 133–139. doi:10.1016/j.biortech.2012.06.028.

[163] EPA, Office of Water and Office of Research and Development. National Rivers and Streams Assessment 2008-2009: A Collaborative Survey (EPA/841/R-16/007), 2016.

[164] K.-J. Appenroth, What are '"heavy metals"' in Plant Sciences?, Acta Physiol Plant. 32 (2010) 615–619. doi:10.1007/978-3-642-02436-8.

[165] P. Gikas, Single and combined effects of nickel (Ni(II)) and cobalt (Co(II)) ions on activated sludge and on other aerobic microorganisms : A review, J. Hazard. Mater. 159 (2008) 187–203. doi:10.1016/j.jhazmat.2008.02.048.

[166] G. Zou, A. Ylinen, F. Di Capua, S. Papirio, A.M. Lakaniemi, J. Puhakka, Impact of Heavy Metals on Denitrification of Simulated Mining Wastewaters, Adv. Mater. Res. 825 (2013) 500–503. doi:10.4028/www.scientific.net/AMR.825.500.

[167] J.E. Ramírez, J.R. Rangel-Mendez, L. Lopes, S.D. Gomes, G. Buitrón, F.J. Cervantes, Denitrification of metallurgic wastewater : mechanisms of inhibition by Fe , Cr and Ni, J. Chem. Technol. Biotechnol. 93 (2017) 440–449. doi:10.1002/jctb.5374.

[168] Y. Pan, L. Ye, B.-J. Ni, Z. Yuan, Effect of pH on N2O reduction and accumulation during denitrification by methanol utilizing denitrifiers, Water Res. 46 (2012) 4832–4840. doi:10.1016/j.watres.2012.06.003.

[169] O. Gylienė, O. Nivinskienė, V. Pakštas, Use of Metallic Iron for Decontamination of Solution Containing Ni(II)– Citrate, Polish J. Environ. Stud. 16 (2007) 397–402.

[170] U.U. Jadhav, H. Hocheng, A review of recovery of metals from industrial waste, J. Achiev. Mater. Manuf. Eng. 54 (2012) 159–167.

[171] D.B. Johnson, K.B. Hallberg, Acid mine drainage remediation options: a review, Sci. Total Environ. 338 (2005) 3–14. doi:10.1016/j.scitotenv.2004.09.002.

[172] D. Wang, Y. Ye, H. Liu, H. Ma, W. Zhang, Effect of alkaline precipitation on Cr species of Cr(III)-bearing complexes typically used in the tannery industry, Chemosphere. 193 (2018) 42–49. doi:10.1016/j.chemosphere.2017.11.006.

[173] Y. Shi, J. Huang, G. Zeng, Y. Gu, Y. Chen, Y. Hu, B. Tang, J. Zhou, Y. Yang, L. Shi, Exploiting extracellular polymeric substances (EPS) controlling strategies for

performance enhancement of biological wastewater treatments : An overview, Chemosphere. 180 (2017) 396–411.

[174] W.-C. Kuo, G.F. Parkin, Characterization of soluble microbial products from anaerobic treatment by molecular weight distribution and nickel-chelating properties, Water Res. 30 (1996) 915–922.

[175] U. Cornell, R. M. and Schwertmann, 13 Formation, in: R.M.C. and U. Schwertmann (Ed.), Iron Oxides Struct. Prop. React. Ocurr. Uses, WILEY-VCH Verlag GmbH & Co., KGaA,Weinheim, 2003. doi:doi:10.1002/3527602097.ch13.

[176] O. Gyliene, M. Salkauskas, R. Juskenas, The Use of Organic Acids as Precipitants for Metal Recover y from Galvanic Solutions, J. Chem. Tech. Biotechnol. 70 (1997) 111–115.

[177] O. Gyliene, J. Aikaite, O. Nivinskiene, Recycling of Ni(II)– citrate complexes using precipitation in alkaline solutions, J. Hazard. Mater. B109 (2004) 105–111. doi:10.1016/j.jhazmat.2004.03.008.

[178] C. Dai, Y. Hu, Fe(III) Hydroxide Nucleation and Growth on Quartz in the Presence of Cu(II), Pb(II), and Cr(III): Metal Hydrolysis and Adsorption, Environ. Sci. Technol. 49 (2015) 292–300. doi:10.1021/es504140k.

[179] X.-M. Wang, T.D. Waite, Iron speciation and iron species transformation in activated sludge membrane bioreactors, Water Res. 44 (2010) 3511–3521. doi:10.1016/j.watres.2010.03.031.

[180] R. Ryall, J. Fielding, The co-precipitation of ferric iron and protein and the reducing capacity of serum as factors affecting the assay os serum iron, Clin. Chim. Acta. 28 (1970) 193–202.

[181] Z. Zhang, M.W. Bligh, Y. Wang, G.L. Leslie, H. Bustamante, T.D. Waite, Cleaning strategies for iron-fouled membranes from submerged membrane bioreactor treatment of wastewaters, J. Memb. Sci. 475 (2015) 9–21.

[182] A.M. Pat-Espadas, F.J. Cervantes, Microbial recovery of metallic nanoparticles from industrial wastes and their environmental applications, J. Chem. Technol. Biotechnol. 93 (2018) 3091–3112. doi:10.1002/jctb.5681.